

Broadband Active Structural Control Using Collocated Piezoelectric Sensors and Actuators

by

Cagri Abdullah Savran

B.S. Mechanical Engineering
Purdue University, 1998

SUBMITTED TO THE DEPARTMENT OF MECHANICAL ENGINEERING IN
PARTIAL FULFILLMENT OF THE REQUIREMENTS FOR THE DEGREE OF

MASTER OF SCIENCE IN MECHANICAL ENGINEERING
AT THE
MASSACHUSETTS INSTITUTE OF TECHNOLOGY

JUNE 2000

© 2000 Massachusetts Institute of Technology. All Rights Reserved.

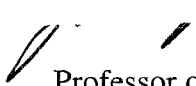
Signature of Author

Department of Mechanical Engineering
May 5, 2000

Certified by

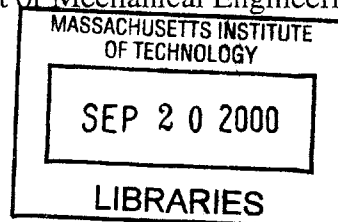
Steven R. Hall
Associate Professor of Aeronautics and Astronautics
Thesis Supervisor

Certified by


Kamal Youcef-Toumi
Professor of Mechanical Engineering
Departmental Reader

Accepted by

Ain A. Sonin
Chairman, Department Committee on Graduate Students
Department of Mechanical Engineering



ENG

Broadband Active Structural Control Using Collocated Piezoelectric Sensors and Actuators

by

Cagri Abdullah Savran

Submitted to the Department of Mechanical Engineering on May 5,
2000, in partial fulfillment of the requirements for the degree of
Master of Science in Mechanical Engineering

Abstract

This thesis presents active structural control experiments performed on a model fuselage testbed, to reduce interior noise. The testbed is a hybrid-scaled model fuselage designed to be representative of complex aircraft structures with rib and stringer construction, which results in a structure with high modal density and complex behavior. Collocated pairs of piezoelectric sensors and actuators were used to achieve robust stability. The sensor/actuator pairs consist of PVDF film and PZT ceramic sheets bonded to the surface of the model fuselage.

Closed-loop control of the fuselage skin was carried out with 30 collocated sensor/actuator pairs, covering approximately 10% of the surface area of the testbed. The disturbance source was a PZT patch bonded to an adjacent panel. Rate feedback was applied to each collocated pair separately but simultaneously (independent loop closure). Accelerometers attached to the panels and microphones located inside the testbed were used as performance sensors. The experimental results show as much as 20 dB reduction in structural acceleration and up to 10 dB attenuation in interior acoustic pressure level, at resonant peaks, over a frequency range of 100-2000 Hz.

Thesis Supervisor: Steven R. Hall

Title: Associate Professor of Aeronautics and Astronautics

Acknowledgements

This research was supported by an Army Research Office Multidisciplinary University Research Initiative (MURI) grant, under the program MURI DAAH 4-95-1-0104, with technical monitor Dr. Gary Anderson.

Special thanks go to my undergraduate colleague Daniel Kwon without whose help, the instrumentation for this research would not be done in a timely manner. I would also like to thank the undergraduate research assistants Christian Garcia and Eric Coulter for the help they provided for the experimental setup. Very special thanks go to Paul Bauer and Dave Robertson without whose help the instrumentation would never be completed. I would like to acknowledge the assistance on thermoplastic adhesives provided by Ken Thompson of 3M Innovation. My profound thanks go to Mauro Atalla, Michael Fripp and Kyung-yeol Song for all the help they provided for my research. I would like to thank my research advisor Steven Hall for his guidance and invaluable insight. I would also like to thank my 16.243 instructor Ed Crawley for telling me that I was a “very lucky boy” for achieving performance with a transfer function that doesn’t roll off. Hale, and Fatih deserve most special thanks for encouraging and supporting me in difficult times. I would like to thank my family members who have always been supportive, considerate, and patient.

Finally, I would like to commemorate and dedicate this thesis to my elementary school teacher Ismail Hakki Kandemir who taught me how to think and be open-minded.

Table of Contents

Acknowledgements	5
Table of Contents	7
List of Figures	9
Chapter 1. Introduction	11
1.1 Motivation	11
1.2 Background	12
1.3 Approach	15
1.4 Overview	16
Chapter 2. Experimental Setup	17
2.1 Testbed	17
2.2 Sensor and Actuator Selection	21
2.2.1 Actuator Selection	21
2.2.2 Sensor Selection	23
2.2.3 Sensor and Actuator Placement	30
2.3 The Active Ply	35
2.3.1 Manufacturing and Bonding the Active Ply	37
2.4 Finalized setup	40
2.5 Summary	42
Chapter 3. Control System Design	43
3.1 An Overview of Structural Control Architectures	43
3.2 Local Control Methods	47
3.3 System Identification	53
3.3.1 Disturbance to Performance Transfer Functions	54
3.3.2 Actuator to Sensor Transfer Functions	56
3.4 Control Law	58
3.5 Summary	70
Chapter 4. Control Implementation and Experimental Results	73
4.1 Control Implementation	74
4.1.1 Digital Approach	74
4.1.2 Analog Approach	78
4.2 Experimental Results	80
4.3 Summary	89

Chapter 5. Conclusions	91
5.1 Summary	91
5.2 Conclusions	94
5.3 Recommendations for Future Work	96
Appendix A Equipment Specifications and Manufacturer Information	99
References	101

List of Figures

2.1	Testbed in anechoic chamber and its CAD drawing.	18
2.2	PZT to accelerometer transfer function.	25
2.3	The curved panel and the schematic of the collocated PVDF-PZT pair.	26
2.4	PZT to PVDF transfer function on the curved panel.	27
2.5	PZT-Copper kapton-PVDF patch.	28
2.6	PZT to PVDF transfer function of the PZT-Copper kapton-PVDF patch.	29
2.7	PZT-PVDF transfer function of the fuselage testbed.	30
2.8	Single panel sensor/actuator placement.	32
2.9	5 PZT-Copper kapton-PVDF patches on a testbed panel.	33
2.10	PZT to PVDF transfer function for the central patch of the panel.	33
2.11	PZT to PVDF transfer functions from 5 patches.	34
2.12	An exploded view of the active ply.	36
2.13	Hot and ground electrode patterns.	37
2.14	A finalized active ply.	39
2.15	Testbed with six active plies.	40
2.16	Schematic of the instrumented area of the testbed.	41
3.1	Mode shape of the testbed at 674 Hz.	46
3.2	Root locus of an arbitrary 3 degree-of-freedom flexible plant with collocated sensors and actuators when controlled by PPF with a pair of complex poles.	49
3.3	Root locus of an arbitrary 3 degree-of-freedom flexible plant with collocated sensors and actuators when controlled by PPF with a single real pole.	50
3.4	Root locus of an arbitrary 3 degree-of-freedom flexible plant with collocated sensors and actuators when controlled by rate feedback.	52
3.5	Schematic of the control problem.	54
3.6	Disturbance to accelerometer open-loop transfer function for Panel 1, Location 1.	55
3.7	Disturbance to microphone open-loop transfer function: The microphone is located behind Panel 2.	55
3.8	PZT to PVDF transfer function for the central patch of Panel 1.	57
3.9	Magnitude of transfer functions for all 5 sensor/actuator pairs of Panel 1.	57
3.10	Force to velocity dereverberated transfer function.	59
3.11	Loop transfer function of a pure rate feedback controller and a PZT-PVDF pair.	60
3.12	$K(s)$ where $\omega_n = 900$ Hz, $\zeta = 0.05$, and $k = 80$	62
3.13	$K(s) \times G_{yu}(s)$ where $\omega_n = 900$ Hz, $\zeta = 0.05$, and $k = 80$	62
3.14	Root locus demonstration of the control system sensitivity to corner frequency in the roll off term of $K(s)$	64
3.15	Controller transfer function for various values of ζ	66
3.16	$K(s)$ where $\omega_n = 3100$ Hz, $\zeta = 0.18$ and $k = 108$	68
3.17	$K(s) \times G_{yu}(s)$ for the sensor/actuator pair at Panel 1-Location 1; where $\omega_n = 3100$ Hz, $\zeta = 0.18$ and $k = 108$	68

3.18	Magnitude of $K(s) \times G_{yu}(s)$ for all pairs of Panel 1.....	69
4.1	Basic digital control system with computer	74
4.2	The chosen controller with and without the additional phase lag (Sampling frequency was assumed to be 4100 Hz).	77
4.3	Analog controller.	78
4.4	Open-loop and closed-loop strain autospectra for Panel 1, Location 1.....	81
4.5	Open-loop and closed-loop acceleration autospectra for Panel 1, Location 4.....	81
4.6	Open-loop and closed-loop acceleration autospectra for Panel 2, Location 1.....	82
4.7	Open-loop and closed-loop acceleration autospectra for Panel 3, Location 3.....	83
4.8	Open-loop and closed-loop acceleration autospectra for Panel 4, Location 2.	83
4.9	Open-loop and closed-loop acceleration autospectra for Panel 5, Location 1.	84
4.10	Open-loop and closed-loop acceleration autospectra for Panel 6, Location 5.	84
4.11	Open-loop and closed-loop average acceleration autospectra integrated in 100 Hz frequency bands.	86
4.12	Open-loop and closed-loop acoustic pressure autospectra for a microphone located behind Panel 2 (#19).	86
4.13	Open-loop and closed-loop acoustic pressure autospectra for a microphone located behind Panel 2 (#21).	88
4.14	Open-loop and closed-loop acoustic pressure autospectra for a microphone located behind Panel 2 (#23).	88
4.15	Open-loop and closed-loop average acoustic pressure autospectra integrated in 100 Hz frequency bands.	89

Chapter 1

Introduction

1.1 Motivation

Excessive interior noise can be a serious problem in aircraft, especially in helicopters. In a commercial helicopter, sound pressure level can reach 95 dB and in a military helicopter, it can exceed 115 dB [Moreland, 1979]. Several reasons exist for these high sound levels. Firstly, helicopters have stiff but light frames to comply with structural requirements. This results in a structure that is composed of thin and lightly damped members. A structure with such members tends to be resonant and transmits sound very easily. Secondly, a helicopter cabin typically undergoes various disturbances from the rotor, transmission, engine, and boundary layer, which result in broadband structural vibration [Niesl, 1994]. Due to structural coupling, the disturbance caused by each source induces vibrations throughout the entire fuselage. Further, structural modes are strongly coupled with many of the acoustic modes of the aircraft interior. This causes noise throughout the cabin. Alleviating this problem may reduce time and cost for maintenance, prevent hearing loss, and improve pilot effectiveness [Leatherwood, 1979] and passenger comfort in general.

A typical helicopter crew member commonly monitors two or three radios. Background noise makes this a very demanding aural task. Besides, effective helicopter operation often depends on a close liaison between crew members and hence on the quality of communication. When manoeuvring to pick up an underslung load or carrying out a rescue operation, the pilot often relies on the messages received from crewmen. While air crew may be able to cope with noisy environment, it is increasingly difficult if others such

as doctors join the intercom for briefing or discussion. For military situations, troops may require direct-voice re-briefing in flight which is made very difficult by high background noise since intercom outlets are limited [Maitland, 1979].

Other than these immediate effects, repetitive and long lasting exposure to high noise levels also has long-term effects. It is possible for a helicopter crew to be exposed to high noise levels for six or eight hours a day. This results in noise-induced fatigue that can limit prolonged helicopter operation and can also result in permanent aural damage.

1.2 Background

One commonly used approach to address the interior noise problem is passive damping. A variety of insulating materials can be mounted on the structure to reduce its resonant behavior by adding damping. Certain foams, polymers, honeycomb structures and multi-layer trim panels can serve as damping materials. Passive damping is a safe method for acoustic quieting since it cannot lead to any form of instability. It is also economical since the required material is relatively easy to find and install. Studies that compare active and passive approaches suggest that passive approach should be used whenever possible [Von Flotow, 1997]. However, to the operator of a helicopter, the extent to which passive damping is acceptable is limited by the extra weight that the insulating material introduces. Especially in military terms, payload may be more important than passenger comfort. Insulating material also tends to absorb other things and when saturated with randomly spilt oil or hydraulic fluid, it becomes a serious fire hazard [Maitland, 1979]. Because of such restrictions, passive damping techniques are undesirable except for high frequency absorption and are ineffective below the frequency range of 1000 - 3000 Hz [Leverson, 1979].

Another approach for acoustic quieting is active control. Researchers have done significant amount of work on Active Noise Control (ANC). ANC relies on the principle of destructive interference between two sound fields. One field is generated by the original or primary sound source, and the other is generated by a secondary sound source set up to interfere with and cancel the unwanted primary sound. The secondary source is usually a loudspeaker with electronically controlled input. Researchers investigated usage of loudspeakers inside the passenger cabin to reduce low frequency tonal noise that results from the rotation of main and tail motors, and achieved reductions up to 10 dB [Elliot, 1997]. Recent developments in digital signal processing (DSP) chips have brought active noise control techniques within the realm of practicality [Elliot, 1999]. However, the space and weight limitations for the integration of the system, and loudspeakers in particular, present challenges [Smith, 1996]. For that reason, researchers have developed lightweight loudspeakers to be used in active control of aircraft noise [Warnaka, 1992]. Though effective in reducing the sound level in small portions of the cabin, ANC does not promise global quieting. The complicated behavior of acoustic waves in three dimensions is a handicap in achieving this goal.

Lightweight systems that apply forces to the aircraft fuselage to reduce interior noise are a relatively new stage in the control of aircraft cabin noise. The process of using such forces, known as Active Structural Acoustic Control (ASAC), has shown much promise. ASAC aims to reduce noise on its transmission path before it is induced in the cabin, as opposed to ANC, which directly attenuates the interior sound field. Studies show that structural-based control systems may outperform the speaker-based ones for reducing interior noise [Rossetti, 1994].

More recent studies on active structural control have involved using surface mounted piezoelectric actuators due to the control authority that they provide [Fuller, 1994].

Researchers at NASA Langley Research Center studied performance of optimized piezoelectric actuator and microphone arrays and successfully predicted best and worst case performances in reducing aircraft interior harmonic noise [Palumbo, 1996]. The majority of ASAC studies concentrated on large-wavelength global modes of the aircraft fuselage for which a strong understanding of the two-dimensional dynamics of the system is sufficient [Concilio, 1996].

Researchers investigated active noise and vibration control of a full scale turboprop aircraft cabin using simple second-order classical compensators. Piezoelectric actuators were designed based on the measured deflection pattern of the aircraft at the blade passage frequency. At this specific frequency, closed-loop results showed acceleration and noise reductions of 20 dB and 15 dB respectively [Grewal, 1997]. Others used a MIMO feedforward control on the same fuselage with a Filtered-x Least Mean Square adaptive algorithm. Their experimental results showed 21.6 dB reduction in vibration and 25.8 dB reduction in interior noise field at the blade passage frequency [Xu, 1998].

Although most ASAC studies aimed at reducing tonal noise components, a limited number of studies were also performed to reduce broadband noise. A section of a full scale DC-9 aircraft fuselage was instrumented with piezoelectric actuators for broadband noise reduction. Actuator locations were selected based on the PZT to microphone transfer functions that were obtained using a finite element based algorithm. The experiment resulted in 8 dB overall noise reduction over a frequency range of 250 - 1200 Hz [Mathur, 1997]. A model-based control design of an aircraft requires an accurate three-dimensional model. Certain fuselage structures can have quite complicated dynamics with high modal density. Hence, an accurate model may require thousands of degrees of freedom. Especially high frequency modes that exhibit uncertainties are difficult to model. These modes also have sensitivity to changes in environmental parameters. Constructing an accurate

model that takes all of these uncertainties into account may not be feasible. Furthermore, using that model for control simulations may exceed the capabilities of a personal computer. Thus, the limited nature of broadband ASAC research is not surprising.

1.3 Approach

The transmission path for many of the structural disturbances to an aircraft runs throughout the fuselage. Thus, in order to achieve global quieting, it is necessary to control the vibration of a large portion of the fuselage without exceeding weight and space limits. The approach presented in this thesis is broadband active structural acoustic control using a large number of distributed sensors and actuators. The distributed nature of sensors and actuators is necessary to achieve control authority over a large portion of the fuselage.

In a previous study at MIT, a model fuselage testbed was designed to investigate control of interior acoustics. Although not a scale model of an actual aircraft fuselage, the testbed emulates many features of a realistic helicopter fuselage, including its modal density and ratio of structural to acoustic frequency. As a part of this study, a two-dimensional model was formed for evaluation of sensors and actuators. Results of control simulations of this model showed that collocated feedback methods are desirable for damping localized structural modes over a broad frequency range. When compared with more sophisticated control laws, collocated local control methods are much more feasible to implement on a fuselage structure [O'Sullivan, 1998].

The study presented in this thesis centers around instrumentation of a portion the fuselage testbed with multiple collocated lightweight strain sensors and actuators. The main goal of the study is to implement multiple classical feedback loops using these sensors and actuators, and thereby achieve broadband vibration and interior acoustic control of the testbed.

1.4 Overview

Chapter 2 presents the experimental setup used in this study and gives a brief description of the model fuselage testbed. This chapter also presents the selection and placement procedure of the sensors and actuators. An active ply with encapsulated sensors and actuators is introduced. A section describes in detail the bonding procedure of these active plies on to the testbed. Pictures and schematics help to present the finalized experimental setup with the performance sensors.

Chapter 3 covers the control design procedure and gives an overview of structural control architectures with a detailed description of commonly used local control methods. Since an accurate model that represents the complex dynamics of the full-size test-bed was not available, control design was based on experimental system identification techniques. Thus, a part of Chapter 3 is dedicated to system identification. A section presents the experimental transfer functions taken from actuators to control sensors, and from the disturbance source to performance sensors. Finally, the chapter presents the control law, and discusses its stability from a frequency domain point of view.

Chapter 4 comprises control implementation and the results of closed-loop experiments that were performed on the testbed. The effectiveness of the control experiment on the structural vibration and the interior acoustics is evaluated by comparing the open-loop and closed-loop performance.

Finally, Chapter 5 summarizes the study, states the conclusions, and gives some recommendations for future work.

Chapter 2

Experimental Setup

This chapter presents the setup that was developed for the structural control experiment. The chapter contains four sections. The first section presents the testbed that was previously developed to be representative of an actual helicopter fuselage. This section outlines the geometrical, material and dynamic properties of the testbed. The second section contains the selection and the placement procedure of sensors and actuators that are necessary to perform control experiments on the testbed. The selection procedure aimed at forming a collocated sensor/actuator pair which is beneficial to achieve robust stability. This section also presents the experimental evaluation of several sensor/actuator pairs. Transfer functions taken from the testbed with the selected sensor/actuator pair are given. The third section of the chapter presents the design and manufacturing of an active ply that contains the selected sensor/actuator pairs in an encapsulated package. Also described in this section is the bonding procedure of multiple active plies onto the testbed. The fourth section of the chapter presents the finalized experimental setup with the location of disturbance sources and performance sensors.

2.1 Testbed

In a previous study at MIT, a fuselage testbed for studying control of interior acoustics was developed [Fripp, 1997; O'Sullivan, 1998]. The testbed was designed to be a simplified representative of a helicopter structure to facilitate control experiments, but the realism of some features that most directly affect the design were maintained.

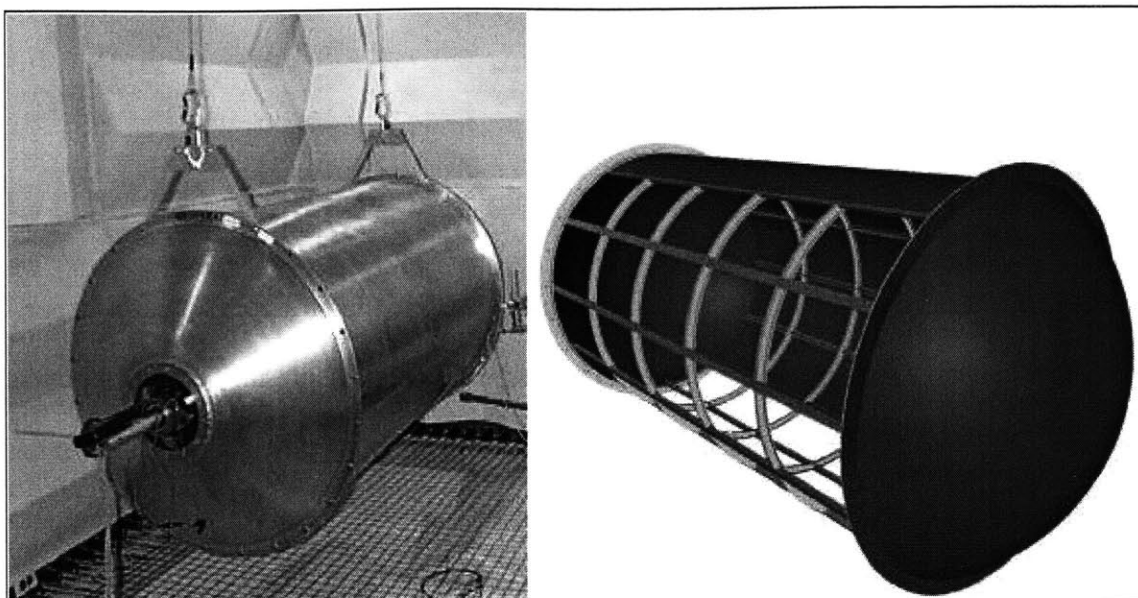


Figure 2.1: Testbed in anechoic chamber and its CAD drawing.

Figure 2.1 shows a picture of the model fuselage and its CAD drawing. The dimensions of the testbed are 91 cm in diameter and 198 cm in length. The testbed consists of six ribs and twelve stringers (frame members) that divide it into sixty panel sub-sections. Each panel is 23.9 cm wide and 30.5 cm long. Similar to many realistic helicopters, the testbed was made of aluminum.

The testbed is one of the most important parts of a study to investigate feasible methods of active structural acoustic control. It must represent the important characteristics of a realistic helicopter fuselage such as global and panel structural dynamics, interior acoustic dynamics, and structural acoustic coupling. The testbed was designed using a hybrid of geometric and dynamic scaling techniques based on the data collected from six aircraft-related structures. The frame and panel geometries of these structures were averaged while maintaining mass and stiffness properties. In addition, the sizes of the structures were

scaled to the diameter of the testbed (91 cm), which was limited by the anechoic facility constraints.

The simplest design would be a geometric scaling of the averaged structures. However, brutal geometric scaling requires components that are difficult and expensive to manufacture. Hybrid scaling parameters were used to maintain the essential structural-acoustic dynamics while ensuring manufacturability of the design [O'Sullivan, 1998]. These parameters include mass per length, length/radius, panel aspect ratio, 1st panel frequency/1st acoustic frequency, panel mass/mass air volume, and bending and torsional inertia of ribs and stringers. These scaling parameters capture three main characteristics of the system dynamics: global dynamics, panel dynamics, and the relative dynamics between frames and panels.

The global stiffness of a thin-walled cylinder is dictated by its thickness. Hence, to capture global dynamics, the global structural stiffness was approximated by smoothing the ribs and stringers to create a thin walled cylinder with constant thickness. Mass per length was used as an equivalent parameter to represent the smoothed thickness.

High frequency modal behavior of aircraft structures is dominated by panels. Hence, panels must be characterized separately. The aspect ratio of a panel determines its modal ordering and frequency spacing. Another important attribute of the panel is the relationship between panel frequency and acoustic cavity frequency. The ratio of these frequencies represents the degree of coupling between structural and acoustic disturbances. This ratio depends on various properties of the panel such as length, width, thickness and density as well as speed of sound in air. These properties of the panel were chosen such that the ratio of 1st panel mode to 1st acoustic mode approximates that of a realistic structure. An exact analytical relation for this ratio appears in the literature [Blevins, 1979]. Another parameter that helps maintain the proper structural acoustic coupling between the panel

and the air is the mass ratio of the panel to a surrounding characteristic volume of air which turns out to be an expression of geometric scaling for homogeneous panels.

Frame members (ribs and stringers) also require appropriate characterization. These members add both local and global stiffness to the structure. The number of frame members of the testbed differs from that of a real structure. Hence, the total frame stiffness was characterized by the sum of the bending and torsional inertias. As the panel size increases, the stiffness and the cross-sectional area of the frames increase but the number of frame members decreases. This helps to maintain the relative deflection between the panels and the frame members.

The nose and the tail of a regular helicopter are fairly complicated and non-regular. Simplified rounded end-caps were designed to reduce cost and to avoid sensor/actuator placement on the ends of the structure. The end-caps are stiffer and more massive than the skin of the testbed. This reduces the structural and acoustic coupling between the end-caps and the cylindrical section of the testbed.

The final consideration of the testbed design is the placement of the rivets that were used to attach the panels to the frame. Fastener spacing was geometrically scaled with the rest of the aircraft parameters and corresponds roughly to one centimeter on the testbed. This spacing is less than a quarter wavelength of the highest frequency of interest and puts the fastener dynamics outside the frequency range of interest (> 9000 Hz).

The reader is referred to the literature [O'Sullivan, 1998] for a more detailed presentation of testbed design. The next section presents in detail the selection and placement of the sensors and actuators to be used for the active structural control of the testbed.

2.2 Sensor and Actuator Selection

The selection of sensors and actuators has crucial importance in a structural control experiment. This is especially true for structures with light damping, high modal density and sensitivity to environmental changes. These aspects introduce modeling difficulties [MacMartin, 1994] and may lead to a control design that solely depends on the experimental identification of open-loop transfer functions taken by using the sensors and actuators. Thus, it is important to choose sensors and actuators that provide good observability and controllability of the structural modes.

The need for sufficient observability and controllability introduces some practical requirements. Achieving authority over a significant portion of the fuselage requires a large number of distributed sensors and actuators. However, strict weight and space limitations render this requirement a rather formidable task to fulfill [O'Sullivan, 1998]. For this reason, the chosen sensors and actuators must be lightweight, compact, and easy to attach to the structure.

2.2.1 Actuator Selection

The actuator has primary importance in a structural control experiment. Space and weight limitations are usually strict. Therefore, the actuator needs to be light and compact. It must be able to excite the structural modes that couple well to the performance metric of the control problem [Fuller, 1991]. The actuator must also be able to provide the required gain without saturation [Crawley, 1999]. Some conceivable choices include electromechanical shakers that can be instrumented inside the testbed and active materials that can be attached on the structure to strain it directly.

An electro-mechanical shaker can apply force to a specific point. Although a shaker provides the advantage of simulating an almost ideal point force actuator, it is massive. In addition, it is relatively difficult to install on a structure. Using a large number of shakers

on the testbed could be somewhat infeasible. The selected actuator should be thin, lightweight and easy to install in large numbers.

Designing a novel lightweight active mechanism to strain the testbed is also a possibility. However, such a mechanism would have to be placed inside the testbed, possibly by fixing it between the frame members. Placing a large number of these mechanisms inside the testbed would be difficult and time consuming. Further, producing such a design in large numbers would also be time consuming and costly.

The utilization of piezoelectric materials as actuators for structural control has received significant attention in recent years, primarily due to their light weight and simplicity. A piezoelectric material deforms upon application of a voltage which allows it to be used as an actuator.

There are two commonly used types of piezoelectric materials: ceramics such as PZT (Lead-Zirconate-Titanate) and polymers such as PVDF (Polyvinylidene-Fluoride). PVDF has been used as actuators to study active vibration control of cantilever beams [Bailey, 1985]. PZT is about twenty times stiffer than PVDF. An actuator requires a large stiffness for effective mechanical coupling to the structure. The dielectric constant which relates the free strain of a piezoelectric element to the applied voltage is an order of magnitude greater for PZT than PVDF. These two properties imply that PZT is a more appropriate actuator than PVDF [Brennan, 1995]. Researchers evaluated the effectiveness of piezoceramic actuators in exciting steady-state resonant vibrations in cantilevered beams and achieved promising results [Crawley, 1987]. Others studied the active suppression of aircraft panel vibrations in the 100 - 500 Hz frequency range using piezoceramic strain actuators and obtained up to 55% reduction in vibrational energy [D'Cruz, 1998].

Difficulties in using piezoelectric actuators do exist. The deformation of a rectangular piezoelectric actuator can be modeled as a combination of in-plane stretching and a couple

at each edge of the rectangle. Hence, it is difficult to assess fully the effects of a piezoelectric actuator on a structure without having an accurate three-dimensional model. In spite of this difficulty, using piezoelectric actuators in structural control experiments has been quite common in recent years.

PZT is commonly used in structural control experiments. It is relatively light, thin and commercially available in different shapes and sizes. Another advantage that PZT provides is high endurance to temperature. This feature of the PZT allows it to be used in smart composites with embedded distributed actuators. One purpose for making these composites is to attach them on the fuselage to control structural vibration. As another alternative, the fuselage can be made of these smart composites. PZT is available in different types (such as PZT 5-A, and PZT 5-H) depending on the strain output produced by a given amount of voltage. PZT 5-A was chosen as the actuator for being able to provide relatively large amount of deformation for a given amount of voltage.

2.2.2 Sensor Selection

A typical helicopter fuselage tends to exhibit complicated dynamics such as high modal density, i.e., closely spaced natural frequencies, sensitivity to environmental parameters and other uncertainties. These structural properties introduce serious modeling difficulties and stability problems. Hence, it is desirable to use a control system that guarantees stability and does not require an accurate model such as a *positive real* control system. A system $G(s)$ is said to be positive real if $Re[G(s)] \geq 0$ for all $Re[s] \geq 0$. This implies that for $s = j\omega$, phase of $G(s)$ is between -90 deg and +90 deg. Thus, $G(s)$ is guaranteed to have a 90 deg of phase margin which implies guaranteed stability.

A common structural control technique is to use collocated and dual sensor/actuator pairs. In a collocated pair, sensing and actuation occur at the same point or area on the controlled structure. A dual pair actuates with a generalized force and senses a generalized

velocity. Thus, the product of the variables of a dual pair is power [Crawley, 1991]. In a collocated and dual pair, a transfer function taken from the actuator to the sensor would show alternating pairs of poles and zeros, resulting in a phase that is bounded by -90 deg and $+90$ deg. Further, a collocated and dual sensor/actuator pair provides a positive real system which is guaranteed to be stable. In this light, the sensor selection was centered around forming a collocated and dual pair with the PZT actuator.

Since the ultimate goal of the control experiment is to reduce the noise inside the fuselage testbed, the internal acoustic pressure is the primary performance metric. Hence, a pressure sensor, such as a microphone may appear as an attractive choice. However, a pressure sensor does not behave in a collocated manner with the PZT. A PZT patch induces local strain in the panel, while a microphone measures acoustic pressure: a quantity that is local to the air inside the testbed. Hence, using a PZT patch and a microphone would result in a great deal of dynamics between the actuator and the sensor. This implies that a transfer function taken from a PZT patch to a microphone would result in a large amount of phase lag which introduces difficulties in closing a feedback loop without having stability problems.

Accelerometers are also commonly used sensors in structural control experiments. They are commercially abundant, simple to attach on a structure like the fuselage testbed and are relatively easy to use. If placed in the vicinity of a PZT, an accelerometer may behave in a collocated manner up to a certain frequency. But an accelerometer can not be truly collocated with the PZT since it only senses translational motion of a point while a PZT patch provides strain in the plane that it actuates. Figure 2.2 shows a frequency response function that was taken by exciting a PZT bonded to a fuselage panel, with broadband random noise, and measuring the output of an accelerometer that is located on the center of the PZT.

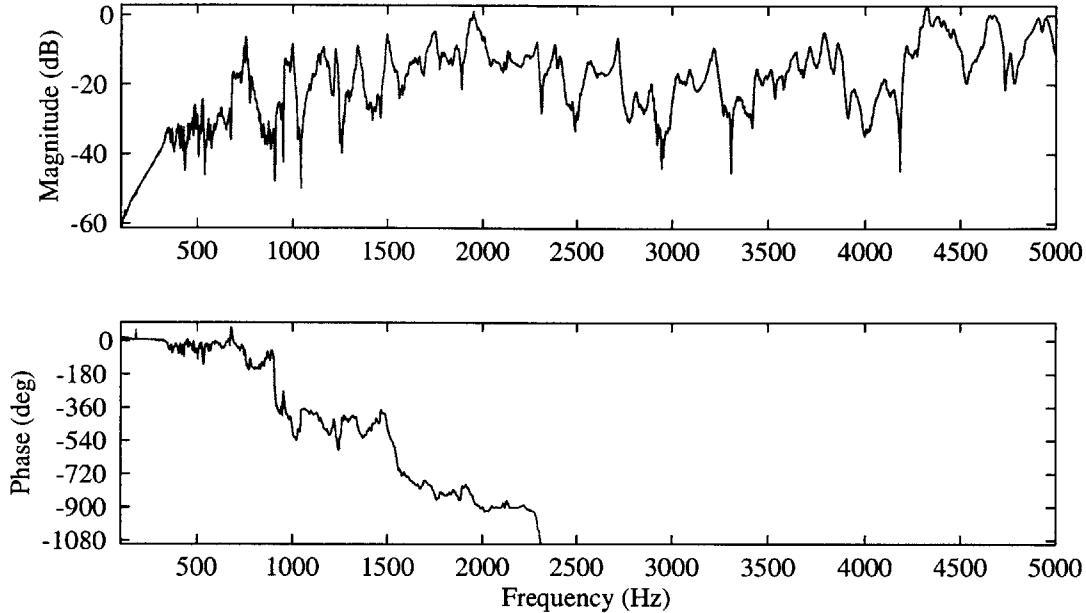


Figure 2.2: PZT to accelerometer transfer function.

Figure 2.2 shows that the accelerometer behaves in a collocated manner with the PZT for frequencies below 900 Hz. However, above 900 Hz, there is a significant amount of phase lag which could introduce stability problems in a feedback control loop. In addition, obtaining a large number of sufficiently sensitive, and small accelerometers may be quite costly. Another drawback is that an accelerometer is a relatively complicated electro-mechanical system. Using a large number of such devices in real aircraft could be unreliable.

Piezoelectric materials can also be used as sensors for structural control. PVDF is a piezo-polymer that is commonly used as a strain sensor. It is economical, light, simple to use and easy to manufacture in various shapes. Furthermore, it is a good candidate to form a collocated pair with the PZT.

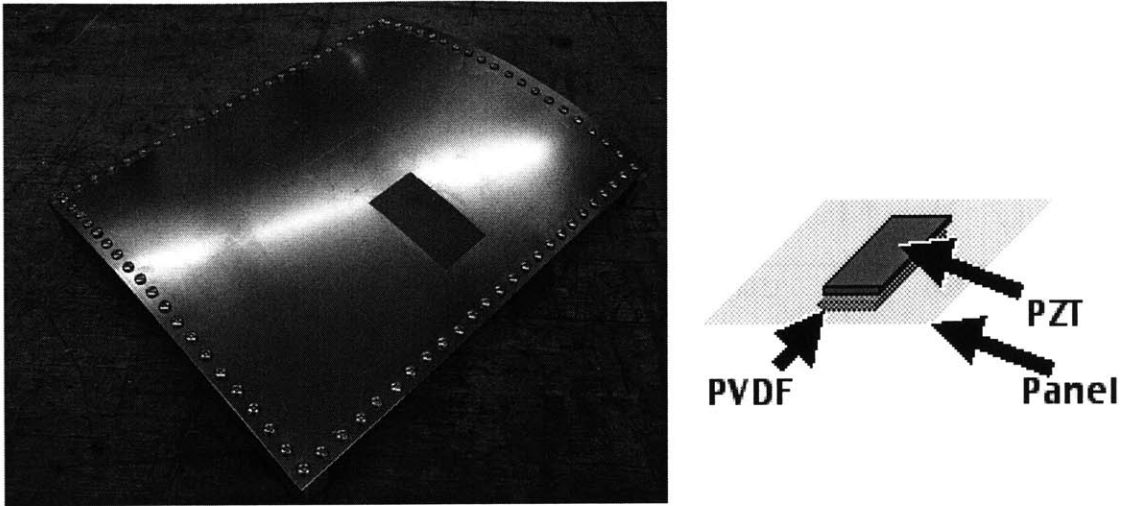


Figure 2.3: The curved panel and the schematic of the collocated PVDF-PZT pair.

Unlike the simple attachment of the accelerometer, bonding PVDF to a metal structure requires a strong glue such as epoxy. Removing an epoxy bond is difficult and has a tendency to damage the testbed. Hence, in order to try various bonding methods without damaging the testbed, an aluminum panel was made. The panel, as shown in Figure 2.3 has the same size, thickness, and curvature as of a testbed panel. It also has similar boundary conditions. A collocated sensor/actuator pair was made by bonding a PZT and a PVDF patch on the opposite sides of the panel as shown in Figure 2.3.

Preliminary transfer functions were taken on this panel to assess the collocated behavior of the PVDF-PZT pair. Collocated behavior only depends on the sensor and the actuator but not on the structure [Crawley, 1999]. Hence, a sensor/actuator pair that shows collocated behavior on the panel is expected to show the same behavior on the testbed.

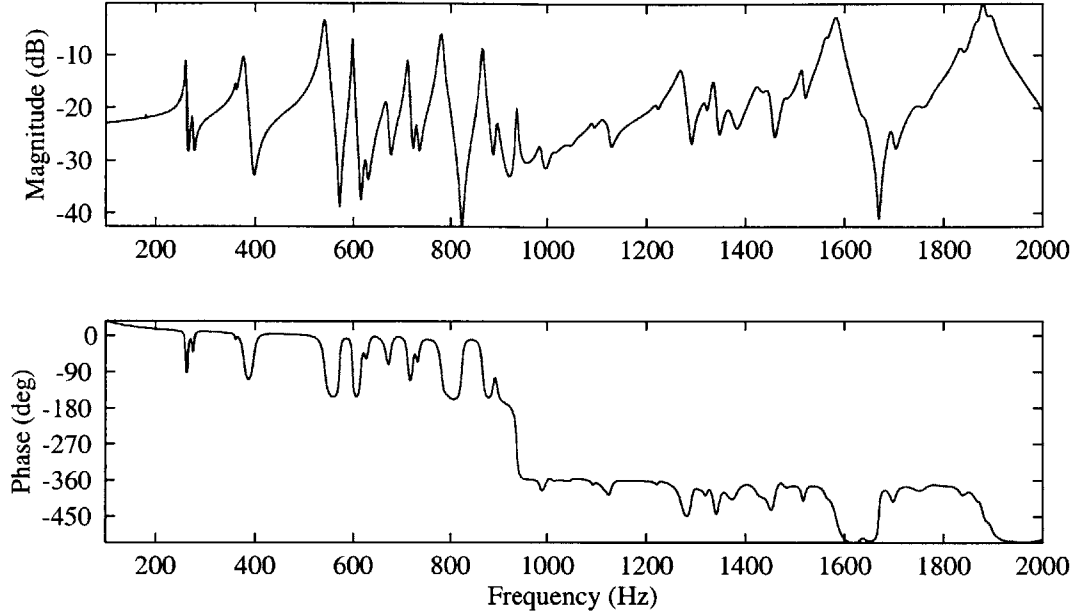


Figure 2.4: PZT to PVDF transfer function on the curved panel.

Figure 2.4 shows a PZT to PVDF transfer function obtained by exciting the PZT with a broadband random signal and measuring the voltage output of the PVDF. The sensor/actuator pair shows collocated behavior below 950 Hz. Deviation from collocated behavior occurs at this frequency and phase lag starts to become significant. Surprisingly, the frequency range of collocated behavior for the designed PVDF-PZT pair is not greater than that of the accelerometer-PZT pair.

The main reason for the PVDF-PZT pair to lose collocation is the combined in-plane and bending actuation of the PZT. This causes the excitation of two types of modes: ones that are dominated by bending of the panel and ones that are dominated by the stretching in the panel. Hence, the local motion observed by the PVDF is a combination of these two kinds of modes. Having the PVDF and the PZT on the opposite sides of the panel results in a difference in the signs of the residues of the two modes.

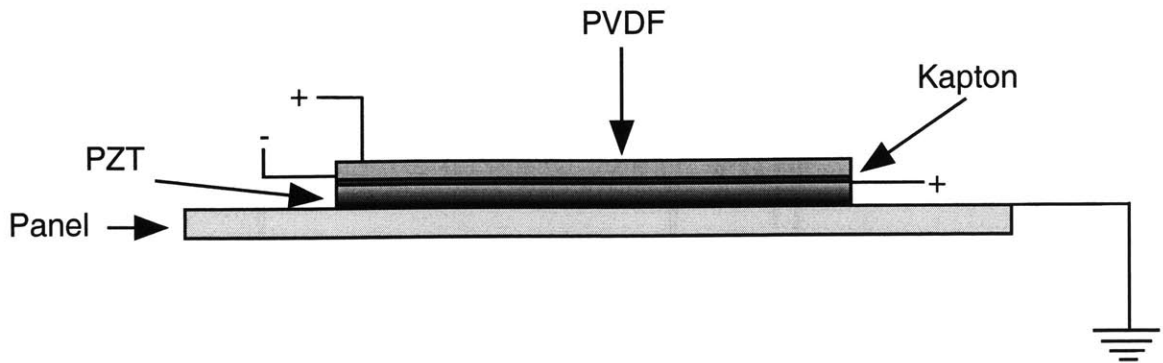


Figure 2.5: PZT-Copper kapton-PVDF patch.

As a result, a zero that occurs at a frequency between the two modal frequencies is “missed” by the sensor [Crawley, 1999]. A missing zero causes an immediate loss of phase at that frequency. In the case of this panel, a numerical study has shown that the first stretching mode occurs at 970 Hz. Hence, the zero that is supposed to occur near 950 Hz is missed. On the other hand, if the PVDF were on the same side as the PZT, bending and in-plane modal residues would have the same sign and a missing zero would not occur. For this reason, an alternative approach was taken by placing the PVDF and the PZT on the same side of the panel. Figure 2.5 shows this new arrangement.

A thin layer of kapton separates the PZT and the PVDF. The bottom side of the kapton is coated with copper to serve as the electrode for the hot (top) side of the PZT. In this particular arrangement, the bottom side of the PZT is hard-wired to the panel. The panel is then grounded to serve as the ground for the PZT. Top side of the kapton is non-conductive. Hence, the silver coating on both sides of the PVDF sheet is used as electrodes.

To test this sensor/actuator arrangement, the PZT was excited with broadband random noise to obtain an actuator to sensor transfer function.

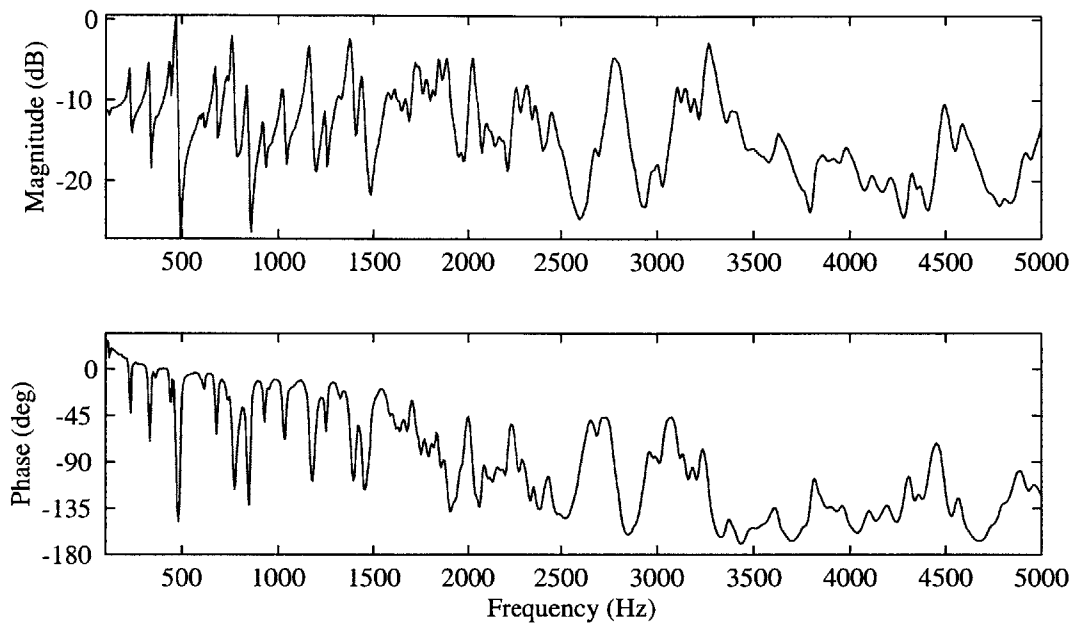


Figure 2.6: PZT to PVDF transfer function of the PZT-Copper kapton-PVDF patch.

Figure 2.6 shows that placing the PVDF on the same side as the PZT recovers the zero near 950 Hz and dramatically improves the frequency range of collocated behavior.

In summary, the sensor selection was based on forming a collocated pair with the PZT. Two different sensors were tested for the frequency range of collocated behavior: the accelerometer and the PVDF. Between the two sensors, PVDF showed the larger frequency range with collocated behavior. Primarily for this reason, it was selected as the control sensor.

The PZT-Kapton-PVDF patch was then bonded on the testbed to verify the frequency range of collocated behavior.

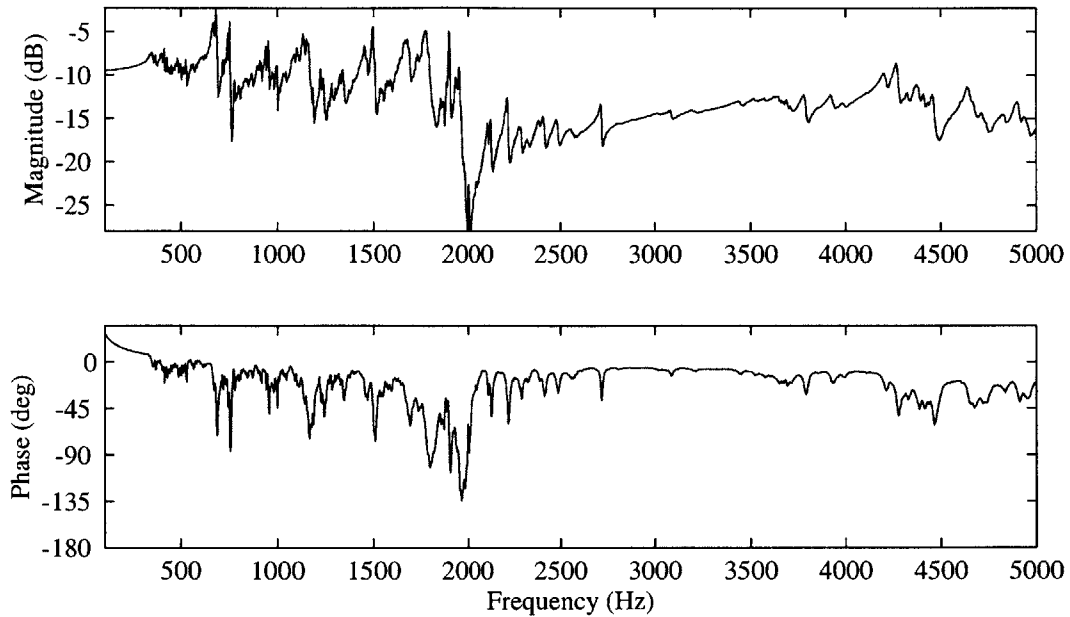


Figure 2.7: PZT-PVDF transfer function of the fuselage testbed.

Figure 2.7 shows a PZT to PVDF transfer function of the fuselage testbed. As expected, the sensor/actuator pair shows collocated behavior over a wide frequency range. The collocated behavior is preserved until 20 kHz which is the highest frequency that experimental equipment could record. The transfer function is plotted until 5000 Hz to better illustrate the high modal density below 2000 Hz. The following section presents the placement method of the chosen sensor/actuator pair.

2.2.3 Sensor and Actuator Placement

A common approach for maximizing the performance of a control experiment is to place the sensors and actuators at the antinodes of each mode in the control bandwidth. However, as Figures 2.2 and 2.7 illustrate, the number of modes that are in the frequency range of interest (0-2000 Hz) is fairly large. In addition, each mode of the structure is likely to have many antinodes. Thus, finding the shape of each mode and locating sensor/actuator pairs at its antinodes is not feasible.

There are numerical methods to assess observability and controllability with a limited number of sensors and actuators. If an accurate state-space model of the system is available, one can calculate the controllability and observability gramians [Crawley, 1999] to quantitatively determine the observability and controllability of each mode.

O'Sullivan developed a state-space model of a cross section of the testbed to evaluate sensors and actuators as well as to study certain control algorithms [O'Sullivan, 1998]. The model was made two-dimensional in order to render the problem computationally feasible. An accurate three-dimensional model would require hundreds of thousands of degrees-of-freedom. With the computational limitations at hand, such a model would not be practical, especially for simulating closed-loop control algorithms.

The two-dimensional model is helpful in predicting the effectiveness of sensors and actuators and assessing the approximate performance of certain structural control algorithms. However, it can not be used to compute the observability and controllability gramians for a given placement of the sensors and actuators on the testbed, as the testbed is a three-dimensional structure.

Although the two-dimensional state-space model was not used with any numerical method, the results of the closed-loop control simulations provided valuable information to predict the appropriate size and location of the sensors and actuators.

The numerical analysis of the two-dimensional model revealed that the sensors and actuators should be placed symmetrically around the center of each panel, covering approximately half of the panel size. A schematic of the proposed placement is given in Figure 2.8. The central patch is necessary to achieve authority over low frequency modes, whereas the patches in the corners provide observability/controllability over high frequency modes. The placement of piezo patches in the corners also provides some advantage in controlling the vibration of ribs and stringers.

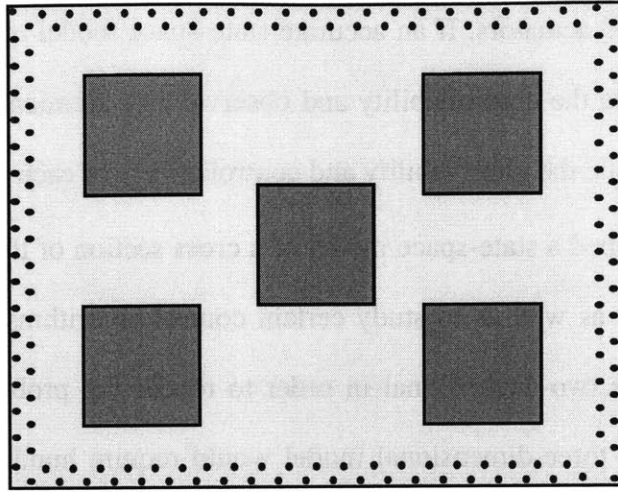


Figure 2.8: Single panel sensor/actuator placement.

The numerical analysis of the two-dimensional model showed that although the internal acoustic behavior strongly depends on the panel vibration, the motion of ribs and stringers also contributes to a certain extent. This implies that the motion of these frame members should also be controlled. Ideally, the most suitable actuator for the ribs and stringers would be a shaker. However, as was discussed earlier, instrumenting the testbed with a large number of electro-mechanical shakers would be extremely time consuming and costly. Furthermore, such an instrumentation would add a significant amount of mass which could change the dynamics of the structure. Frame members are much stiffer than panels. Hence, whether piezoceramics can provide significant authority over the frames is somewhat unclear. However, some level of actuation authority over the frames may be achieved by placing piezoelectric sensor/actuator pairs close to the corners of the panel.

In order to investigate the possibility of closing stable feedback loops on the testbed, one panel of the structure was instrumented with five collocated sensor/actuator pairs. Figure 2.9 shows the five sensor/actuator pairs bonded on the testbed, based on the proposed placement method.

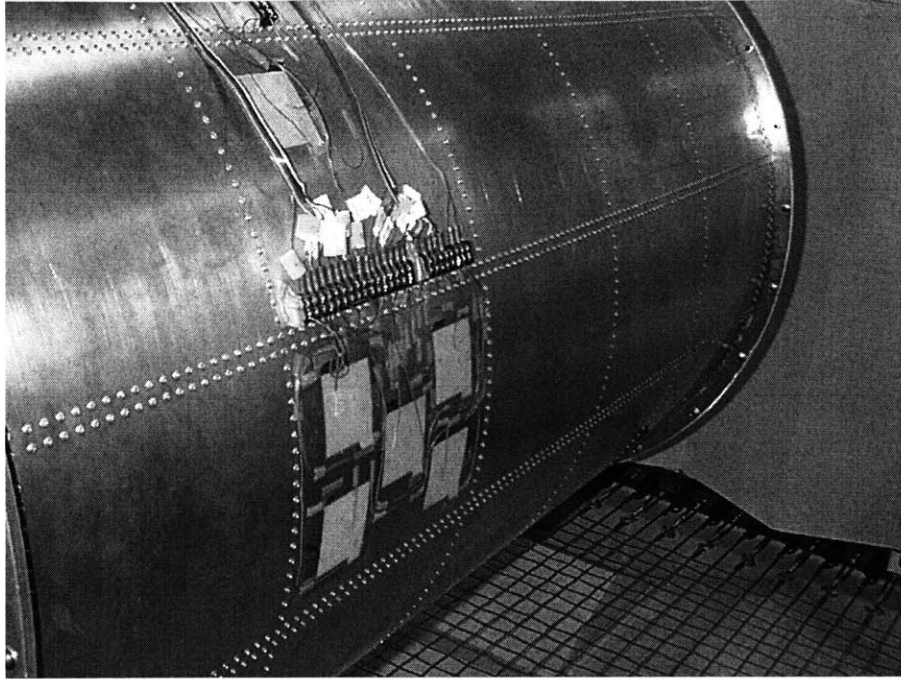


Figure 2.9: 5 PZT-Copper kapton-PVDF patches on a testbed panel.

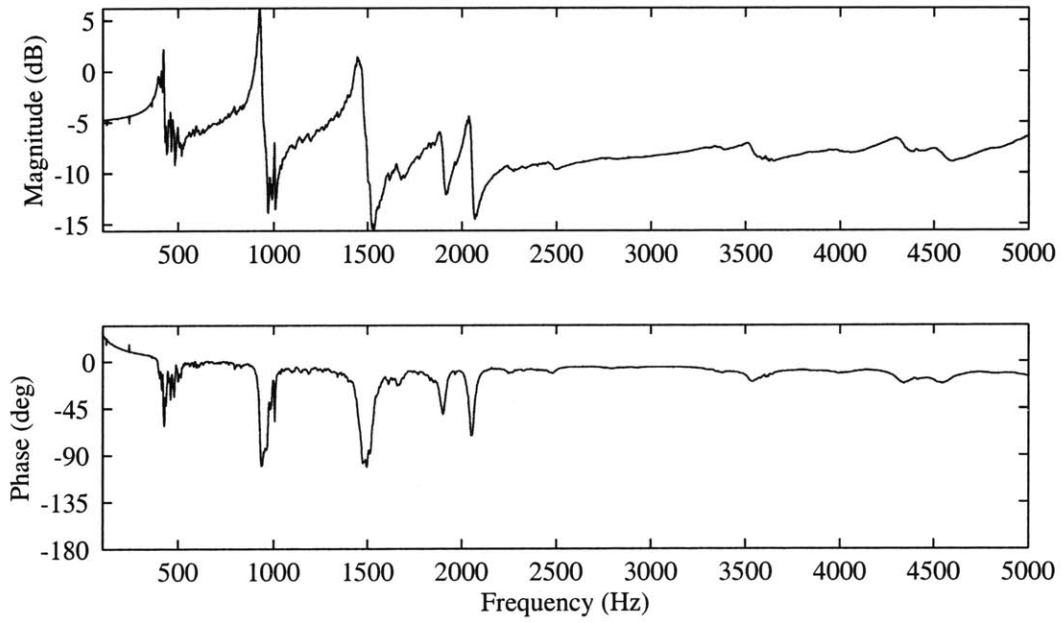


Figure 2.10: PZT to PVDF transfer function for the central patch of the panel.

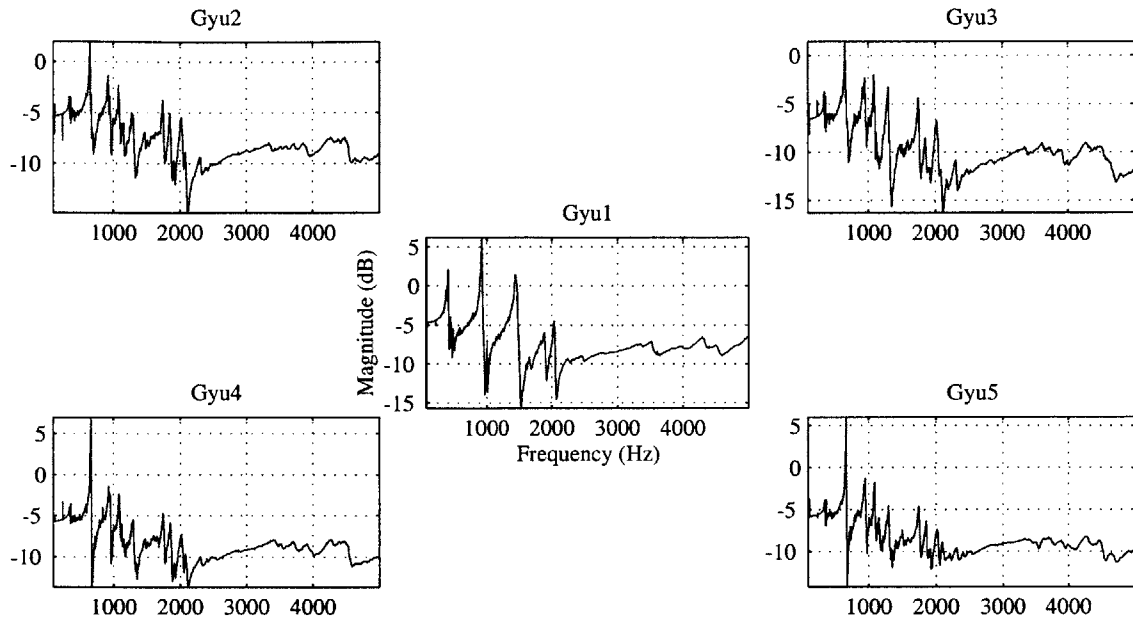


Figure 2.11: PZT to PVDF transfer functions from 5 patches.

PZT to PVDF transfer functions were taken for each of the five sensor/actuator pairs to verify their functionality and collocated behavior. These transfer functions are shown in Figures 2.10 and 2.11. Figure 2.10 shows the typical pattern of a collocated transfer function with alternating poles and zeros. Because the phase is bounded by 0 deg and -180 deg as opposed to -90 deg and +90 deg, the system is not positive real. This is because the sensor/actuator pair is not dual, i.e. the sensor measures a generalized displacement (strain) as opposed to a generalized velocity (*strain rate*). However, a positive real system may still be achieved by designing an appropriate controller. For example, the phase of the transfer function may be shifted up by +90 deg by differentiating the signal that is measured by the sensor. This issue will be discussed in further detail in Chapter 4 (control system design). Figure 2.11 shows the magnitude of transfer functions taken from all five sensor/actuator pairs. The subplots were arranged in a way similar to sensor/actuator placement scheme as

a visual aid. The phase plots of these transfer functions are not given in this figure to prevent redundancy.

Controlling the local vibration of a single panel of the testbed is unlikely to have a significant effect on the interior noise level or the vibration of a large portion of the structure. Thus, the main purpose of this instrumentation was not to achieve closed-loop performance but to assess the stability and feasibility of multiple separate classical feedback loops. Hence, details of this intermediate control experiment are not going to be presented here. Five independent simple control loops were stably implemented using a PC. As a result, the structural acceleration in the panel was reduced by as much as 10 dB at certain resonant peaks over the frequency range of 100 - 2000 Hz.

The results of the intermediate control experiment indicated that a larger number of testbed panels be instrumented with sensors and actuators. Further, a larger number of sensors and actuators are necessary to reduce the structural vibration over a significant portion of the structure. However, the performed instrumentation was lengthy and complicated. Further, as shown in Figure 2.9, there was a great deal of wiring. The wires were individually connected to a terminal block for strain relief and then transferred to the computer. The dangling wires on the panel were secured with plastic tapes. Repeating this procedure on a larger number of panels could be excessively time consuming. As an immediate result, the study aimed towards developing an improved and more robust method of instrumentation. An active ply with encapsulated sensors, actuators, and wiring was developed.

2.3 The Active Ply

The main goal for developing the active ply was to minimize the instrumentation time that is spent on the testbed. The testbed is a relatively massive structure and is not easy to move around. Neither is it convenient to work on.

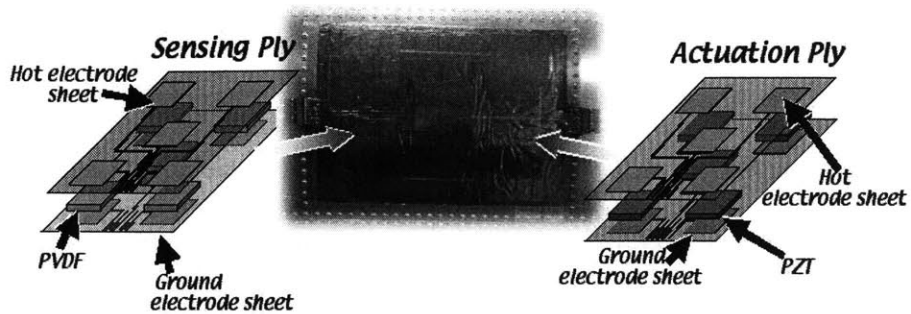


Figure 2.12: An exploded view of the active ply.

Instrumenting every component of the sensors and actuators on the fuselage individually leads to numerous bonding steps and consumes a great deal of time. Instead, forming a ply that contains the sensors, the actuators and the wiring in it, reduces the number of instrumentation steps dramatically.

Figure 2.12 shows an exploded view of the active ply with encapsulated collocated PVDF-PZT pairs. The active ply has two sub-sections: the sensing ply and the actuation ply. The actuation ply has 5 PZT patches sandwiched between two layers of copper-kapton. Each kapton layer was etched to form an appropriate electrode and wiring pattern. The sensing ply was prepared in the same manner, only the sandwiched material was the PVDF. It was then glued on top of the actuation ply to form a single active ply. Fripp et al reported on the use of similar active plies for modal isolation techniques [Fripp, 1999].

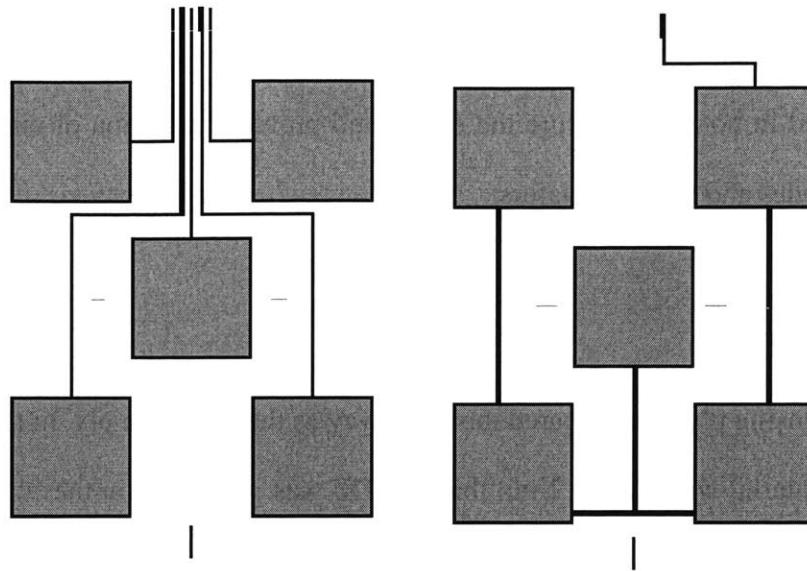


Figure 2.13: Hot (on the left) and ground (on the right) electrode patterns.

2.3.1 Manufacturing and Bonding the Active Ply

Actuation Ply

The first step of the manufacturing procedure was to form the electrode pattern for the actuators. This was accomplished by etching a sheet of copper-kapton to form the appropriate pattern. The actuation ply has two different electrode patterns: the ground electrode pattern and the hot electrode pattern. These patterns are shown in Figure 2.13.

The ground electrode pattern has five squares, each one corresponding to a PZT wafer. These squares are simply shorted to enable using a single ground source. The hot electrode pattern enables application of separate signals to each PZT patch. Each electrode pattern was printed on the copper coated side of a kapton layer, using a laser printer. Then, the printed section of the pattern was painted with a magic marker to form an etch mask. After that, the unpainted copper was etched using the Kepro Ferric-Chloride. Finally, the

mask paint was washed away with acetone. Five square PZT wafers (63.5mm x 63.5mm) were sandwiched between the ground and hot electrodes with epoxy. The sandwich was then placed in hot press to cure the epoxy and prevent formation of air bubbles between the electrodes and the PZT wafers.

Sensing Ply

The sensing ply was prepared the same way as the actuation ply. In this case, the sandwiched material was PVDF. 2 mil thick PVDF was purchased in the form of 8.5x11 inch sheets. Each sheet had silver electrode coating on both sides. This coating was removed with acetone, and five squares, each being the same size as a PZT patch, were cut out of the sheet. These squares were then sandwiched between the hot and the ground electrodes with epoxy. The ply was then cured in the hot press.

As the final step of the manufacturing procedure, sensing ply was bonded on the actuation ply with epoxy. This was done carefully to ensure that the PVDF patches of the sensing ply were collocated with the PZT patches of the actuation ply. An additional sheet of copper-kapton was placed between the sensing and the actuation plies. Grounding this sheet during the control experiment serves as a shield against capacitive coupling between the two plies.

Figure 2.14 shows the picture a completed active ply. The plastic connectors were crimped onto the copper wiring at both ends of the active ply. Six active plies were manufactured and bonded on the fuselage testbed for the active control experiment.

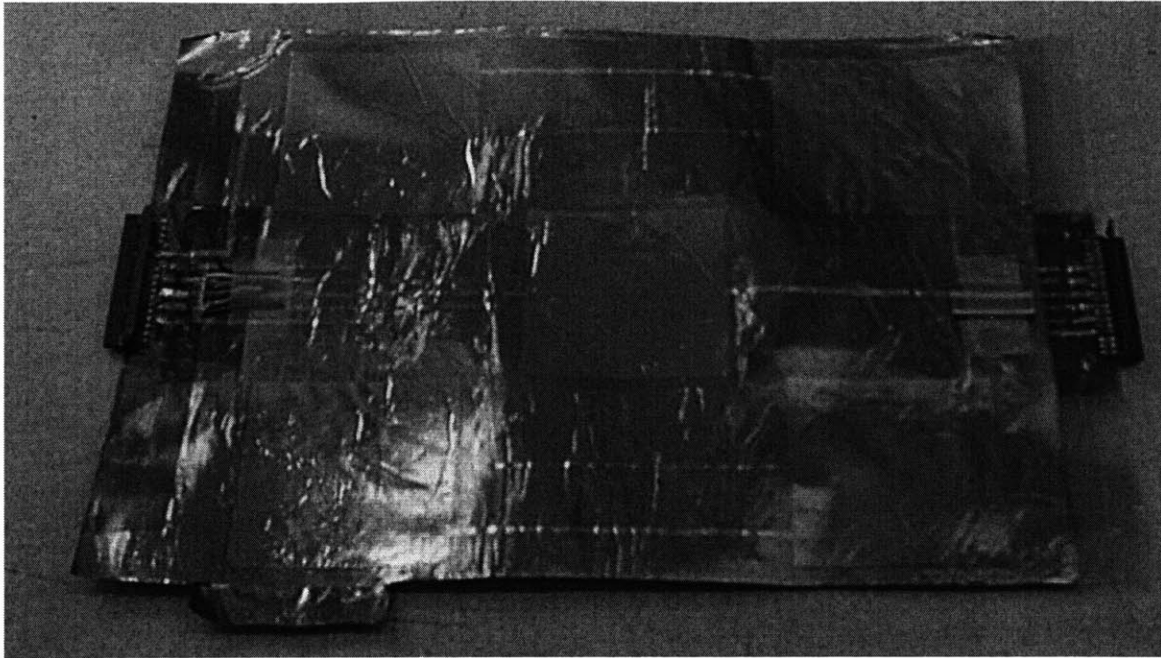


Figure 2.14: A finalized active ply.

The active plies were bonded on the testbed using a thermoplastic adhesive to mandate removing them easily, in case they needed to be replaced. The selected model for the current application was the 2.5 mil thick 3-M Thermobond 557EG which is the thinnest thermoplastic adhesive available. The Thermobond is available in the form of 8.5x11 inch polymer sheets. The sheet melts when heated; then, with the application of pressure, it forms a bond between the active ply and the structure. It is possible to break the bond and remove an active ply by simply reheating the adhesive. This is much easier than breaking bonds that are formed with strong liquid adhesives such as epoxy.

A thermoplastic polymer sheet was placed between each active ply and the fuselage testbed. Heat was applied by placing a Watlow flexible heater to the opposite side of the panel (inside the testbed). The required pressure was applied by means of a typical vacuum bagging procedure: the vacuum bag was taped to the structure, sealing off the active ply. Air was sucked out of the interior of the bag by means of a vacuum pump.

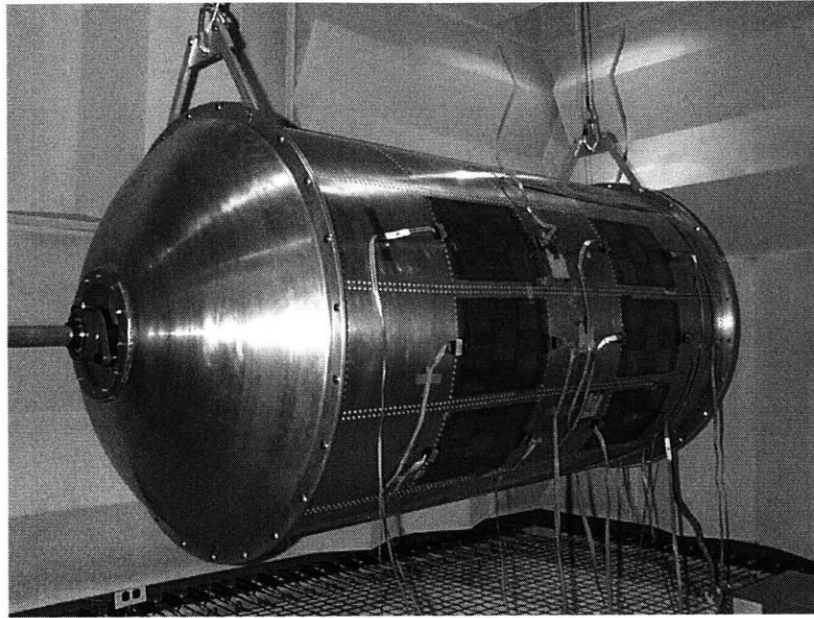


Figure 2.15: Testbed with six active plies.

Figure 2.15 shows the testbed after the bonding procedure has been completed. Ribbon cables were used to connect the sensor/actuator pairs in the active plies to the controllers. Two ribbon cables were connected to each active ply: one cable for sensors, one for actuators. Each ribbon cable contains ten lines: five hot lines and five ground lines. Hot lines, i.e., the lines that carry the sensor or actuator signals, and the ground lines were alternated to prevent cross-talk between the hot signals.

2.4 Finalized setup

The instrumentation of the testbed was completed by attaching the performance sensors that measure structural acceleration. An accelerometer was attached on the inside of each fuselage panel that was instrumented with an active ply. The microphone array had been instrumented during the development of the testbed itself.

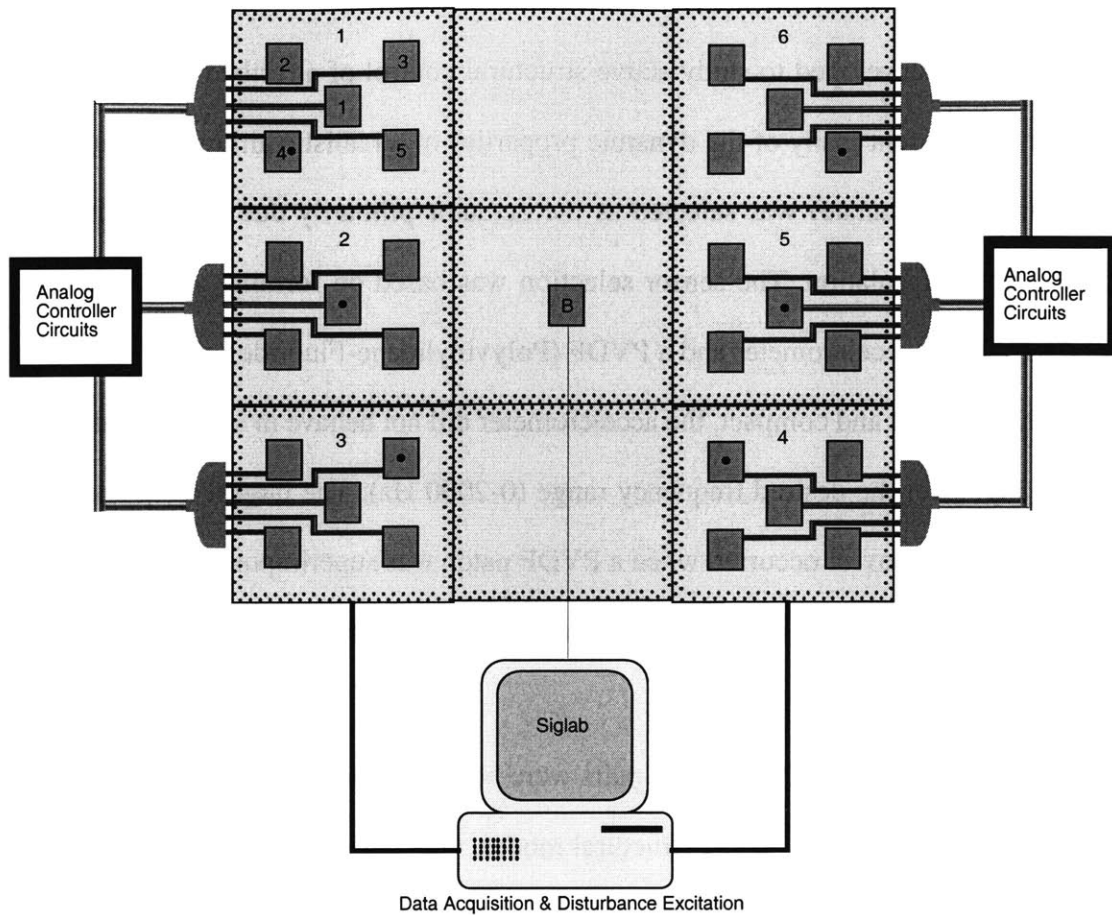


Figure 2.16: Schematic of the instrumented area of the testbed.

Figure 2.16 shows a schematic of the instrumented area of the testbed with the PVDF, PZT and accelerometer locations. The dark gray squares indicate the PVDF-PZT pairs, while black dots represent the accelerometer locations. The PZT patch bonded to the middle panel (labeled “B”) is the disturbance source. Figure 2.16 also illustrates the numbering scheme of the panels, sensor/actuator pairs and accelerometers. For example, Panel 2, Location 1 corresponds to the central patch of the middle panel in the left-most column of Figure 2.15. The disturbance signal was generated using a PC with a Siglab interface. Outputs of the performance sensors were measured with the same interface.

The following chapter discusses the design and the implementation of the controllers.

2.5 Summary

A setup was developed to study active structural control of a testbed which had been designed to represent many of the dynamic properties of a realistic aircraft fuselage. PZT (Lead-Zirconate-Titanate) was selected as the actuator primarily due to its light weight and ease of encapsulation. The sensor selection was based on forming a collocated pair with the PZT. An accelerometer and a PVDF (Polyvinylidene-Fluoride) patch were tested. Though lightweight and compact, the accelerometer did not behave in a collocated manner with the PZT over the desired frequency range (0-2000 Hz). The largest frequency range with collocated behavior occurred when a PVDF patch was superimposed on a PZT patch. Further, PVDF is light and simple to use. Hence, it was chosen as the sensor for this control study.

Five square collocated PVDF-PZT pairs were bonded on a testbed panel and tested for observability/controllability of the structural modes. One pair was bonded to the center of the panel and the others were bonded to the four corners. After verifying that the chosen sensor/actuator pairs and the placement method provided acceptable observability/controllability of many structural modes, an active ply was developed. The active ply contains the sensor/actuator pairs in an encapsulated package. Six active plies were manufactured and bonded on six panels of the testbed. Two kinds of performance sensors were used: accelerometers and microphones. Six accelerometers were attached on the structure: one behind each panel that has an active ply. A number of microphones had been instrumented in the interior of the testbed in an earlier study and were used as the acoustic performance sensors for this study. The microphone array is located on the boom that runs across the testbed.

Chapter 3

Control System Design

This chapter presents the design of a controller for the testbed instrumented with collocated piezoelectric sensors and actuators, described in Chapter 2. The chapter starts with a brief overview of common control architectures. Low authority control, which is generally used to control localized modes is discussed. Further, a detailed description of common local control methods is presented. General benefits and disadvantages of these methods are evaluated by analyzing an arbitrary reduced order plant that exhibits resonant dynamics. Since an accurate model of the testbed does not exist, system identification techniques were used to assess the dynamics of the testbed and to design the control law. The results of system identification are presented with actuator to sensor and disturbance to performance transfer functions. Finally, the design of control law is presented in detail.

3.1 An Overview of Structural Control Architectures

In complicated structures, it is difficult to observe the exact system behavior and actuate the system in real time with a single central controller. For this reason, it is common to separate the system into smaller components that can be coped with individually [Siljak, 1991]. Generally, the control architecture is divided into levels with various degrees of authority on the structure.

A well-known approach to structural control is the use of a combination of high authority and low authority control (HAC/LAC). Generally, high authority control concentrates on the global or low frequency modes that can be accurately modeled. Low authority

control is generally used for local or high frequency modes of the system, which tend to be difficult to model. A HAC controller usually operates on a multi-input multi-output (MIMO) basis, while LAC controllers can operate with separate local control loops, independent from the HAC controller. In other words, HAC and LAC controllers can use separate sensors and actuators [O'Sullivan, 1998]. Though this provides flexibility in implementing HAC and LAC controllers separately, in a complicated structure like an aircraft fuselage, control spillover problems may occur.

Hall et al. developed a hierarchic control scheme, which is a more sophisticated version of combined HAC/LAC control [Hall, 1991]. Their scheme offers the possibility of avoiding spillover by allowing HAC and LAC controllers to share information. Hence, HAC and LAC controllers are required to have some sensors and actuators in common. One disadvantage of this control scheme is that it requires full state feedback which is not feasible for a realistic structure.

As discussed in Chapter 2, the two-dimensional model of the testbed showed that frame members also contributed to interior noise generation by coupling to low frequency modes of the system. This implies that frame motion, i.e., the motion of the ribs and stringers, also needs to be controlled to maximize performance. Also discussed in Chapter 2 was the fact that the motion of panels couples well to the high frequency modes. Based on these facts, an appropriate control method would be to implement LAC controllers on the panels and HAC controllers on the frames of the structure [O'Sullivan, 1998].

Significant work has been done in controlling low frequency modes of aircraft. Grewal et al. studied the narrowband control of global modes of a turboprop aircraft [Grewal, 1997]. They developed a high authority control method by placing piezoelectric actuators to match the deflection pattern of the aircraft at its blade passage frequency (approximately 61 Hz). A weighted average of a group of accelerometers was used as the sensed

quantity for three separate control loops. Second order classical compensators were designed sequentially, that is with previous loops closed before designing new ones. Closed-loop results showed interior noise attenuation as high as 14.8 dB, and fuselage vibration reduction as high as 20 dB at the blade passage frequency. Xu et al. performed multi-input multi-output (MIMO) feedforward control with a Filtered-x Least Mean Square (LMS) adaptive algorithm on the same fuselage [Xu, 1998]. They achieved reductions as high as 21.6 dB in the fuselage vibration and 25.8 dB in interior sound field at 61 Hz.

In the majority of the HAC work in literature, either the exact deflection pattern of the aircraft at a certain frequency is well known, or a finite element model of the structure is available. Since the global modes can be represented with the deflection pattern of a cross-section of the structure, a two-dimensional model may be formed with a relatively course mesh. It is then possible to use this model to design a high authority controller for global modes that have large wavelengths.

Finite element methods are typically used to model a structure and are sometimes capable of modeling the lowest frequency modes accurately. However, in the region of high modal density, any model is likely to be inaccurate. Models of structures with closely spaced modes tend to be extremely sensitive to parameter changes in predicting natural frequencies and especially mode shapes. Consequently, the actual structure may be significantly different from the model that is developed for control simulations [MacMartin, 1991]. Furthermore, modeling high frequency modes of a realistic structure in three dimensions requires a very fine mesh, which may push the limits of computational availability. These requirements make it infeasible to control high frequency modes with a model based controller. Not surprisingly, the amount of work done in broadband control of high frequency modes of aircraft structures is limited.

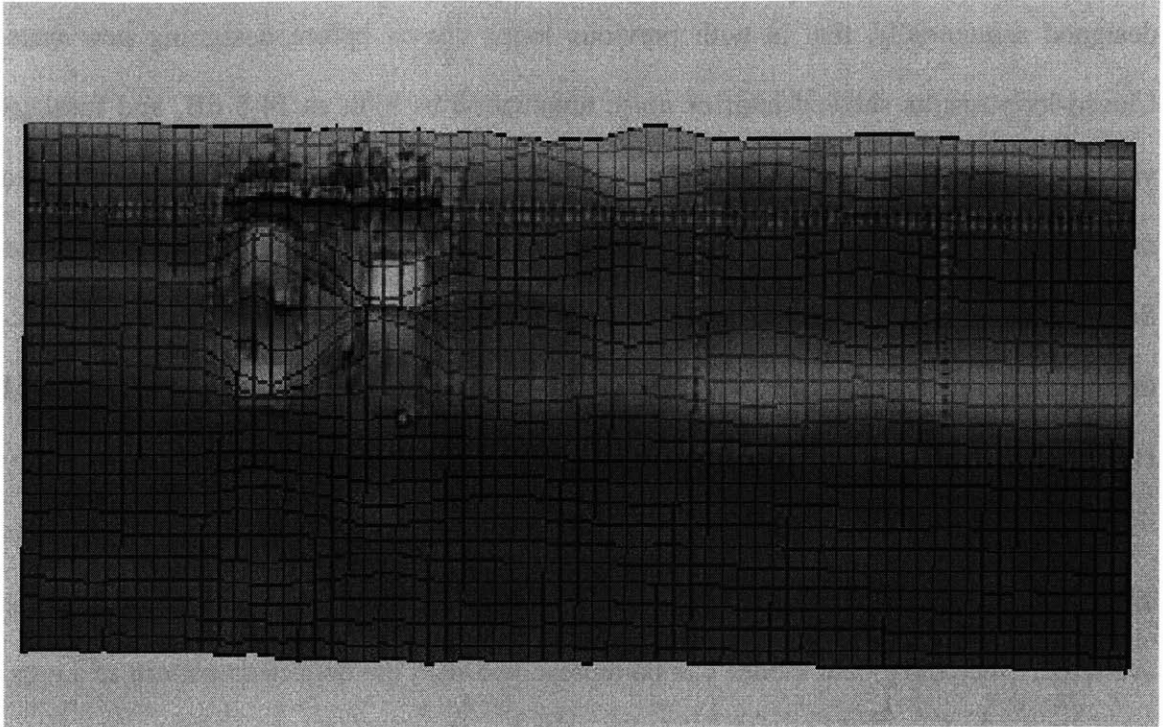


Figure 3.1: Mode shape of the testbed at 674 Hz.

Control design in this thesis focuses on low authority broadband control of localized shorter wavelength modes that are poorly modeled or are not modeled at all.

As discussed in Chapter 2, each panel is surrounded by stiff frame members that have significantly smaller deflections. Hence, frame members (ribs, stringers) constitute the local boundaries of each panel. Figure 3.1 illustrates a mode shape that was experimentally determined by exciting the PZT actuators at Location 1 and 2 (central and top left corner) by a random signal with a 2 kHz bandwidth. A Polytech laser vibrometer was used to measure the frequency response of the structure and to determine the mode shape related to each natural frequency. Figure 3.1 is a side view of the testbed, excluding the end caps. The greatest motion occurs at the excited panel, while less motion exists at the neighboring panels. This fact implies some level of coupling between the panels, that is, a disturbance induced on a specific panel causes the motion of other panels and results in

sound radiation from these panels. Hence, controlling a large number of panels is essential to reduce the effect of a structural disturbance on interior acoustics. The mode shape that is shown in Figure 3.1 is that of a localized 2-2 panel mode, i.e., the panel mode with four anti-nodes. This implies that the chosen sensor/actuator placement effectively excites localized modes and permits the frame members to be treated as local boundaries.

Implementing local or low authority controllers on the testbed does not interfere with a possible future study on high authority or combined HAC/LAC control, since it is possible for the HAC and LAC controllers to operate independently. In the case of a combined HAC/LAC control architecture, local control would provide robustness to the high authority global controller by damping out the high frequency modes and preventing the HAC controller from spilling over. The next section presents some commonly used local control techniques.

3.2 Local Control Methods

The objective of this study is to control interior acoustics by reducing the structural motion. Structural motion can be reduced by removing energy from the system. Adding damping to the system is one way to accomplish this goal. It is important to remember that structural control can only have an effect on the acoustic modes that couple well to the structural modes. However, as will be demonstrated in the next section, the modal density of the system is extremely high, that is the natural frequencies of the system are very closely spaced. Thus, it is difficult to determine which structural modes couple well with the acoustic modes of the system. Furthermore, preliminary transfer functions taken on the testbed showed that the dynamics of the system is sensitive to environmental parameters, such as temperature. For systems with such sensitivities, an appropriate controller would be the one that adds damping over a broad frequency range, in a robust manner.

One popular structural control algorithm is Linear Quadratic Gaussian (LQG) control [Crawley, 1999]. LQG is a Linear Quadratic Regulator (LQR) combined with a Kalman Filter. Solution of the LQR problem gives optimal feedback gains based on full state feedback from the system [Freidland, 1986]. The Kalman Filter is the optimal estimator for the system [Kalman, 1961]. The drawback to using LQG on a complex structure is that it requires an accurate model, which is not available for the testbed. Even in the case of simpler structures, LQG is generally used for well modeled low frequency modes. This implies that the model must be appropriately reduced to include the first few modes. Although LQG is guaranteed to be stable on a reduced model, there is a possibility that the modes that are truncated from the model can destabilize the system when the controller is implemented on the real structure.

A simpler control method that does not require an accurate model is Positive Position Feedback (PPF). PPF was first introduced as by Goh et al. as a means to damp the vibrations of large space structures [Goh, 1985]. Such structures have a high number of flexible modes within the bandwidth of the controller, some of which are not targeted for control. Presence of these modes within the control bandwidth results in the well-known phenomenon of *spillover* [Fanson, 1990]. Spillover is the coupling of the control system to the residual dynamics, which occurs because the sensors and actuators are not continuously spatially distributed. Spillover can destabilize the control system, especially at higher frequencies where the dynamics of the structure is poorly modeled [Schaechter, 1981]. PPF promises to prevent the spillover from destabilizing the system by causing the poles of the system to migrate towards the left half of the complex plane. PPF is a low-pass filter whose realization is simple and straightforward. It can be implemented as a pair of complex poles. The location of these complex poles may be adjusted in order to damp specific modes. One drawback to PPF is that it does not guarantee stability.

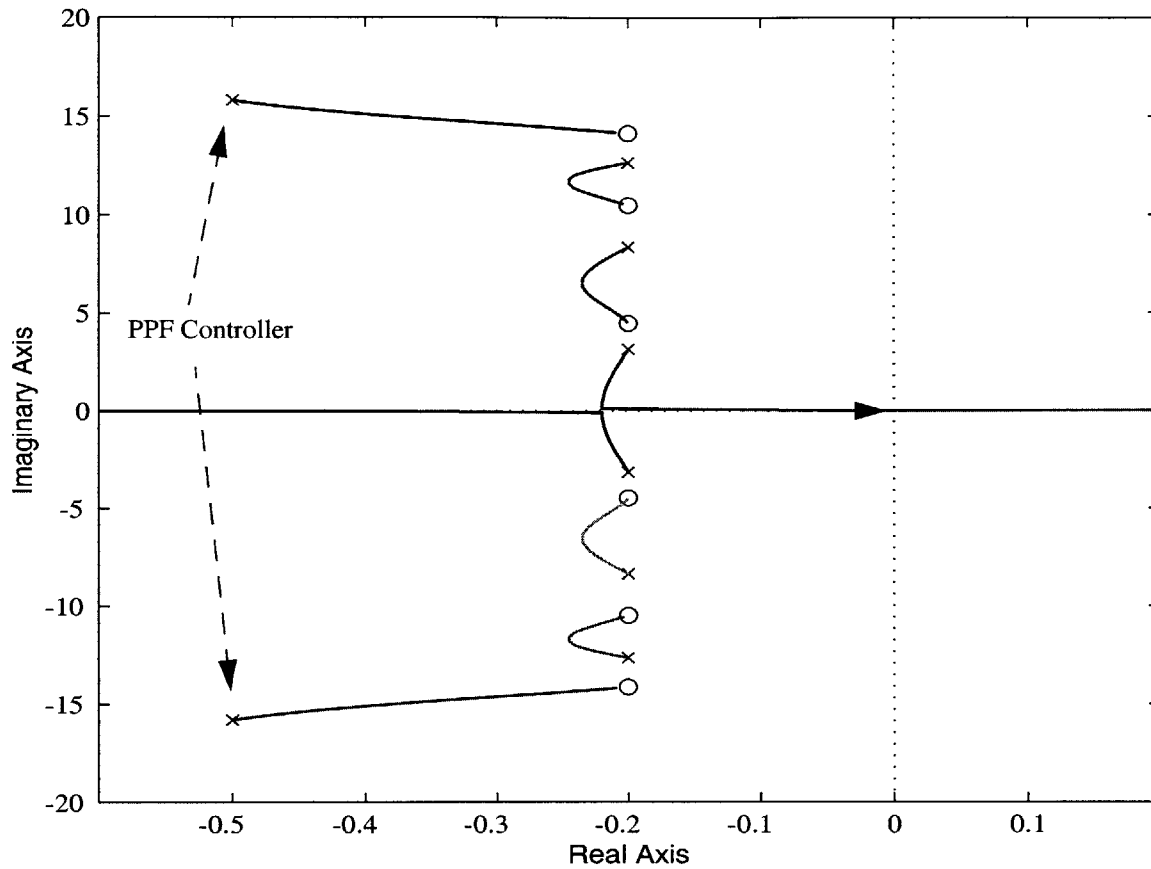


Figure 3.2: Root locus of an arbitrary 3 degree-of-freedom flexible plant with collocated sensors and actuators when controlled by PPF with a pair of complex poles.

Figure 3.2 illustrates the stability problem of PPF by showing the root locus of an arbitrary resonant plant with collocated sensors and actuators. The plant has three natural frequencies. The alternating pole-zero pattern shows the collocated nature of the system. The complex pole pair with high damping represents the PPF controller. The stiffer poles of the structure start migrating towards the zeros underneath them. Since these poles initially move towards the left half plane, they can be damped by choosing an appropriate gain. However, the remaining (low frequency) poles migrate towards the real axis. As the gain is increased, one of the poles moves to the right half plane and results in instability.

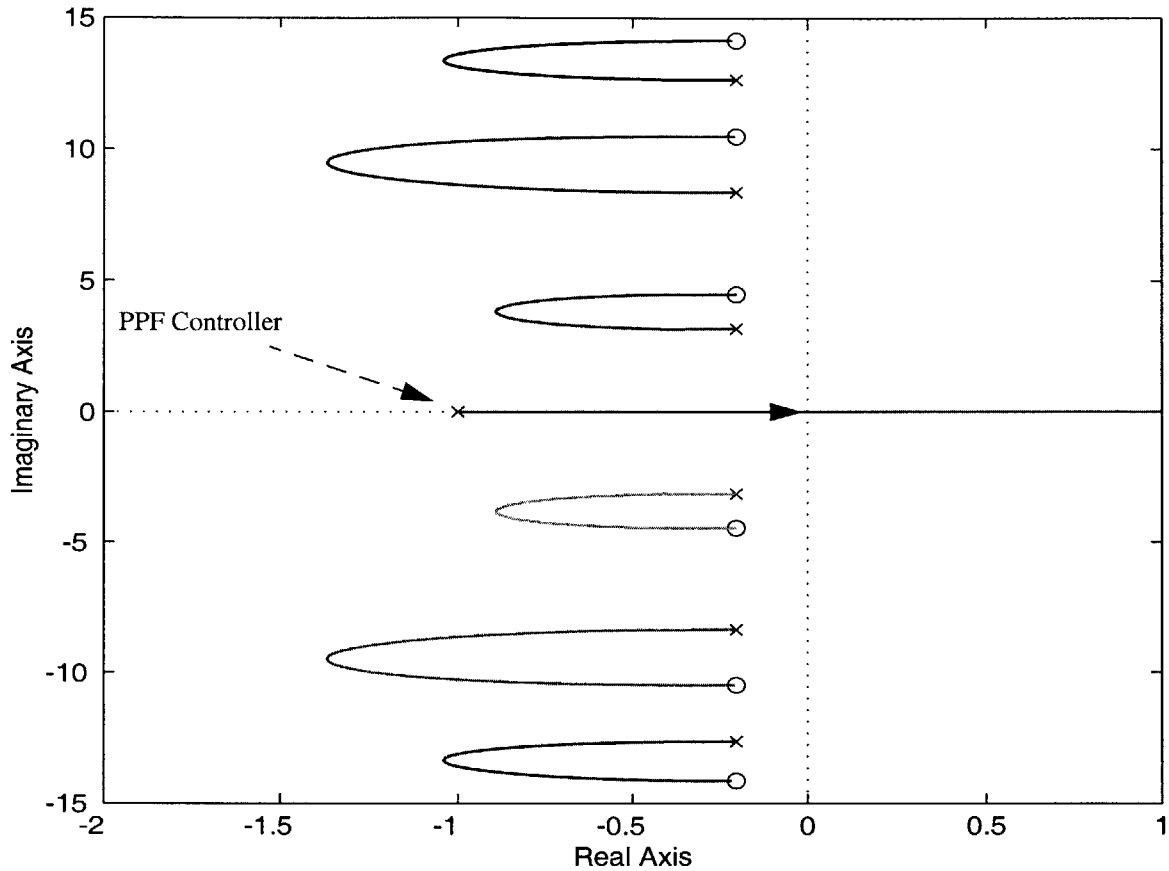


Figure 3.3: Root locus of an arbitrary 3 degree-of-freedom flexible plant with collocated sensors and actuators when controlled by PPF with a single real pole.

Note that too high of a gain also degrades the performance, since the closed-loop poles become attracted by the open-loop zeros and start moving towards the right half plane. The gain should be high enough to achieve sufficiently damped closed-loop poles but low enough to prevent instability.

PPF can also be applied by using a real pole on the left half plane. Figure 3.3 shows the root locus of the same resonant plant as in Figure 3.2, when it is controlled by PPF with a single pole on the negative real axis. When compared with the controller with a complex pair of poles, this method seems to add more damping to the system. However, it does not guarantee stability either. As the gain is increased, the real pole that is introduced

by the controller moves towards the right half of the complex plane and eventually becomes unstable. Consequently, in a PPF control system, stability is not guaranteed and is sensitive to the chosen value of gain.

One structural control method to add damping with guaranteed stability is collocated rate feedback (RF). Ideally, this control technique is applied to a collocated force actuator/velocity sensor pair. The product of these parameters is power. A control loop with a negative feedback of velocity reduces the energy of the system, resulting in improved performance [Crawley, 1991]. An advantage of collocated rate feedback is that it guarantees stability. A collocated force to velocity transfer function has alternating pole-zero pairs, and its phase is bounded by -90 deg and $+90$ deg. A negative proportional feedback results in 90 deg of phase margin, which guarantees a stable loop. Researchers have proven by using the Lyapunov function that a system with collocated negative velocity feedback is always asymptotically stable no matter how large the feedback gain is set [Hu, 1999].

Laugwitz et al. studied the active vibration control of a thin rectangular plate by means of rate feedback and achieved an increase in the modal damping coefficients by a factor of 40 [Laugwitz, 1998]. Martin et al. studied the attitude control of a flexible spacecraft where they developed low-order controllers to damp a number of vibration modes that are excited by the control torque. They developed low-order collocated rate feedback controllers and compared them with a full-order optimal controller. Their results showed that the low-order controllers can provide near optimal performance and are significantly less sensitive to modeling errors [Martin, 1980]. Applying rate feedback with a non-collocated pair can lead to instability because of the time delay from the sensor to the actuator. However, in the case of an ideal collocated pair, this time delay is considerably small. Hence, the collocated nature of the sensor/actuator pairs on the testbed is a significant advantage.

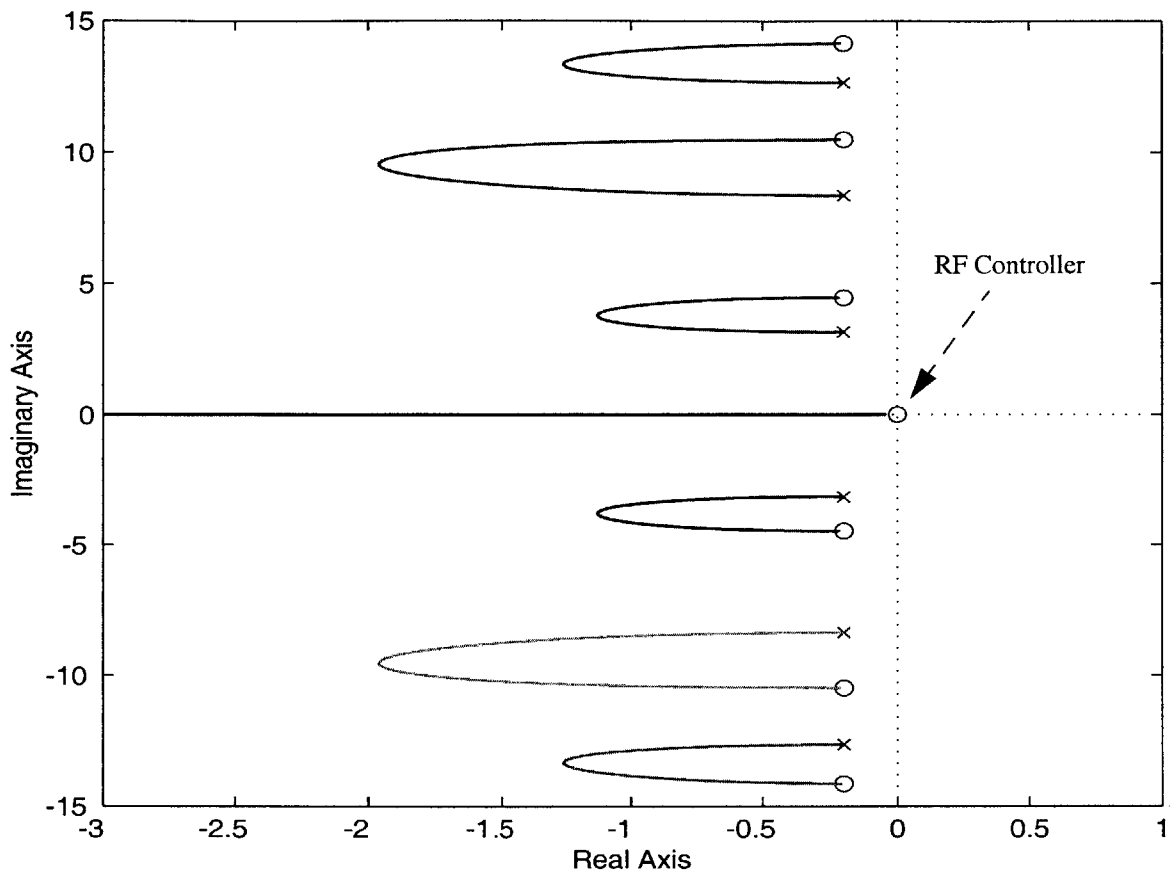


Figure 3.4: Root locus of an arbitrary 3 degree-of-freedom flexible plant with collocated sensors and actuators when controlled by rate feedback.

Figure 3.4 illustrates the guaranteed stability of a rate feedback control system. Given in this figure is a root-locus of the same flexible plant as in Figure 3.2 when rate feedback is used. The zero located at the origin of the complex plane represents the rate feedback controller. All pole pairs migrate towards the zeros. Since they initially move towards the left, they can be damped by choosing an appropriate gain. Regardless of the gain of the controller, there are no poles that pass to the right half plane, hence the system is guaranteed to be stable.

Although the above scenarios concerned an arbitrary sixth order system (or a three degree-of-freedom plant, with three natural frequencies), rate feedback would be stable for

any ideal system with collocated sensors and actuators. This, however, is not true for positive position feedback. The gain and the location of the real pole (or complex pair of poles) of the PPF controller are crucial for the stability of the system. This renders rate feedback a more favorable method for robust structural control when uncertainties in the system are possible.

Previous studies have also confirmed that rate feedback is an effective structural control method. In a study performed on the two-dimensional model, rate feedback was applied to multiple collocated piezoelectric sensor/actuator pairs of a panel where a separate controller was used for each sensor/actuator pair [O'Sullivan, 1998]. The closed-loop simulations showed reductions in interior acoustic pressure that reach 20 dB at certain resonant peaks.

At this point, although using multiple independent rate feedback loops seems to be an appropriate control method for the testbed, it is important to remember that measuring strain rate with the sensors instrumented on the testbed is not possible. The sensors located on the testbed are PVDF patches and they measure strain. This requires the differentiation of the signal measured by the sensors. A frequency domain analysis is necessary to predict the consequences of this action. Unfortunately, as stated before, a full prediction of the controller effects on the testbed requires an accurate model. Since such a model is not available, it is necessary to assess the behavior of the testbed by utilizing experimental system identification techniques.

3.3 System Identification

In this study, system identification is used to understand the dynamics of the structure, to determine the observability/controllability of structural modes provided by the sensors and actuators, and to predict the effects of the chosen control algorithm on the structure.

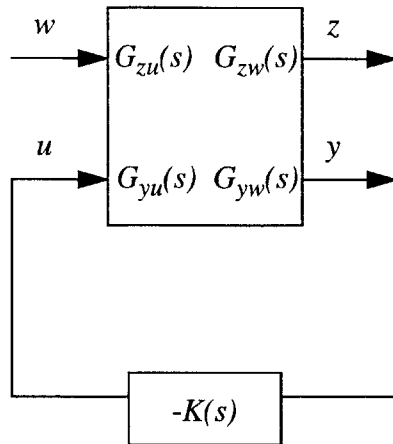


Figure 3.5: Schematic of the control problem.

System identification of the testbed was accomplished by taking actuator to sensor ($G_{yu}(s)$) and disturbance to the performance ($G_{zw}(s)$) transfer functions.

Figure 3.5 shows a generic schematic of the control problem where u , y , w , and z represent actuator (PZT) input, sensor (PVDF) output, the disturbance, and the performance metric respectively. The objective of the control experiment is to design a controller $K(s)$ that minimizes the performance metric z , when the plant is subjected to disturbance w . The disturbance w is provided by a PZT bonded to an adjacent panel on the testbed (as illustrated in Figure 2.16 of Chapter 2). Accelerometers and microphones are the two kinds of performance sensors. The open-loop transfer functions taken from the disturbance source to these performance sensors are presented next.

3.3.1 Disturbance to Performance Transfer Functions

Figure 3.6 shows an open-loop transfer function taken from the disturbance PZT to the accelerometer located on the center of Panel 1 (inside the testbed).

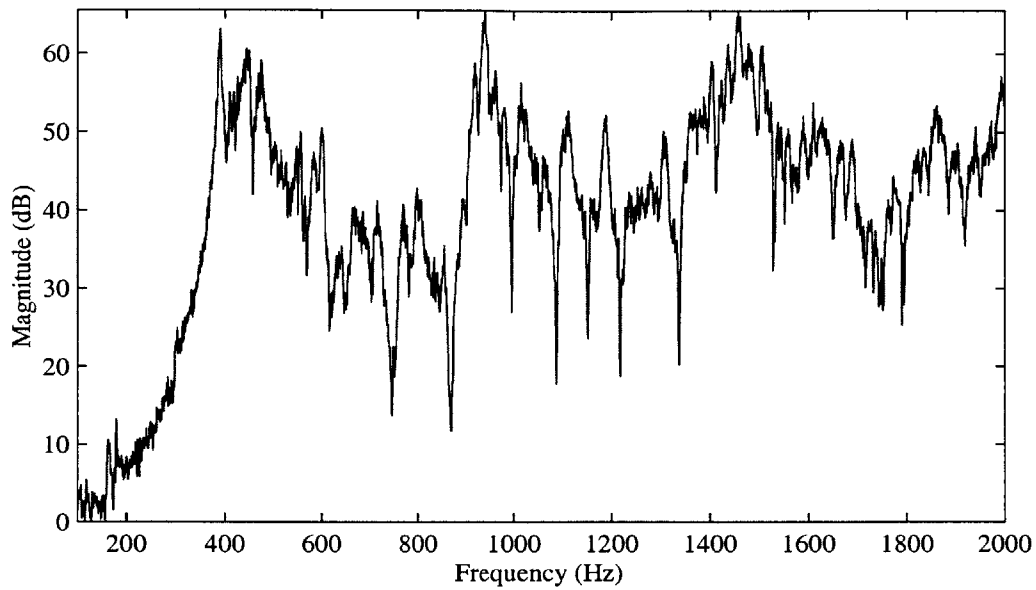


Figure 3.6: Disturbance to accelerometer open-loop transfer function for Panel 1, Location 1.

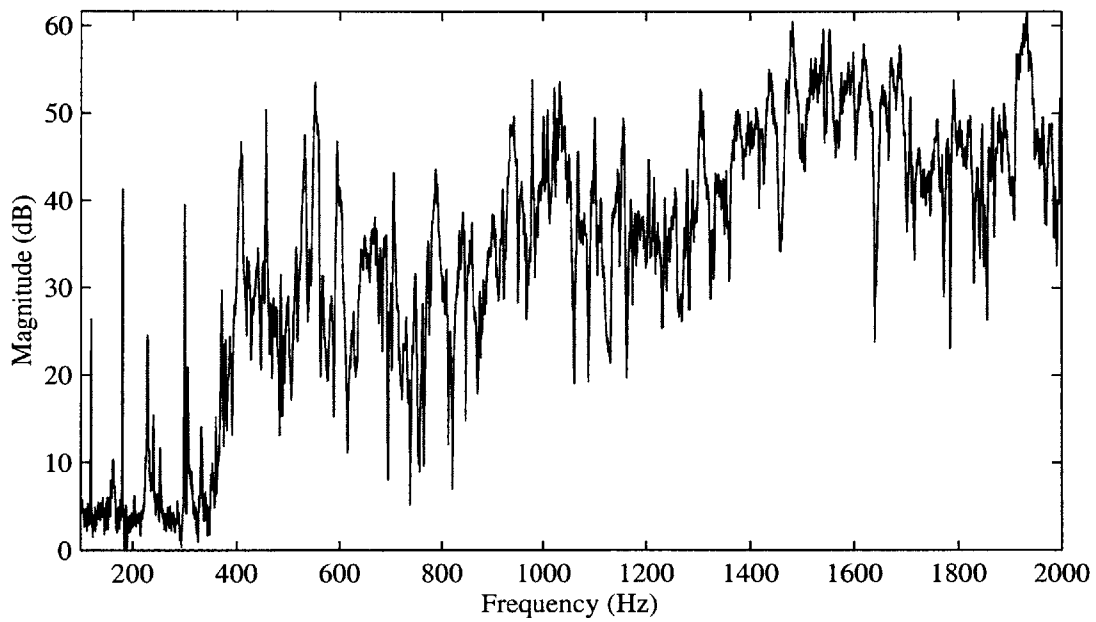


Figure 3.7: Disturbance to microphone open-loop transfer function: The microphone is located behind Panel 2.

Figure 3.7 illustrates a transfer function taken from the same disturbance source to one of the three microphones located behind Panel 2. It is clear from Figures 3.6 and 3.7 that the modal density of the system is extremely high, i.e., the modes of the system are very closely spaced. Figures 3.6 and 3.7 also imply that the type and the placement of the disturbance source are appropriate for stimulating a large number of structural and acoustic modes over a wide frequency range. Transfer functions were taken using five other accelerometers and two other microphones. When compared with Figures 3.6 and 3.7, these transfer functions show similar behavior (see Chapter 4). Since acoustic radiation results from the out-of-plane motion of fuselage panels, strain in a panel is not a direct performance metric. Hence, disturbance to sensor (PVDF) transfer functions (G_{yw}) do not constitute an important part of system identification for this study.

3.3.2 Actuator to Sensor Transfer Functions

Actuator to sensor transfer functions are important, because they are explicitly used to design the control law. Open-loop actuator to sensor transfer functions were taken separately for each of the 30 collocated pairs by exciting a PZT actuator with broadband random noise, and measuring the output of the collocated PVDF sensor.

Figure 3.8 shows a transfer function that was taken from the central collocated PVDF-PZT pair of one of the 6 instrumented panels. The plot displays alternating poles and zeros, which is a typical pattern of a collocated transfer function. Note that the phase is bounded by 0 and -180 degrees, instead of -90 and +90 degrees. This is because the sensor measures strain (displacement) instead of strain rate (velocity).

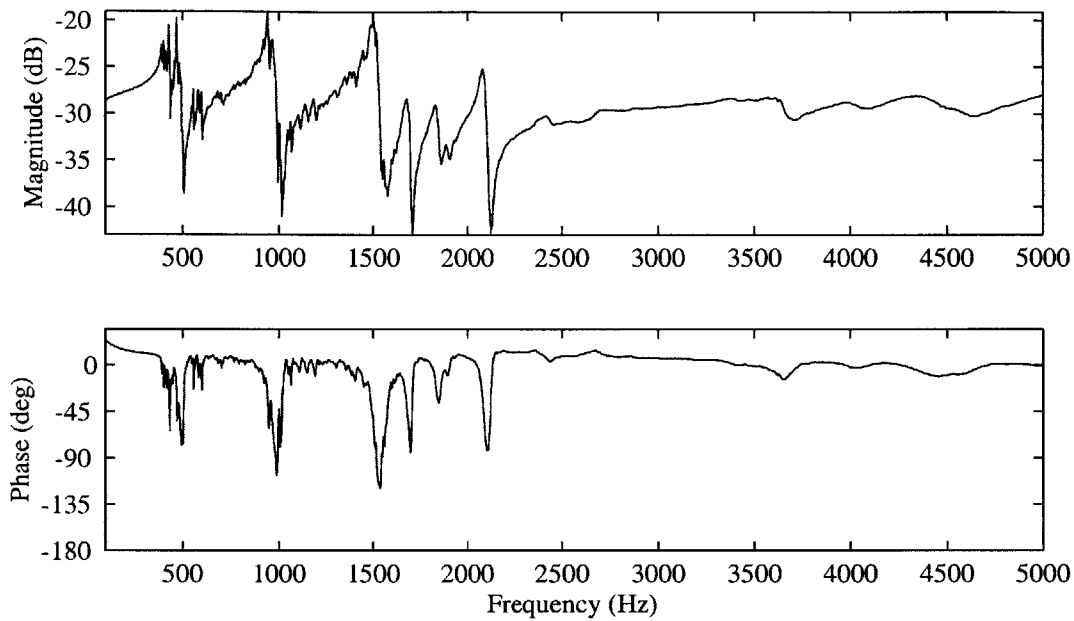


Figure 3.8: PZT to PVDF transfer function for the central patch of Panel 1.

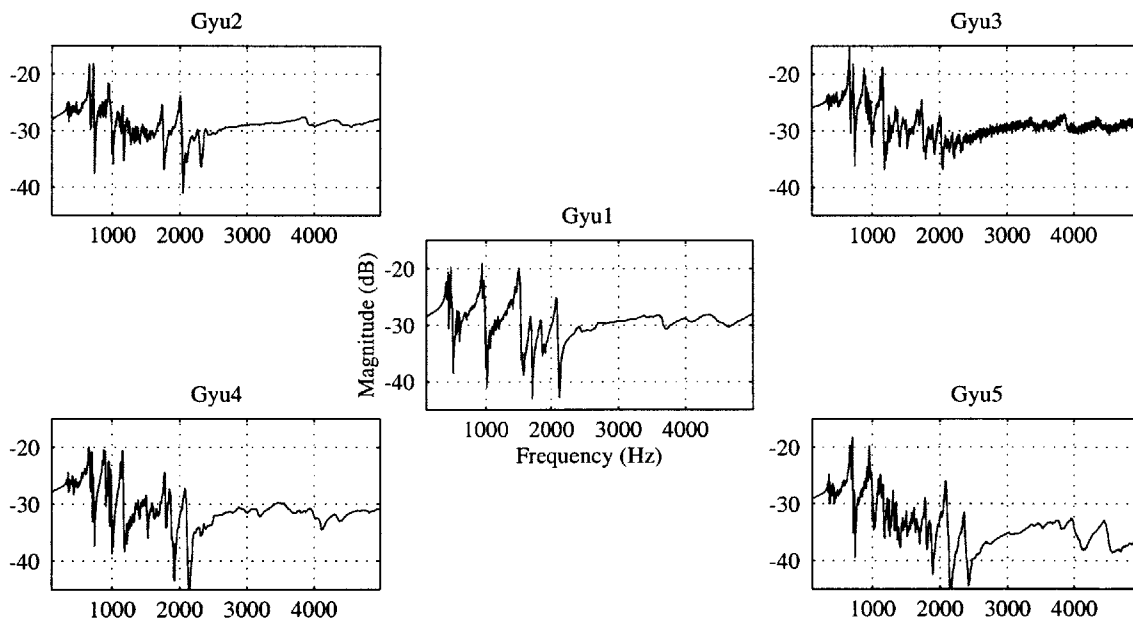


Figure 3.9: Magnitude of transfer functions for all 5 sensor/actuator pairs of Panel 1.

Another important point to note is that negligible dynamics is observed above 2000 Hz, and the phase does not deviate significantly from 0 degrees in that range. This is because the PVDF patch senses the average local strain over its area. Modes with wavelengths that are smaller than the sensor size tend to average out, producing average strain readings much smaller than the maximum strain. In structural dynamics, this phenomenon is referred to as *spatial filtering*.

Figure 3.9 shows that all pairs of panel 1 exhibit collocated behavior and that they all filter the resonant dynamics above 2000 Hz. Figure 3.9 also shows that there are modes in some transfer functions that are not present in the others, which indicates that during control action, a mode that is missed by one pair can be controlled by another one. There are also some modes that are present in more than one transfer function, which indicates that for those modes, control authority is reinforced by multiple sensors and actuators. There may also be modes that are not observed/controlled well by any pair. For these modes, closed-loop control is not expected to produce significant performance.

Transfer functions were taken from all 30 sensor/actuator pairs. They show behaviors that are very similar to those illustrated in Figures 3.8 and 3.9, i.e, they all show alternating pole-zero pairs, and exhibit filtered dynamics above 2000 Hz.

3.4 Control Law

Rate feedback is a desirable structural control law, because it adds damping and is simple to implement. For a system with a force actuator and a velocity sensor, the control input is simply: $u = -ky$, where y is the velocity output. It was shown in the last section that rate feedback guarantees stability. However, rate feedback is only effective with a transfer function that rolls off [Crawley, 1999].

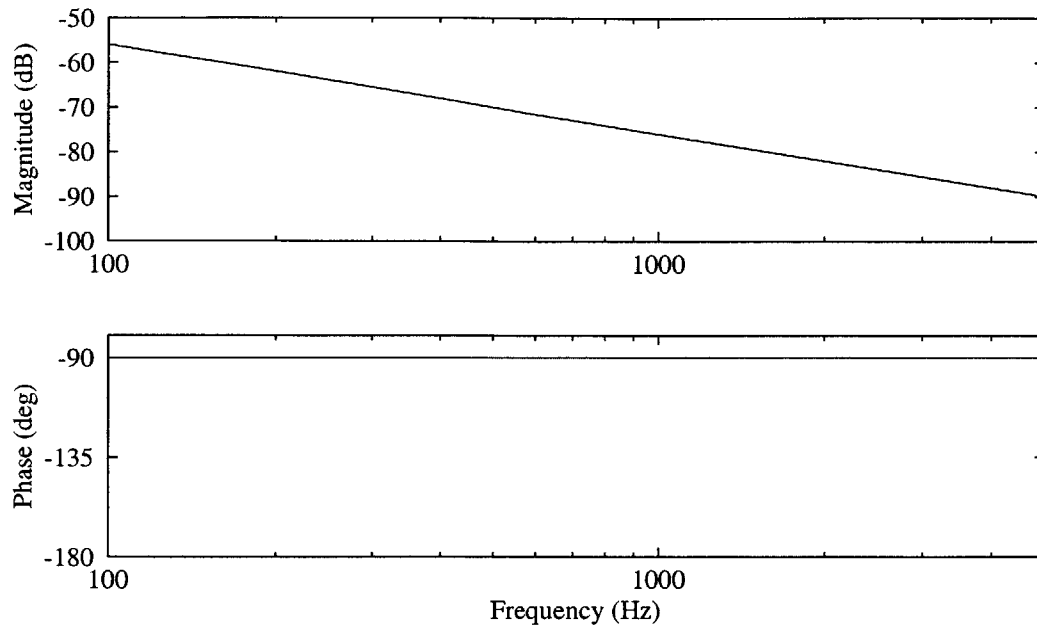


Figure 3.10: Force to velocity dereverberated transfer function.

Figure 3.10 shows a generalized force to velocity transfer function. Figure 3.10 also approximates a *dereverberated* transfer function taken from a collocated force/velocity pair, i.e., it excludes any flexible dynamics that the system may exhibit. For this system, a control law of the type $u = -ky$ results in 90 degrees of phase margin. The magnitude rolls off with a slope of -20 dB/dec, which is beneficial to prevent instability at high frequency.

Unfortunately, the magnitude of a PZT to PVDF transfer function, as illustrated by Figure 3.8, does not roll off at all. Since PVDF measures strain, rather than strain rate, pure rate feedback control requires a derivative action: $u = -k\dot{y}$ where \dot{y} is the time derivative of the sensor output. The Laplace transform of the required controller is of type:

$$K(s) = ks. \tag{3.1}$$

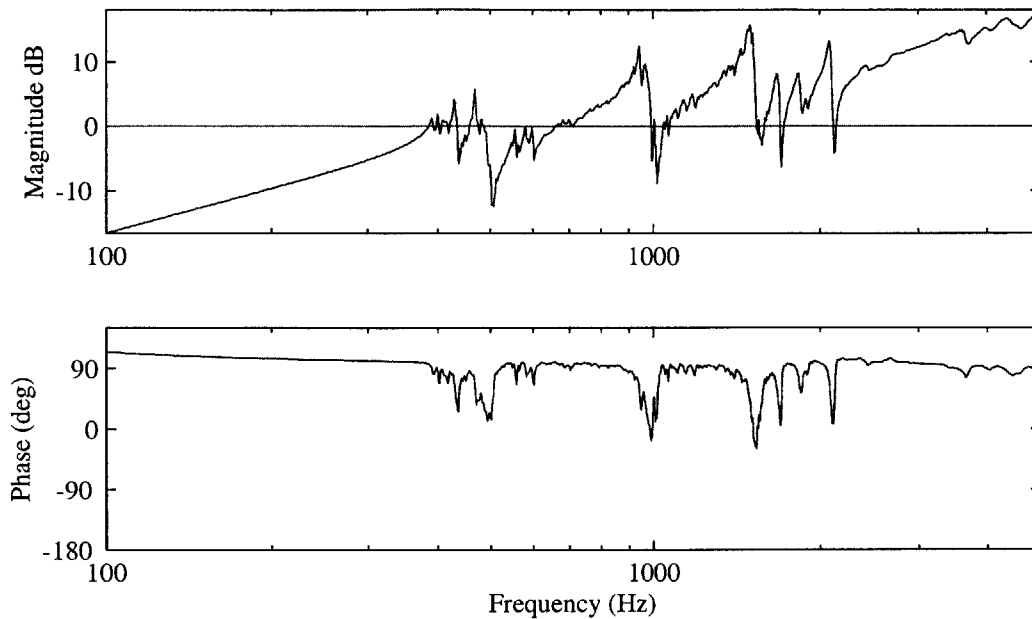


Figure 3.11: Loop transfer function of a pure rate feedback controller and a PZT-PVDF pair.

Figure 3.11 shows the loop transfer function ($K(s) \times G_{yu}(s)$) for the central sensor/actuator pair of Panel 1. Although phase indicates stability, the magnitude has a positive slope which is extremely undesirable. It may be tempting to think that the system is stable since the phase never becomes -180 deg or $+180$ deg at crossover frequencies. However, the transfer function in Figure 3.11 is somewhat idealized, i.e., it does not take any possible time delays into account. Time delays can occur during the experiment because the signals travel a finite distance between the sensor/actuator pairs and the controllers. As will be discussed in the control implementation section of Chapter 4, a time delay results in a phase lag that increases linearly with frequency. Hence, even an infinitesimal time delay can destabilize a control system whose transfer function does not roll off. Therefore, it is necessary for the magnitude of the loop transfer function to roll off to prevent high frequency instability.

An appropriate controller transfer function would be the one that applies rate feedback up to a certain frequency and rolls off for gain stabilization of high frequency dynamics. This can be represented by a control law of the form:

$$K(s) = \frac{k\omega_n s}{s^2 + 2\zeta\omega_n s + \omega_n^2} \quad (3.2)$$

In this equation, k is a static gain, ω_n is the corner frequency for roll off, and ζ is the damping ratio. The numerator of this transfer function applies rate feedback until a desired frequency ω_n . At ω_n , the magnitude starts to roll off. Since the numerator provides a +20 dB/decade slope, the denominator is required to be second-order to provide a -20 dB/decade slope at high frequency.

The second-order roll off term in the controller introduces additional phase lag, especially above the corner frequency. The phase of the function $K(s)$ is 90 deg at low frequency. As the frequency approaches ω_n , the phase starts to decrease and above ω_n , it becomes -90 degrees. Strictly speaking, this control law does not guarantee stability, because a flexible mode that occurs above ω_n could make the system unstable. Thus, care is needed when selecting the controller parameters. The corner frequency must be set to a value greater than the last modal frequency in the control bandwidth. If ω_n is placed near a modal frequency, the phase lag introduced by the second-order roll off term and that associated with the system pole combine, which could make the control loop unstable. This scenario is illustrated in Figures 3.12 and 3.13. Figure 3.12 shows a bode plot of the controller in Equation 3.2 with parameters: $\omega_n = 900$ Hz, $\zeta = 0.05$, and $k = 80$, and Figure 3.13 shows a loop transfer function ($K(s) \times G_{yu}(s)$) with the same controller for the central pair of Panel 1.

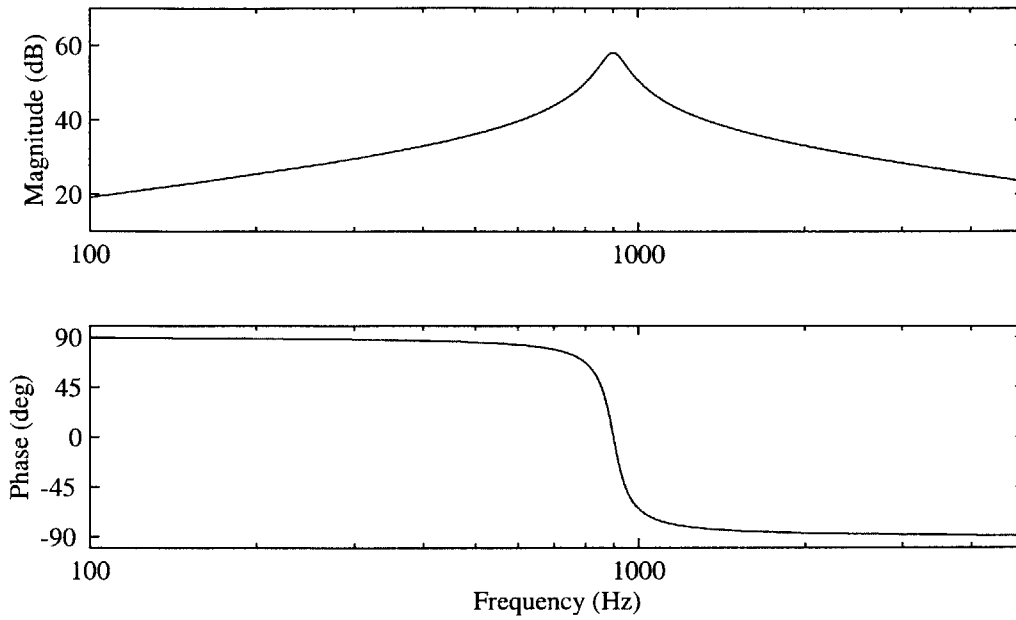


Figure 3.12: $K(s)$ where $\omega_n = 900$ Hz, $\zeta = 0.05$, and $k = 80$.

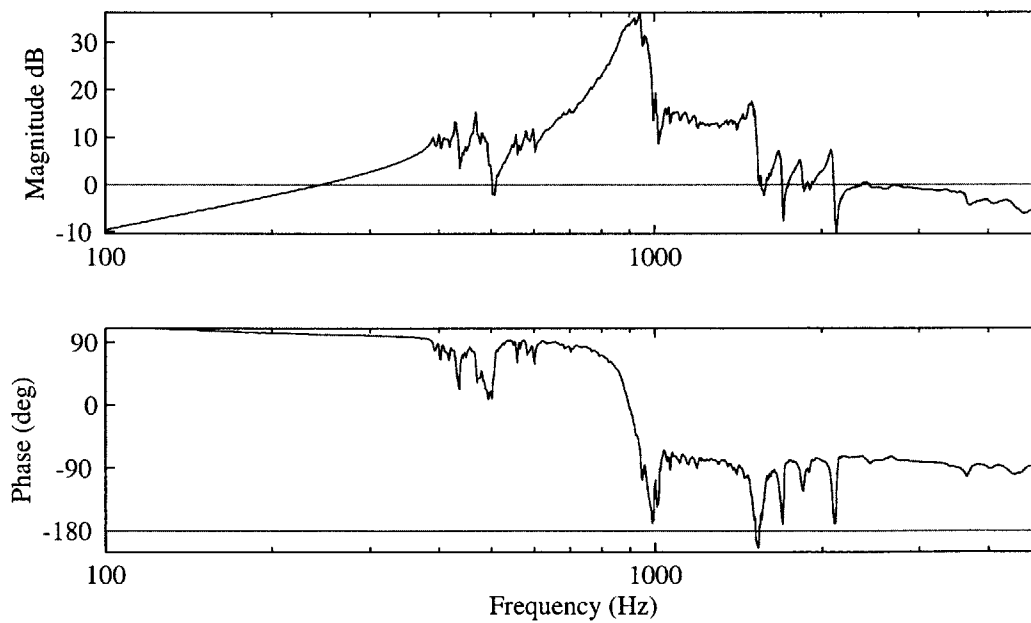


Figure 3.13: $K(s) \times G_{yu}(s)$ where $\omega_n = 900$ Hz, $\zeta = 0.05$, and $k = 80$.

Figure 3.12 shows a controller transfer function that applies rate feedback over the frequency range 100 - 900 Hz and rolls off beyond this range. The stability of the feedback loop can be evaluated from the loop transfer function, shown in Figure 3.13. Instability occurs if the phase of the loop transfer function is less than or equal to -180 deg or greater than $+180$ deg at the frequency where the magnitude crosses 0 dB. For the current case, the first crossover occurs at 500 Hz. At this particular frequency, the phase is approximately $+10$ deg, which does not result in instability. The second crossover occurs at 1650 Hz where the phase is less than -180 deg. The phase at the third and the fifth crossovers is almost -180 deg. This control loop is clearly unstable.

The main reason for the instability is the phase lag introduced by the second-order term in the denominator of the controller transfer function. When the corner frequency is placed near a modal frequency, the phase lag of the system pole and that introduced by the controller combine, and cause instability. Thus, it is imperative not to place the corner frequency near a frequency where significant resonant behavior is observed [Crawley, 1999].

As discussed in the system identification section, all actuator to sensor transfer functions showed negligible dynamics after 2000 Hz due to spatial filtering. Although this implies that the control bandwidth is limited by 2000 Hz, the advantage provided by spatial filtering is indispensable. Since resonant dynamics is negligible above 2000 Hz, the variation in phase is also very small. Figure 3.8 shows that the phase of the PZT to PVDF transfer function above 2000 Hz does not deviate significantly from 0 deg. This implies that if the value of ω_n is set to a larger value than 2000 Hz, the phase of the loop transfer function will not deviate significantly from -90 deg, resulting in a stable control loop. Thus, the roll off in the controller must start after the last modal frequency in the control bandwidth.

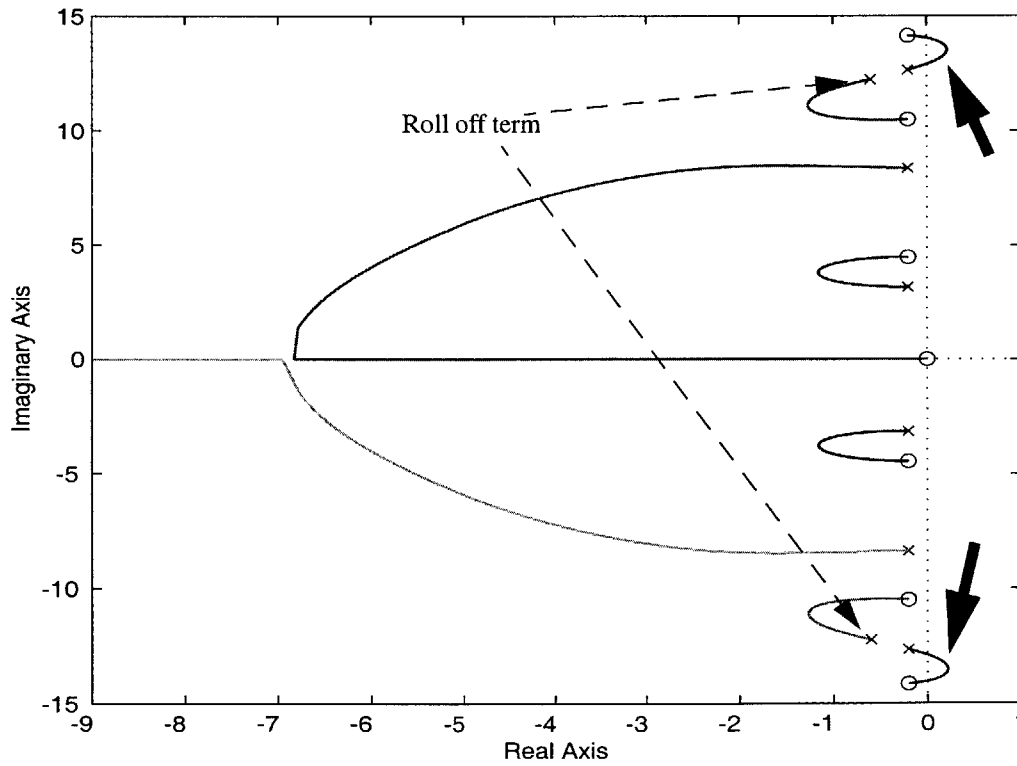
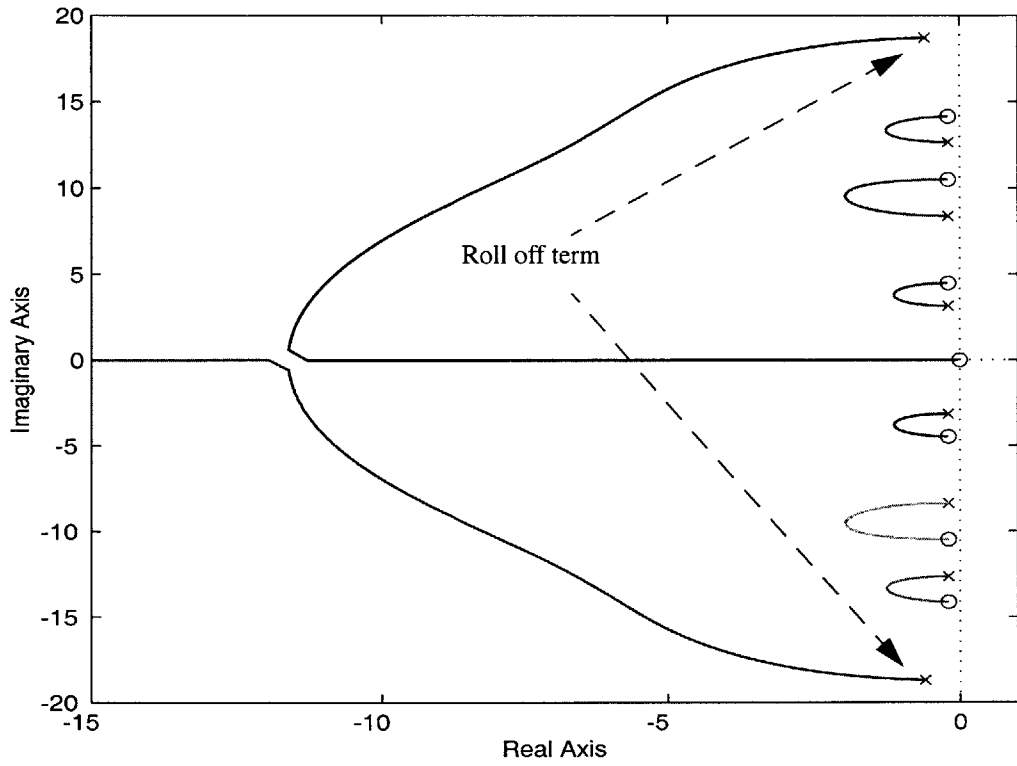


Figure 3.14: Root locus demonstration of the control system sensitivity to corner frequency in the roll off term of $K(s)$.

Figure 3.14 shows the root locus plots of an arbitrary flexible plant that is controlled by collocated rate feedback. The complex pair of poles that serves for roll off are indicated with dashed arrows on both plots. The top plot represents the control system where the corner frequency of the second-order roll off term is above the last modal frequency, i.e., the *stiffest* pole pair. There are no poles in the right half plane, and hence, the system is stable. As the gain is increased, closed-loop poles migrate farther left and become more damped. Again, the gain must be chosen appropriately to achieve optimum performance. Too high of a gain makes the poles move back towards the right half plane, degrading the performance. But the system is guaranteed to be stable regardless of the gain.

The bottom plot of Figure 3.14 shows the root locus when the complex pole pair of the controller is placed in the vicinity of the poles of the plant. As the gain is increased, the pole pair with the highest natural frequency goes unstable. This instability is indicated with bold arrows. Figure 3.14 confirms the argument that was made by Figures 3.12 and 3.13: the roll off must start above the last modal frequency in the control bandwidth.

The designed controller is not expected to add damping at all frequencies. As discussed before, rate feedback is applied only over the frequency range where the loop magnitude rolls up at 20 dB/decade. As frequency increases, the effectiveness of damping control degrades. Rate feedback occurs at low frequencies, where the phase is near +90 deg. As frequency increases, a *transition region* starts, and the phase decreases, which implies that less damping is added. As frequency approaches the corner frequency ω_n (where the magnitude forms a peak), the decrease in the phase becomes more dramatic. At ω_n , the phase is 0 deg which implies that the controller adds stiffness rather than damping. Above ω_n , the phase assumes negative values which implies an *anti-damping region* where damping is actually reduced. As shown in Figure 3.15, the variation in the phase is strongly related to the damping ratio ζ in the controller transfer function.

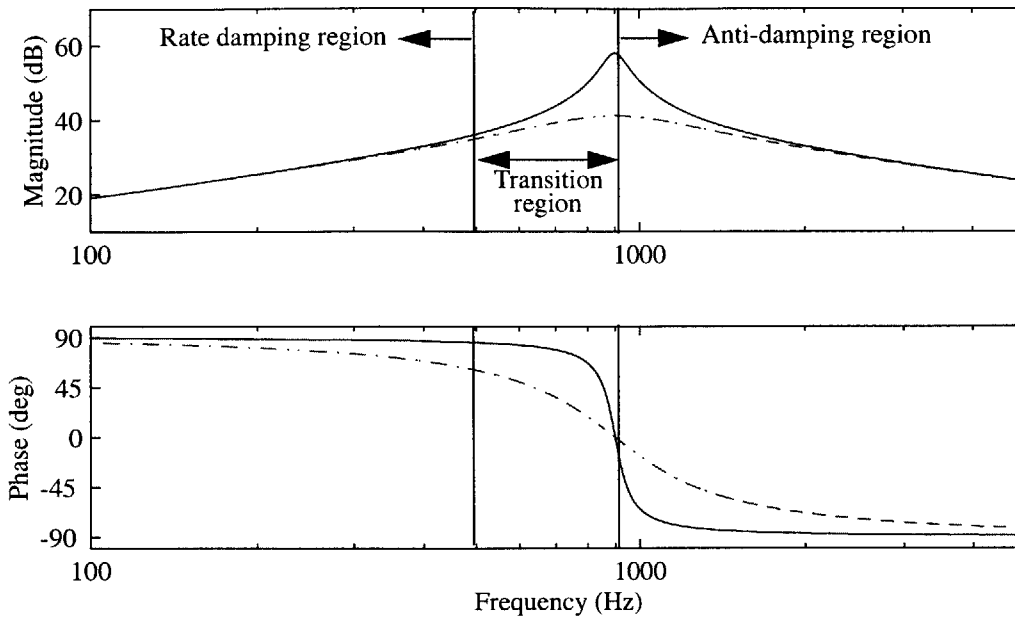


Figure 3.15: Controller transfer function for various values of ζ .

Figure 3.15 shows a plot of the controller transfer function over a frequency band of 5 kHz with a high and a low damping ratio. The solid curve and the dashed curve correspond to damping ratios of $\zeta = 0.1$ and $\zeta = 0.5$ respectively. As shown in Figure 3.15, a larger damping ratio results in a wider peak. Further, the decrease in the phase starts at a lower frequency, i.e., the transition region becomes wider, and the rate damping region becomes narrower.

If there is absolutely no flexible dynamics above the corner frequency, i.e., the phase of the actuator to sensor transfer function is exactly 0 deg, the damping ratio may be set equal to 0, to maximize the frequency range for rate damping. However, if there are slight variations in the phase above the corner frequency, or there is some uncertainty in the high frequency dynamics of the system, it is beneficial to set the damping ratio to a nonzero value.

It was stated earlier that ω_n should be placed above the last modal frequency in the control bandwidth. If roll off starts above the last mode of interest, the phase margin of the control system is near 90 deg at high frequency where the resonant dynamics is spatially filtered. Hence, the sensitivity of the system to the value of ζ is reduced by increasing ω_n . Consequently, the value of ζ can be set to a relatively small value to ensure damping over a large frequency range, provided that ω_n is sufficiently larger than the last modal frequency of interest.

The final parameter in the controller transfer function is the static gain k . Since the control loop can be phase stabilized by choosing a sufficiently large value for ω_n , it may be tempting to make gain k as large as possible. However, in order to achieve maximum damping, the controller and the system must be *impedance matched*. That is, maximum energy dissipation is obtained if the impedance of the compensator is the complex conjugate of the impedance of the load, which in this case is the structure. Hence,

$$K_{opt}(s) = \frac{1}{G_{yu}^{dr}(-s)} \quad (3.3)$$

where $G_{yu}^{dr}(s)$ is the *dereverberated* actuator to sensor transfer function of the system. This requires that the product of the dereverberated transfer function and the controller transfer function be unity. However, in order to have a stable closed-loop system, Equation 3.3 requires a non-causal controller which can not be implemented in real time [MacMartin, 1991].

Another interpretation of Equation 3.3 is that the “backbone” of the loop transfer function must be at 0 dB. Unfortunately, before the corner frequency ω_n , the backbone of the loop transfer function has a positive slope; hence, it is not possible for the controller to be impedance-matched everywhere. However, the constant gain k might be chosen such that the backbone crosses 0 dB in the middle of the frequency range of interest.

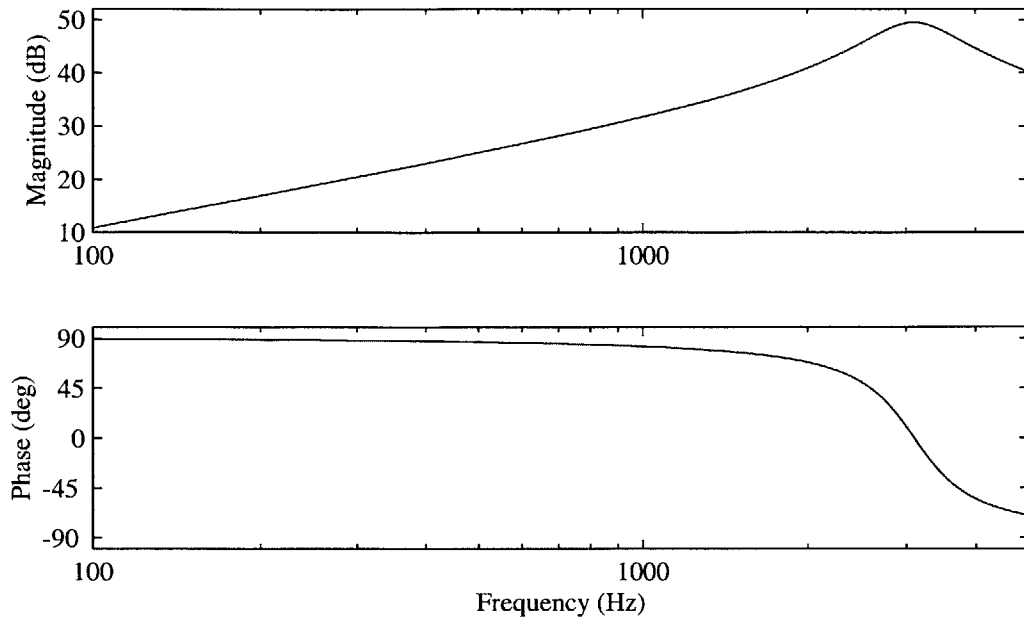


Figure 3.16: $K(s)$ where $\omega_n = 3100$ Hz, $\zeta = 0.18$ and $k = 108$.

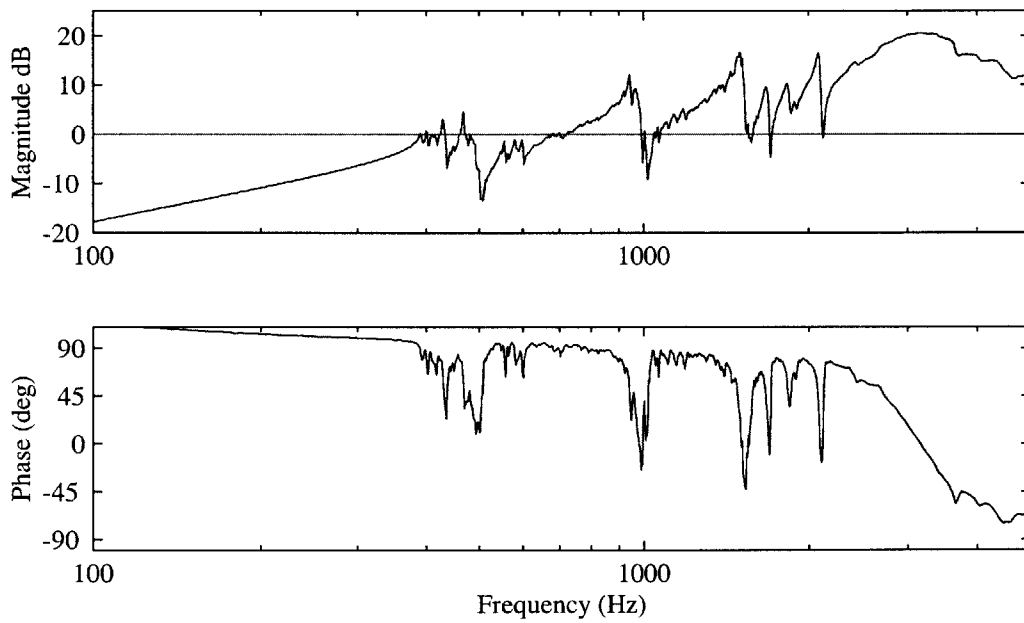


Figure 3.17: $K(s) \times G_{yu}(s)$ for the sensor/actuator pair at Panel 1-Location 1; where $\omega_n = 3100$ Hz, $\zeta = 0.18$ and $k = 108$.

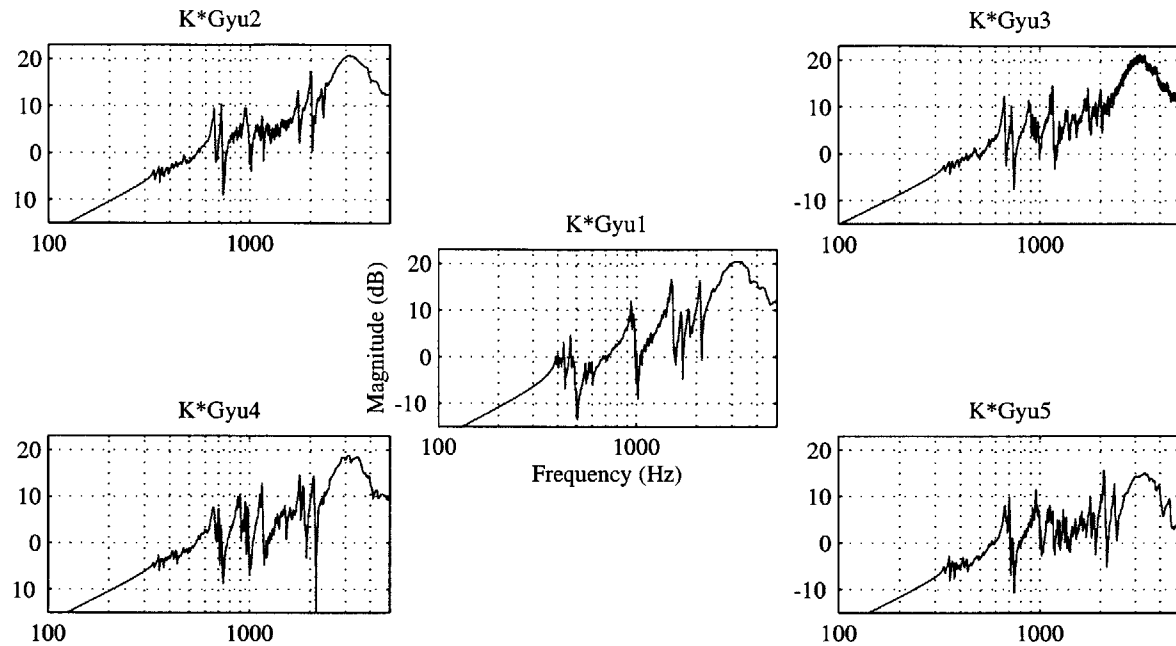


Figure 3.18: Magnitude of $K(s) \times G_{yu}(s)$ for all pairs of Panel 1.

Figure 3.16 shows a plot of the controller transfer function with parameters $\omega_n = 3100$ Hz, $\zeta = 0.18$ and $k = 108$. The value of corner frequency is sufficiently larger than the last modal frequency in the control bandwidth of 2000 Hz. The specific value of the damping ratio was chosen to be as small as possible and fine-tuned during the actual experiment. Figure 3.17 shows the loop transfer function of the central PVDF-PZT pair of Panel 1. The plot indicates a stable system, i.e., the phase is far from -180 deg at crossover frequencies. There is another crossover above 5000 Hz which is not shown in Figure 3.17. Instability at that crossover frequency is not a concern because, it is known that negligible resonant dynamics exists beyond 2000 Hz, hence the phase of the loop transfer function is supposed to be almost flat around -90 deg. Figure 3.17 also shows that the chosen value for k is appropriate to keep the dereverberated transfer function as close to the 0 dB line as possible. Since the chosen control law will be applied to each of the 30 sensor/actuator pairs separately, the loop transfer function for each pair was checked individually. Figure 3.18

shows the magnitude of loop transfer functions of all sensor/actuator pairs in Panel 1. It is apparent that the chosen controller parameters yield similar results for all sensor/actuator pairs of Panel 1. Loop transfer functions were also plotted for the sensor/actuator pairs of the remaining five panels and stability of each loop was individually checked.

The main purpose of the control implementation is to apply the chosen control law to 30 sensor/actuator pairs separately and simultaneously. Each control loop is to operate independently from the remaining 29 control loops without getting any information from them. This should not introduce doubts of instability because every individual feedback loop has a collocated sensor/actuator pair, i.e., any disturbance that is observed by a PVDF sensor will be controlled by the collocated PZT actuator. Similarly, if the effect of a disturbance is not observed by the sensor, it can not be controlled by its collocated actuator. Hence, instability of the feedback loop is not a concern.

3.5 Summary

A local control design was performed based on system identification methods. Among various local control techniques, rate feedback was chosen because of its robust stability and simplicity. Rate feedback provides the best results when the system has a collocated actuator to sensor transfer function that rolls off. Although a sensor/actuator pair on the testbed exhibits collocated behavior, its transfer function does not roll off. Furthermore, since the chosen sensors measure strain rather than strain rate, applying pure rate feedback requires a derivative action which results in a transfer function that continuously rolls up. Hence, a complex pair of poles were introduced to the denominator of the controller transfer function to provide the desired roll off. Simulations of loop transfer functions and root locus plots show that corner frequency of the roll off term must be sufficiently larger than

the last modal frequency in the control bandwidth to ensure stability. Implementation of the designed controller and the closed-loop results are presented next, in Chapter 4.

Chapter 4

Control Implementation and Experimental Results

This chapter describes the results of the experiment performed by using the feedback control methods discussed in Chapter 3. The first section of the chapter discusses possible methods to implement multiple independent controllers, each operating with the designed control law. Basics of digital control implementation using a PC are briefly discussed; where benefits and disadvantages of digital control are evaluated. Though flexible and simple, digital methods introduce phase lag which may reduce the performance of the control system or lead to instability. Although analog methods are not as flexible as the digital techniques, they generally do not cause as much phase lag. Hence, the control implementation of this study was performed using an analog approach with electrical circuits. The first section describes this implementation procedure in detail.

The second section presents the results of the closed-loop experiment performed by exciting the disturbance PZT with a broadband random noise. Accelerometers attached to six different locations on the testbed skin were used to evaluate the effectiveness of the control system on structural vibration. Three microphones located inside the testbed were used to assess the interior acoustic behavior of the system. The chapter discusses the control performance by means of comparing the closed-loop results with the open-loop behavior of the system.

4.1 Control Implementation

4.1.1 Digital Approach

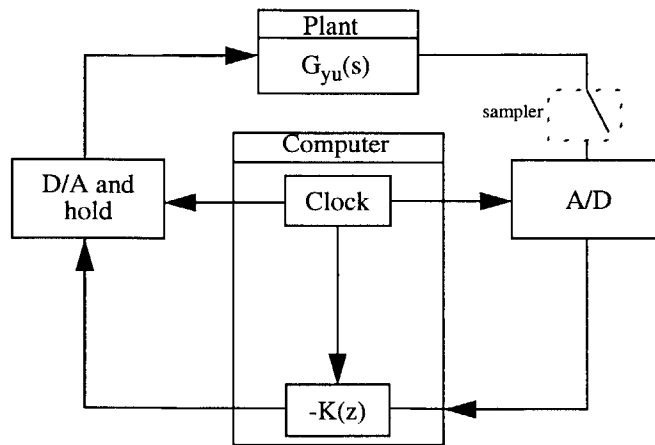


Figure 4.1: Basic digital control system with computer.

Thanks to the extremely fast pace of computational advancements, it is becoming more and more common to control physical systems with digital computers. Many electro-mechanical servo systems that exist in aircraft, mass-transit vehicles, oil refineries and chemical plants are currently operated with digital control systems. Digital control is desirable mainly because of the flexibility it gives the designer in implementing the control logic. The designer generally writes a code that represents the controller in discrete time. The computer then interprets the code into digital instructions and applies them to the incoming sensor signal.

Figure 4.1 shows the schematic of a basic digital control system that is implemented on a computer. The continuous sensor output (usually electrical voltage) that represents the behavior of the plant is first discretized by sampling it at every T_s seconds. The A/D converter then acts on the sampled signal and converts it into a stream of numbers. The clock is a part of the computer logic which supplies a pulse or *interrupt* at every T_s seconds and the A/D converter sends a number to the computer every time the interrupt

arrives. The computer then applies the discretized control law that was previously coded in it and sends it to the D/A converter. The resulting discrete signal then goes through a zero order hold (ZOH) and is eventually sent to the actuators.

Digital control is flexible because the controller parameters may be changed easily by modifying the computer code that comprises the control law. Numerous digital signal processing (DSP) interfaces that can be instrumented inside a PC are commercially available. Many of the commercial DSP interfaces are compatible with MATLAB. This makes implementation even easier by eliminating the procedure of writing complicated codes and enabling the usage of certain toolboxes such as Simulink.

The most important drawback to digital control is the time delay that is introduced by sampling of the incoming sensor signal. A delay in any feedback loop degrades the stability of the system [Franklin, 1998]. During sampling, each discrete value is held constant until the next value is available. This results in an average time delay of $T_s/2$ between the sampled and the actual measured signal. In addition to the effective time delay caused by sampling, there is a delay T_c , due to the time required to perform the digital calculations. Hence, the total time delay can be expressed as:

$$T = \frac{T_s}{2} + T_c. \quad (4.1)$$

Depending on the complexity of the computation, T_c can be as large as T_s . Thus, it is common and safe to assume a total time delay of $1.5T_s$. A time delay of $1.5T_s$ corresponds to a phase lag of

$$\delta\phi = -1.5\omega T_s, \quad (4.2)$$

which must be considered while designing the controller. If the sampling time is small, i.e., for a high sampling frequency, this additional phase lag may not be significant. However, for large values of T_s , this phase lag may have detrimental effects on the stability of

the control loop.

The purpose of the experiment is to implement 30 independent control loops. Digital implementation requires using 30 input (A/D) and 30 output (D/A) channels. A simple experiment was performed on a personal computer to understand the effects of the number of utilized A/D and D/A channels on the sampling frequency, i.e., $1/T_s$. The PC was equipped with a 300 MHz Pentium microprocessor, 128 MB of RAM, 1.96 GB of hard drive space and a dSpace card. The dSpace interface had 32 A/D and D/A channels. The sampling frequency was observed to be as high as 42000 Hz when a single A/D and a single D/A channel were used. This value is sufficiently high since the desired control bandwidth is only 2000 Hz. Unfortunately, the sampling frequency was found to be as low as 4100 Hz when 30 A/D and D/A channels were used. This sampling frequency is only high enough to prevent aliasing but may introduce significant phase lag.

Figure 4.2 shows a transfer function of the controller that was discussed in Chapter 3. The solid curve is the ideal controller without any additional phase lag. The dashed curve shows the controller with the additional phase lag approximated by Equation 4.2, assuming a sampling frequency of 4100 Hz. This value was determined to be the maximum sampling frequency when 30 A/D and D/A channels were used. It is clear that the control system acquires a significant amount of phase lag when it is implemented in digital. As expected from Equation 4.2, phase lag becomes significant as frequency increases. The additional phase lag is -90 deg at 1000 Hz. As a practical matter, it is not safe to perform closed-loop control above this frequency, since the phase of the loop transfer function may become even more negative if the system exhibits flexible dynamics above 1000 Hz. It was already discussed that the flexible dynamics of the testbed is observed/controlled up to 2000 Hz.

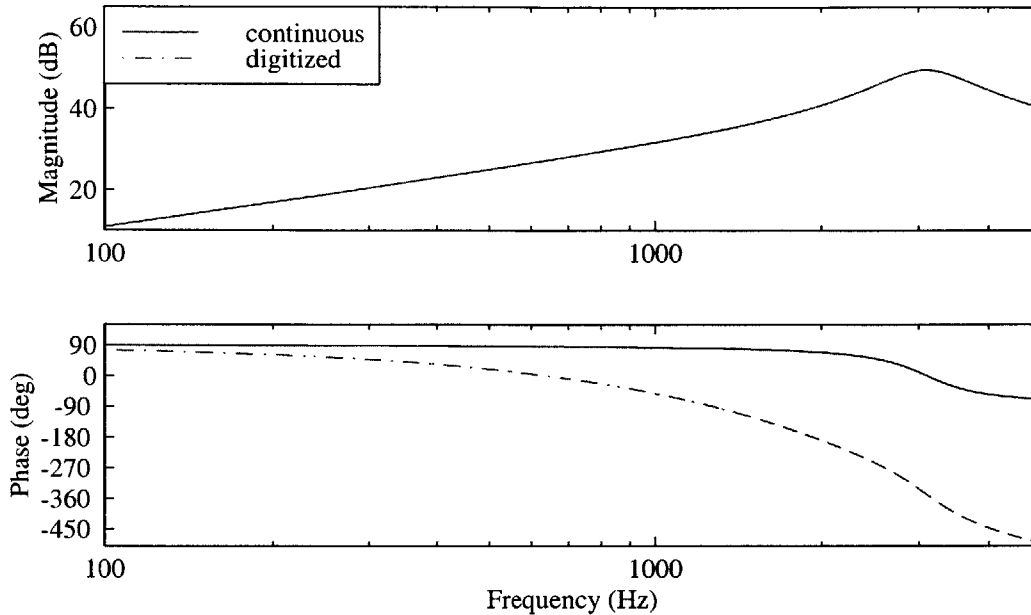


Figure 4.2: The chosen controller with and without the additional phase lag (Sampling frequency was assumed to be 4100 Hz).

Phase lag can be reduced by increasing the sampling frequency. However, it was experimentally confirmed that the maximum sampling frequency with 30 A/D and D/A dSpace channels was 4100 Hz.

As discussed before, Grewal et al. implemented digital controllers to damp a global mode of an aircraft that occurs at 61 Hz using a small number of sensors and actuators [Grewal, 1997]. It is convenient to perform narrowband or tonal control of low frequency modes using digital methods. However, the objective of this experiment is to damp localized high frequency modes over a broad frequency range. Unfortunately, implementing the designed control law using digital methods is not feasible. Therefore, the implementation of the control system was done using analog techniques, and is presented next.

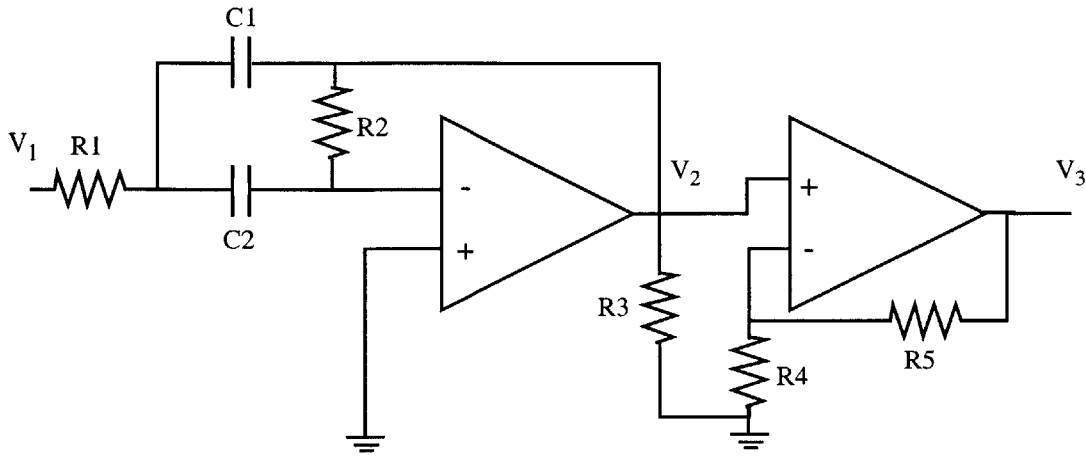


Figure 4.3: Analog controller.

4.1.2 Analog Approach

Analog approach comprises the implementation of the controller using electrical circuitry. One disadvantage of analog implementation is the difficulty of adjusting the parameters of the controller. This is especially true if there are multiple controllers, as in the current case. Another disadvantage is that analog circuits may require a great deal of wiring which consumes time. Excessive wiring may also introduce noise problems, unless care is taken to prevent electromagnetic coupling between the wires. The most significant advantage of using analog implementation is the elimination of time delay. Since no sampling is required, no time delay is introduced. This in turn, eliminates the undesired phase lag that was shown in Figure 4.2.

The chosen controller is a band-pass filter and can be implemented in analog using simple op-amp circuitry. Figure 4.3 shows a schematic of the analog controller. The op-amp on the left is used to implement the band pass filter with the transfer function:

$$\frac{V_2}{V_1} = \frac{-\frac{s}{R_1 C_1}}{s^2 + 2\zeta\omega_n s + \omega_n^2} \quad (4.3)$$

where

$$\omega_n = \frac{1}{\sqrt{R_1 R_2 C_1 C_2}} \quad (4.4)$$

$$\zeta = \frac{\sqrt{\frac{C_1}{C_2}} + \sqrt{\frac{C_2}{C_1}}}{2\sqrt{\frac{R_2}{R_1}}} \quad (4.5)$$

Once C_1 and C_2 are arbitrarily chosen, R_1 and R_2 can be calculated for the required values of ω_n and ζ . Note that the low pass filter has a fixed DC gain rather than the desired gain k in Equation 3.2. The op-amp circuit on the right is a non-inverting amplifier that is used to obtain the desired DC gain. Its transfer function is simply:

$$\frac{V_3}{V_2} = 1 + \frac{R_5}{R_4} \quad (4.6)$$

The value of R_3 is not critical and is usually set to a high value.

The preparation for the closed-loop experiment was completed by building the controller circuitry in Figure 4.3 for each of the 30 sensor/actuator pairs separately. Two breadboards were used for the implementation, each accommodating 15 circuits. The connections between the sensor/actuator pairs and the controller circuits were made using BNC cables to minimize signal corruption due to noise.

Recall that control system design and stability analysis were based purely on the PZT to PVDF transfer functions. Hence, certain experimental imperfections, such as the time delays due to finite length of wiring, were not considered. As a result, some of the control loops initially became unstable. However, stability was recovered by fine tuning gain k for these specific feedback loops. This was done simply by changing the value of R_5 .

4.2 Experimental Results

The closed-loop experiment comprised measuring the disturbance to performance transfer functions when the analog controllers were on and off. As illustrated in Figure 2.16 of Chapter 2, the disturbance source was a PZT bonded to an adjacent panel. This PZT was excited with 0-2 kHz random noise to simulate a broadband structural disturbance. There are two important performance metrics for this control experiment: structural vibration and interior noise. Structural vibration was measured with six accelerometers that were attached on the inside of panels instrumented with active plies. The effectiveness of closed-loop control on the interior noise level was assessed by measuring the output of the microphones located inside the testbed.

Although accelerometers and microphones are primary performance sensors, the output of the control sensor (PVDF) was also measured to determine the effectiveness of the control system. The upper plot in Figure 4.4 shows the autospectra of PVDF sensor number 1 on Panel 1, with and without feedback control. The open-loop spectrum is plotted in gray; the closed-loop spectrum is plotted in black. The main goal of the control experiment is to determine the reduction in the performance metrics (interior acoustics and structural acceleration), rather than to find an absolute measure of the system response. Hence, no sensor calibration was made and the magnitude is arbitrary. The bottom plot is simply the ratio of the open-loop and closed-loop spectra, expressed in decibels. The response is reduced by as much as 20 dB near 1000 Hz, and by more than 10 dB near 1500 Hz. Furthermore, the reduction is greater than 0 dB over the entire range from 0-2000 Hz, except for a small frequency range near 1750 Hz. Thus, it appears that the controller is damping the panel modes over a wide frequency range.

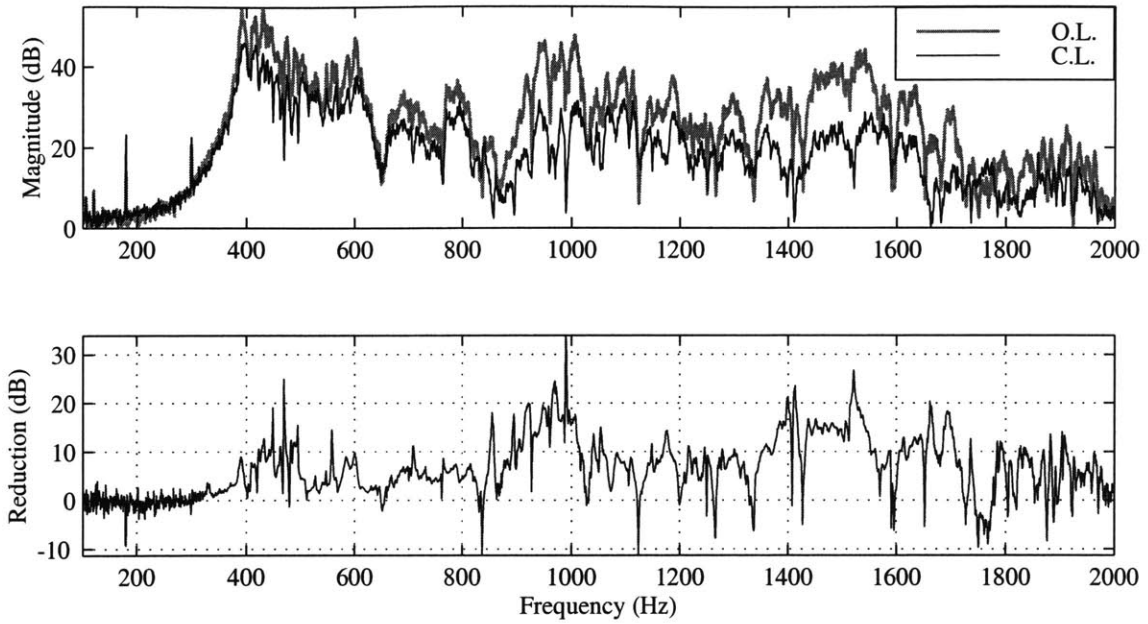


Figure 4.4: Open-loop and closed-loop strain autospectra for Panel 1, Location 1.

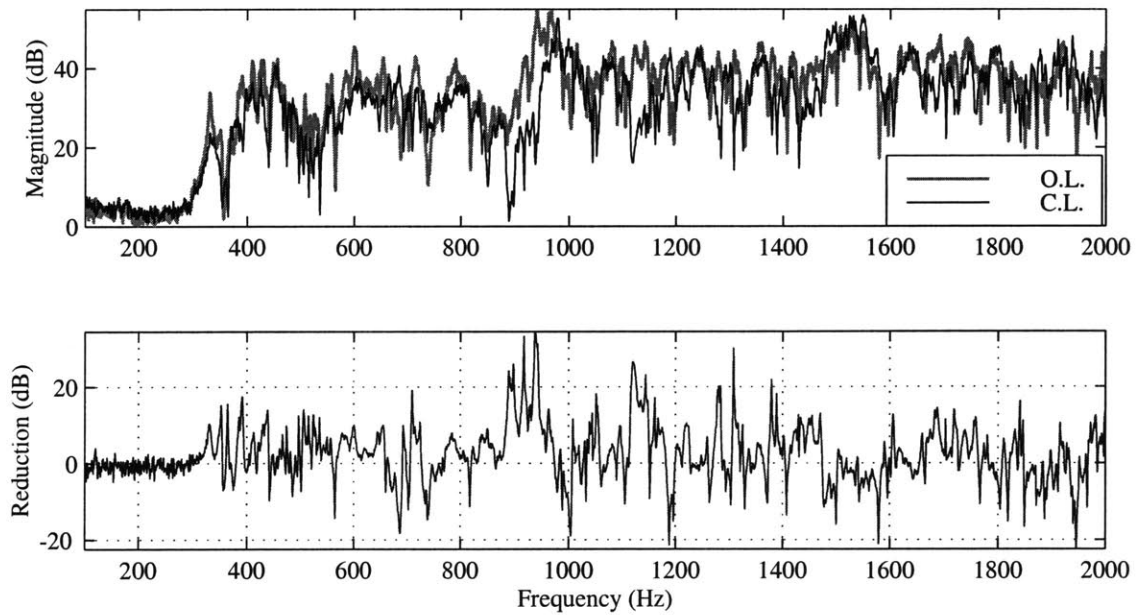


Figure 4.5: Open-loop and closed-loop acceleration autospectra for Panel 1, Location 4.

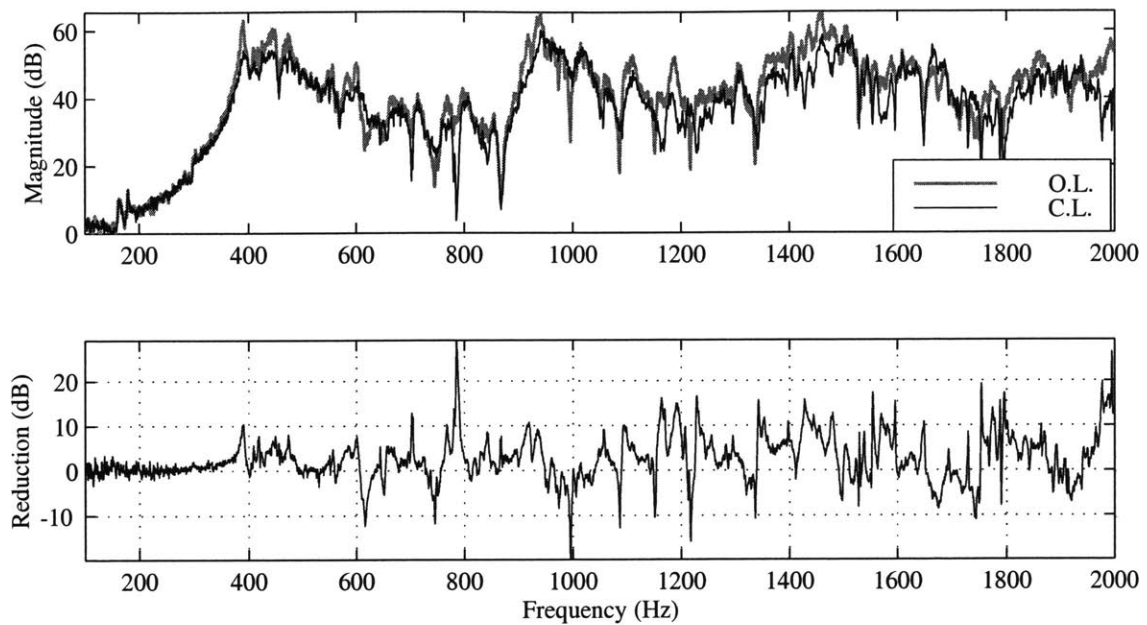


Figure 4.6: Open-loop and closed-loop acceleration autospectra for Panel 2, Location 1.

A better measure of the controller performance is the panel acceleration, since it is the motion of the panel that causes radiation of sound into the interior of the fuselage. Figure 4.5 shows the autospectra of the structural acceleration at Location 4 (bottom-left location) of Panel 1 (top-left panel) with and without feedback control. The best improvement in performance, i.e., the greatest decrease in acceleration occurs near the peaks at 400 Hz and 950 Hz. This is as expected since (a) the most observable modes occur at these frequencies and (b) the loop gain has magnitude near 0 dB at these frequencies, so that there is a good impedance match between the dynamics and the controller. Recall from Figure 3.17 that this impedance match is better at 950 Hz than at 400 Hz. Hence, there is more reduction in structural acceleration near 950 Hz. Similar behavior is observed at the remaining five accelerometer locations [Savran, 2000].

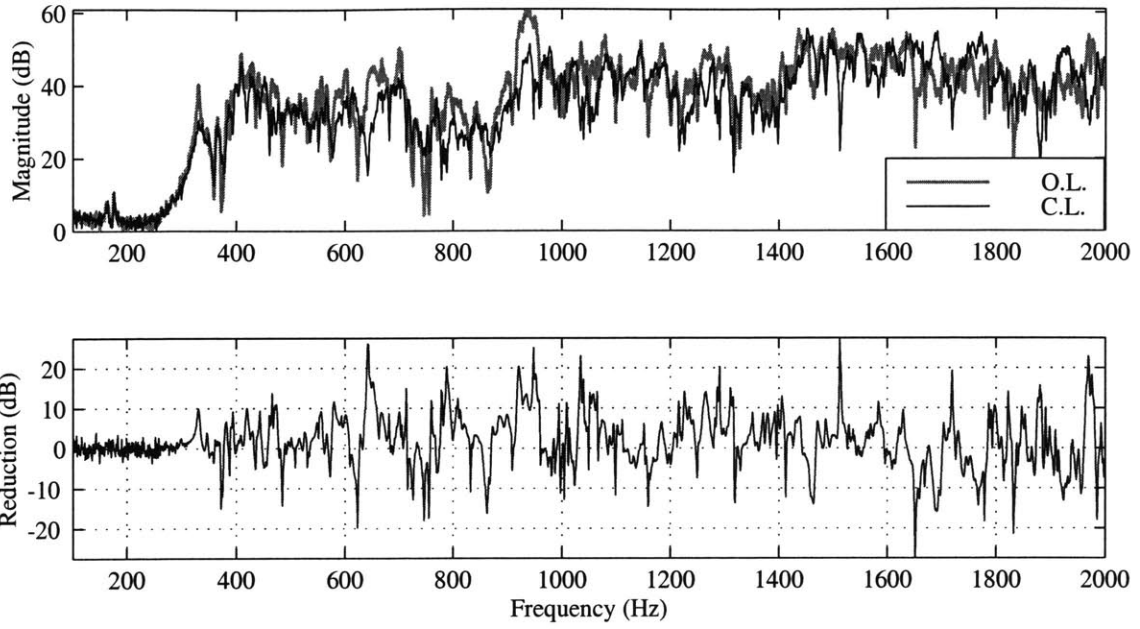


Figure 4.7: Open-loop and closed-loop acceleration autospectra for Panel 3, Location 3.

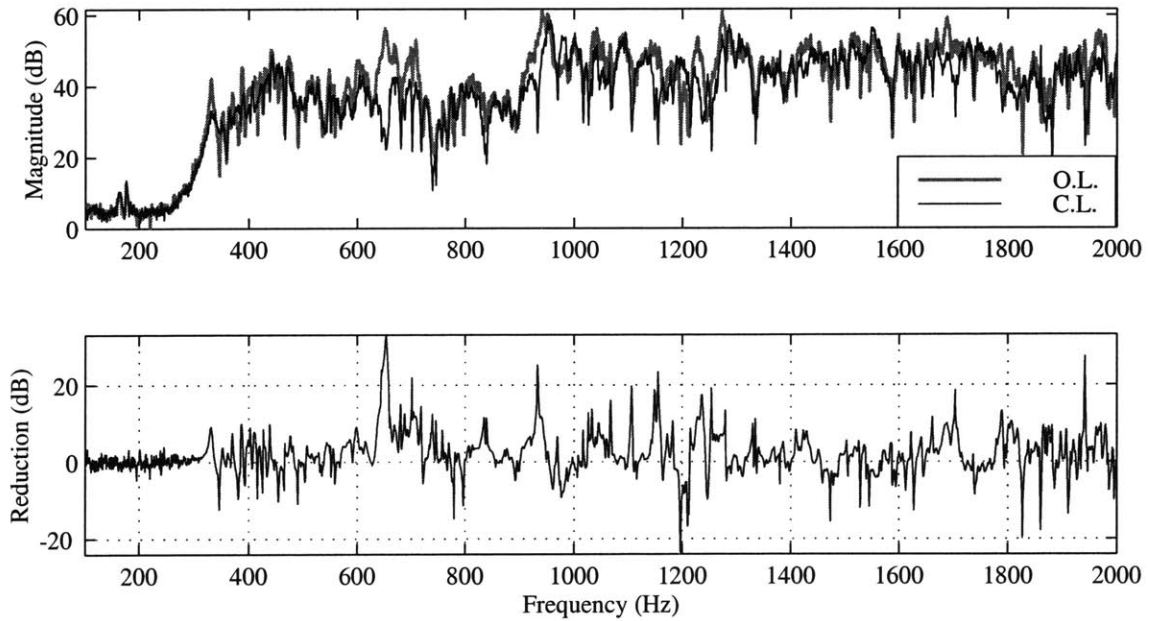


Figure 4.8: Open-loop and closed-loop acceleration autospectra for Panel 4, Location 2.

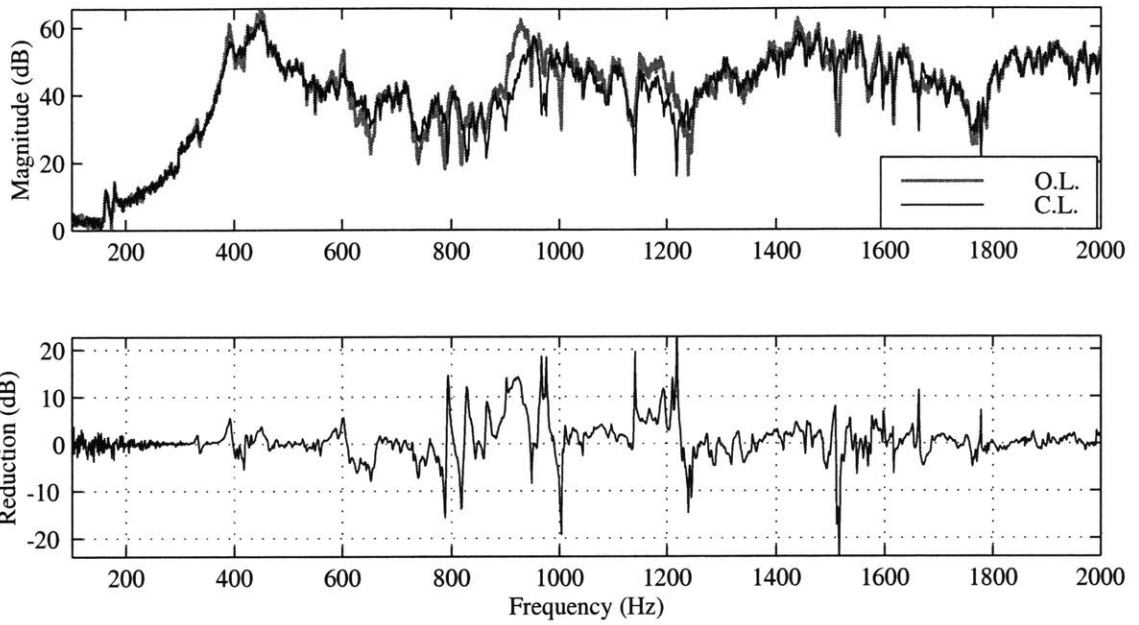


Figure 4.9: Open-loop and closed-loop acceleration autospectra for Panel 5, Location 1.

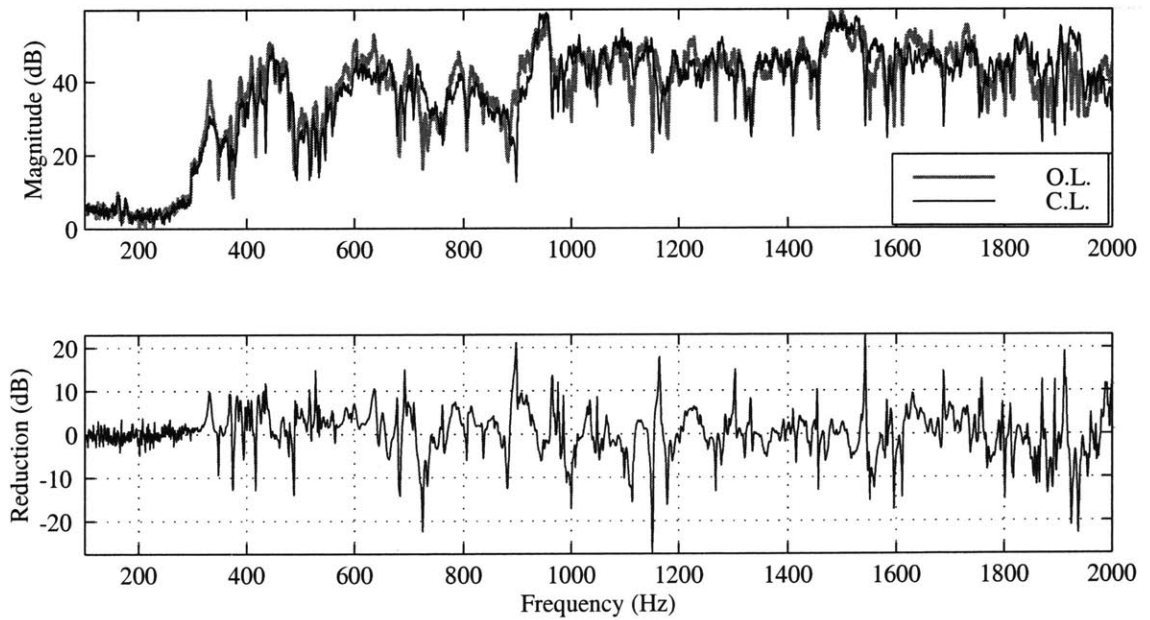


Figure 4.10: Open-loop and closed-loop acceleration autospectra for Panel 6, Location 5.

Note that in Figures 4.7, 4.8 and 4.10 (locations 3-3, 4-2 and 6-5) there is significant attenuation at resonant peaks near 650 Hz. This is as expected since in Figure 3.18 (multiple loop transfer functions) it was seen that the PVDF-PZT pairs at the four corners of the panel have good observability/controllability of the local modes in the frequency range of 600-700 Hz. On the other hand, the PVDF-PZT pair at the center of the panel does not have the same observability/controllability in the same frequency range. Hence, Figures 4.6 and 4.9 (Locations 2-1 and 5-1) show relatively low reduction in structural vibration near 650 Hz. In contrast, structural acceleration at the central location was reduced near 1450 Hz. This is because the central PVDF-PZT pair has good observability/controllability for the modes near this frequency. Recall that the PVDF-PZT pairs located in the four corners have relatively poor observability/controllability near 1450 Hz. Hence, closed-loop performance at the corners is relatively low near this frequency.

To quantify the performance gain from closed-loop control, the autospectra of the six accelerometers (Figure 2.16) were integrated and averaged in 100 Hz wide frequency bands. Closed-loop and open-loop responses were compared in each frequency band. Figure 4.11 shows that the control action was effective in reducing the structural acceleration in all but a few frequency bands, over a bandwidth of 2000 Hz. There is a reduction of 5 dB in the 300-400 Hz frequency bin. The greatest reduction is 8-10 dB, which occurs in the 900-1000 Hz bin, and in the 1400-1500 Hz bin. This is not surprising since, as already discussed, the modes in this frequency range have fairly good observability/controllability by the collocated sensor/actuator pairs.

The effectiveness of the control action in reducing acoustic behavior inside the testbed was tested using three microphones, located behind Panel 2. Figure 4.12 shows a comparison of the open-loop and closed-loop acoustic pressure autospectra for one of the microphones.

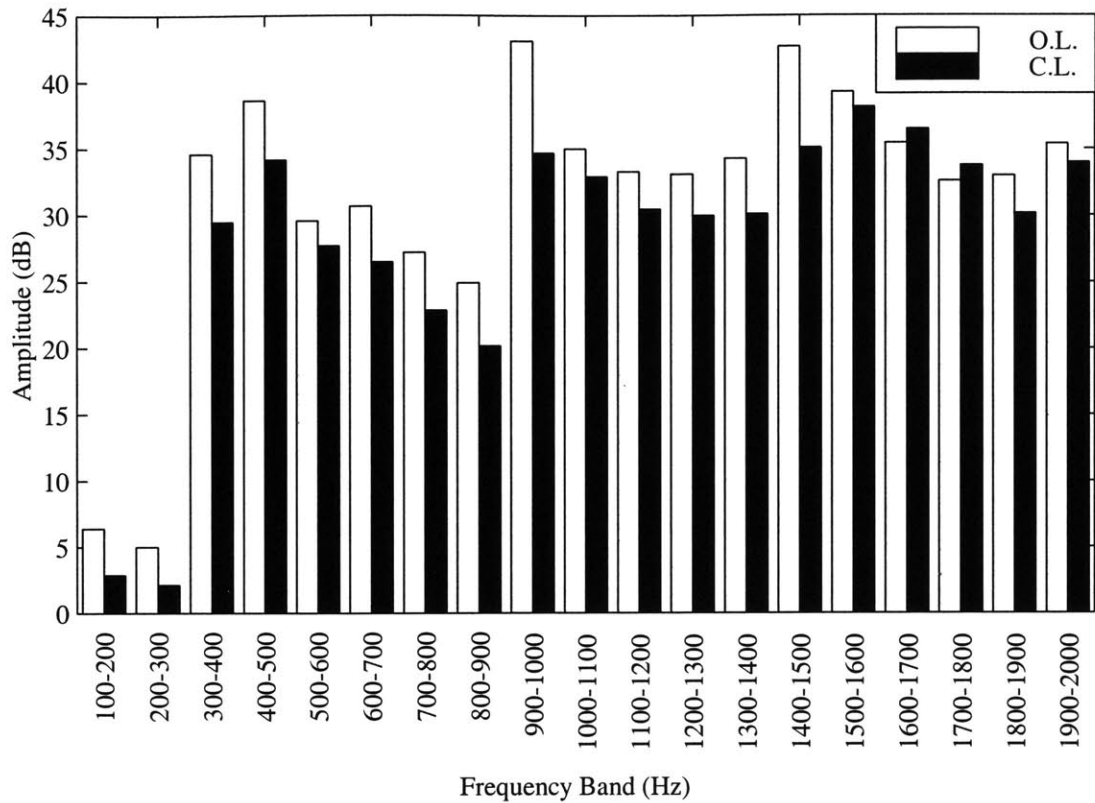


Figure 4.11: Open-loop and closed-loop average acceleration autospectra integrated in 100 Hz frequency bands.

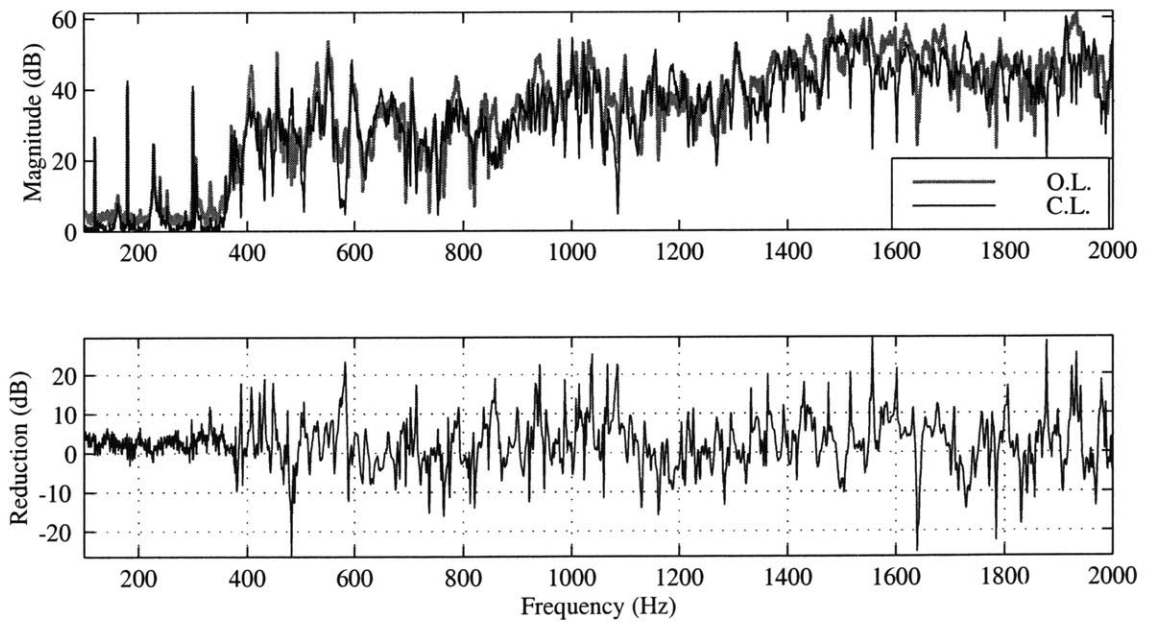


Figure 4.12: Open-loop and closed-loop acoustic pressure autospectra for a microphone located behind Panel 2 (#19).

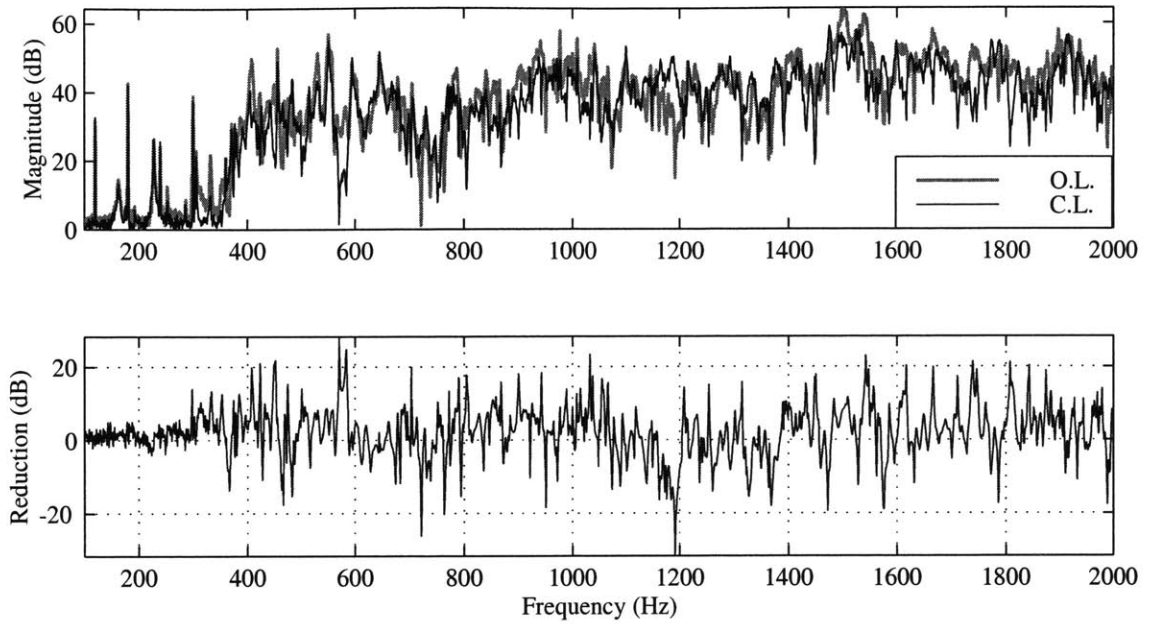


Figure 4.13: Open-loop and closed-loop acoustic pressure autospectra for a microphone located behind Panel 2 (#21).

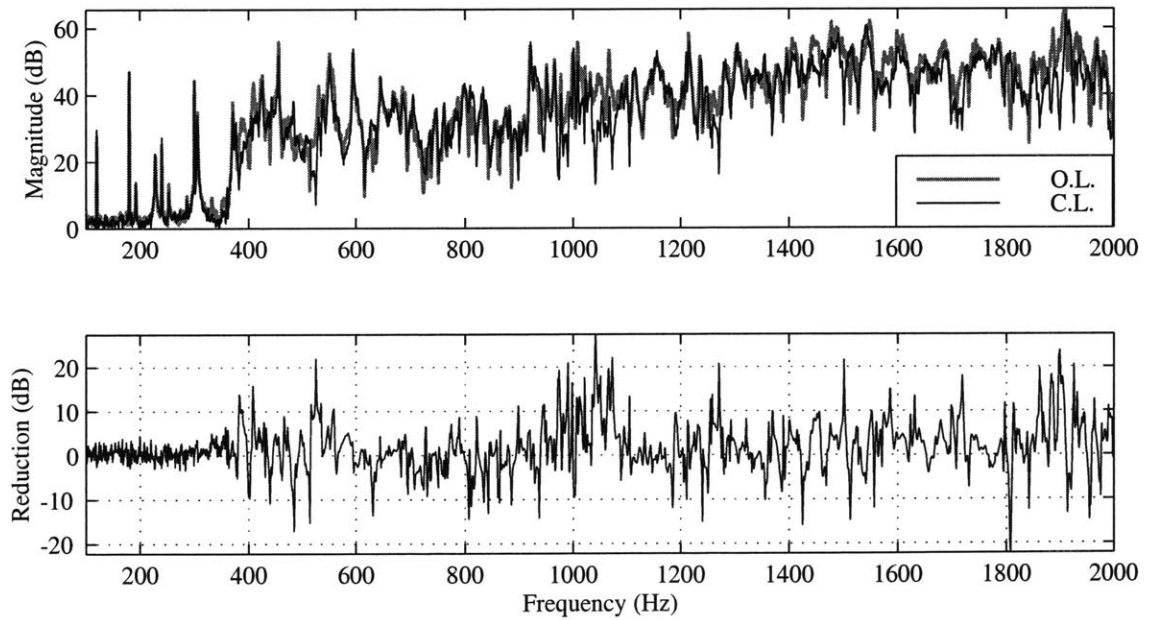


Figure 4.14: Open-loop and closed-loop acoustic pressure autospectra for a microphone located behind Panel 2 (#23).

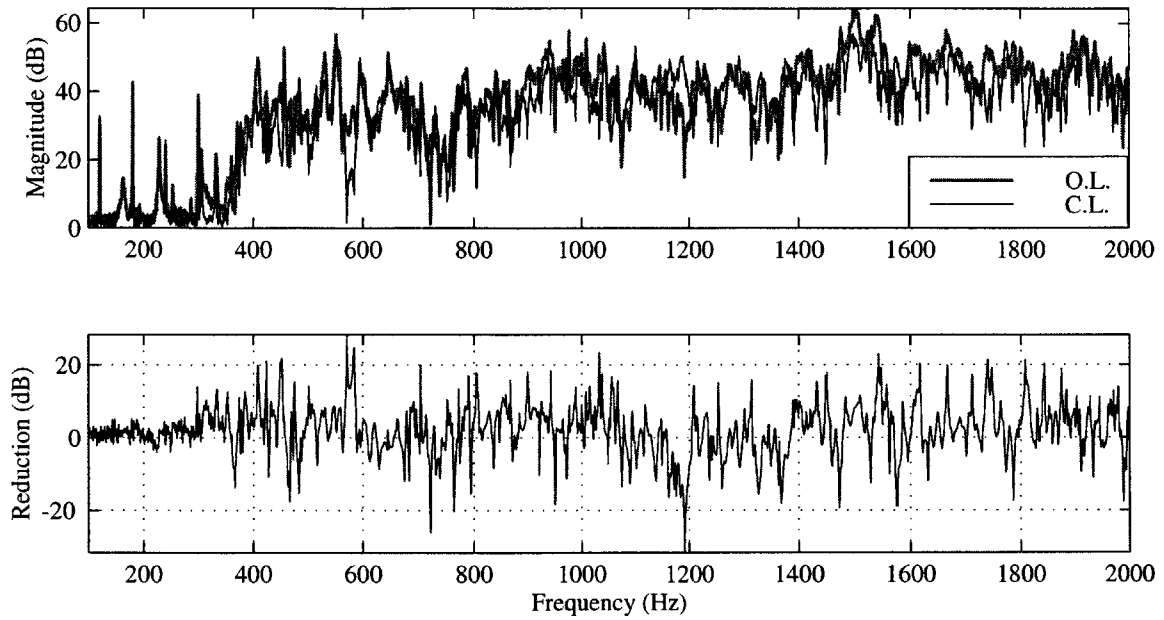


Figure 4.13: Open-loop and closed-loop acoustic pressure autospectra for a microphone located behind Panel 2 (#21).

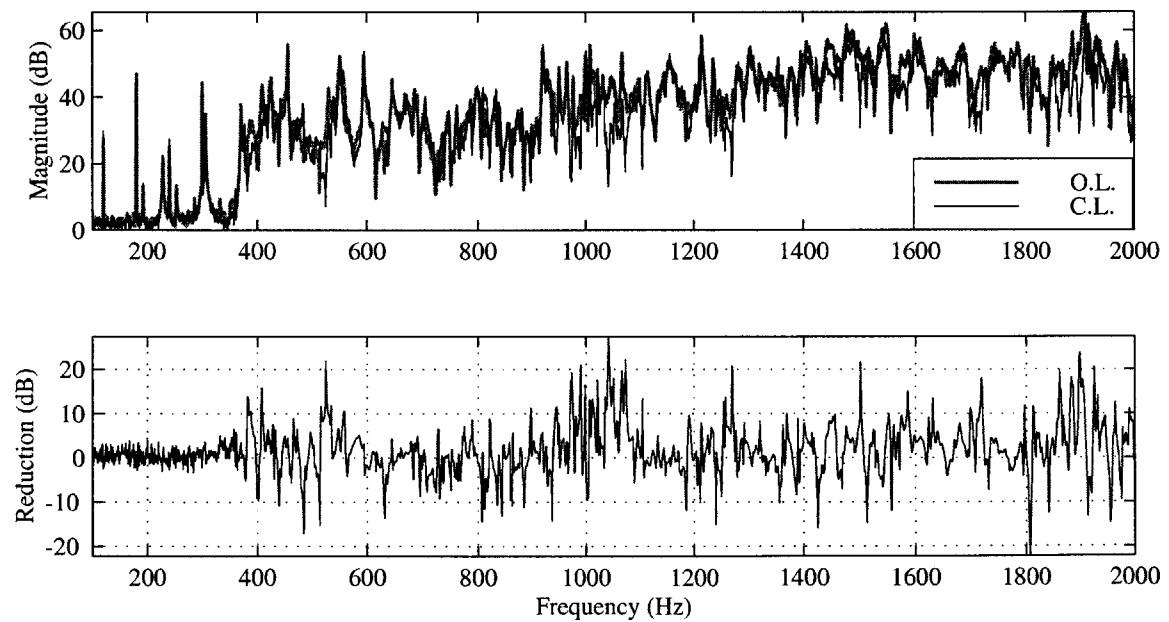


Figure 4.14: Open-loop and closed-loop acoustic pressure autospectra for a microphone located behind Panel 2 (#23).

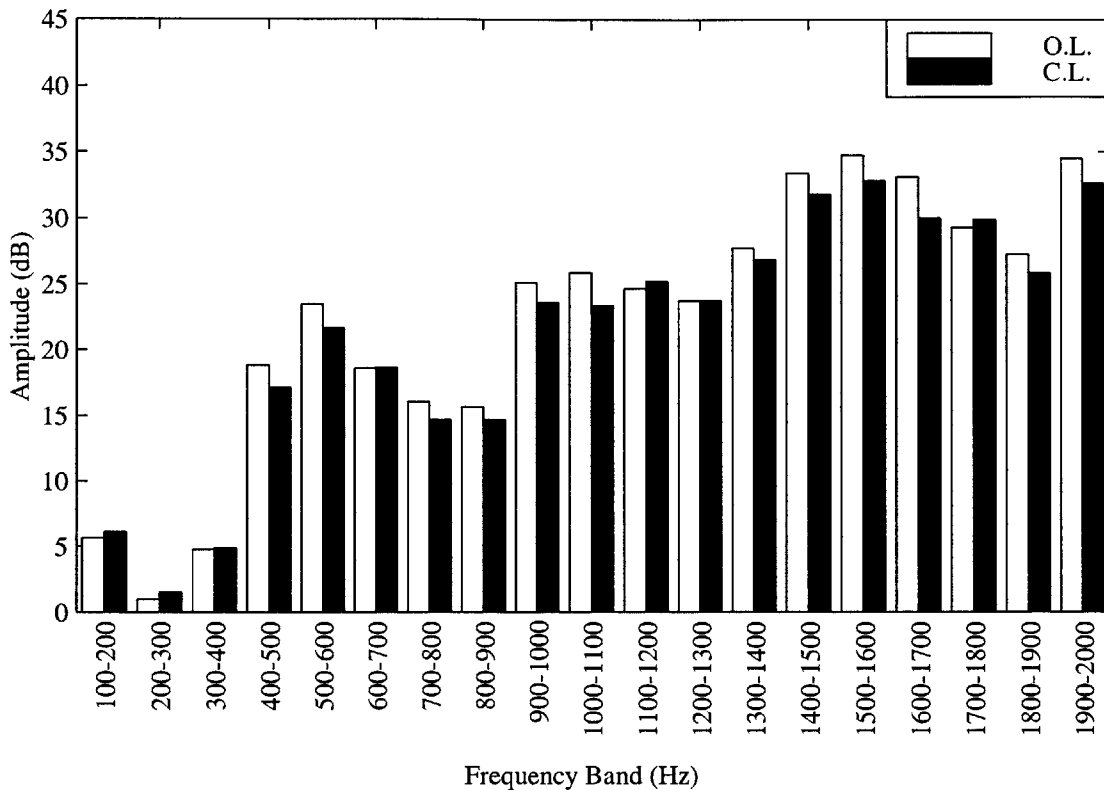


Figure 4.15: Open-loop and closed-loop average acoustic pressure autospectra integrated in 100 Hz frequency bands.

4.3 Summary

A total of 30 independent feedback loops were implemented based on the feedback methods discussed in Chapter 3. It was initially planned to implement each controller digitally on a personal computer equipped with a dSpace DSP card. Unfortunately, attempts to implement all 30 loops simultaneously have not been successful, primarily due to computational limitations. As a result, the controllers were implemented using analog circuits based on op-amps.

Control experiment was performed by applying the rate feedback control law to each PVDF-PZT pair separately. The disturbance source was a PZT patch bonded to an adja-

cent panel. This patch was excited with a 2 kHz bandwidth random signal to simulate a structural disturbance. Accelerometers attached to panels and microphones located inside the testbed were used as performance sensors. The open-loop and closed-loop autospectra of the performance sensor signals were analyzed and compared, to determine the effectiveness of the control system. Experimental results show reductions as much as 20 dB in structural acceleration and up to 10 dB of attenuation in the interior acoustic pressure level at some resonant peaks, over the frequency range of 100-2000 Hz. Maximum reduction was achieved at the frequencies where structural modes had good observability/controllability by the collocated PVDF-PZT pairs and where there was a good impedance match between the controller and the plant.

Chapter 5

Conclusions

5.1 Summary

In this thesis, a study of active structural acoustic control performed on a model fuselage testbed was presented. The study concentrated on broadband damping of localized panel modes. A setup was developed to carry out structural control experiments on a testbed, designed to be a simplified representative of a helicopter structure, in a previous study [O'Sullivan, 1998]. The most significant part of this setup was the selection and placement of the sensors and actuators that are required for active control. Weight and space restrictions in aircraft are severe. Hence, light and compact sensors and actuators were selected. PZT (Lead-Zirconate-Titanate) ceramic sheets were used as the actuators primarily due to their ease of utilization in large numbers. Although the PZT has a relatively high density, each PZT ceramic used in the experiment weighs far less than many electro-mechanical actuators.

The sensor selection was driven by the requirement that the sensor form a collocated pair with the PZT actuator. Though a microphone is capable of measuring the primary performance metric directly, it could not be used to form a collocated pair with the PZT. This is because a PZT patch generates local strain on the structure it is bonded to, while a microphone senses acoustic pressure: a quantity that is not exactly local to the structure. Accelerometers were also tested as sensors, but do not exhibit the desired collocated behavior. The PVDF (Polyvinylidene-Fluoride) film, a light and compact piezo-polymer,

is a good candidate to form a collocated pair with the PZT. The PVDF film is also simple to use and easy to attach on the structure. Hence, it is an appropriate sensor for this study.

Five square collocated PVDF-PZT pairs were bonded on a testbed panel and tested for observability/controllability of the structural modes. One of the patches was bonded to the center of the panel and the others were bonded near the four corners. This placement technique was chosen to ensure that most of the structural modes are observed and controlled over a broad frequency range. The actuators and sensors were sized to spatially filter the modes that occur beyond the frequency band of interest (0 - 2000 Hz). After verifying that the chosen sensor/actuator pairs and the placement method yielded acceptable observability/controllability of many structural modes, an active ply was developed that encapsulates the sensor/actuator pairs in the chosen placement pattern. Each active ply contained five PVDF patches collocated with five PZT patches. These patches were sandwiched with epoxy between two copper-kapton layers that were etched to form an appropriate electrode pattern. Six active plies were manufactured and bonded on six panels of the testbed, resulting in 30 collocated PZT-PVDF pairs. Instrumentation was completed by placing the performance sensors; the accelerometers were attached to the inside of the panels while the microphones were located on the boom that runs through the testbed.

Like many realistic fuselages, the model testbed exhibits complicated dynamics, such as high modal density and sensitivity to environmental changes. These characteristics make a model-based controller design infeasible. Hence, the control design was performed based on some experimental system identification methods that were used to assess the general dynamic behavior of the system. PZT to PVDF transfer functions were taken using each of the 30 collocated pairs to identify the system dynamics local to each sensor/actuator pair. These transfer functions were then used to design a control law that adds damping to local structural modes.

Among various local control techniques, rate feedback was chosen because of its robust stability and simplicity. Rate feedback is effective when the system has a collocated transfer function that rolls off, i.e., decreases with frequency. Although the sensor/actuator pair on the testbed exhibits collocated behavior, its transfer function does not roll off. Furthermore, since a PVDF sensor measures strain rather than strain rate, applying a pure rate feedback controller requires a derivative action which results in a transfer function with magnitude that increases with frequency. Hence, a complex pair of poles were introduced to the denominator of the controller transfer function to provide the desired roll off. This approach was only possible because of the spatial filtering inherent to the sensors and actuators.

The control law was applied to each of the 30 collocated PZT-PVDF pairs independently. The initial plan was to perform the implementation digitally on a PC with a digital signal processing (DSP) interface. However, attempts to close all of the loops simultaneously were not successful, due to computational limitations. The sampling frequency was found to depend on the complexity of the control law and the number of implemented controllers. The maximum sampling frequency to implement 30 independent controllers was as low as 4100 Hz. This introduced severe phase lag, which destabilized some of the feedback loops. As a result, the controllers were implemented using analog circuits based on op-amps.

The control experiment was performed by implementing the analog rate feedback controller for each PVDF-PZT pair independently. A PZT patch bonded to an adjacent panel was used as the disturbance source. This patch was excited with a 2 kHz bandwidth random signal to simulate a structural disturbance. Accelerometers attached to panels and microphones located inside the testbed were used as performance sensors. The open-loop and closed-loop autospectra of the performance sensor signals were analyzed and com-

pared, to determine the effectiveness of the control system. Experimental results showed reductions of as much as 20 dB in structural acceleration, and up to 10 dB of attenuation in the interior acoustic pressure level at some resonant peaks, over the frequency range of 100-2000 Hz. As expected, maximum reductions were achieved at frequencies where structural modes had good observability/controllability by the collocated PVDF-PZT pairs, and where there was a good impedance match between the controller and the plant.

5.2 Conclusions

Performing broadband control on aircraft structures is a challenging task. Many modern control approaches require an accurate mathematical representation of the system: either a state-space model or a set of transfer functions with poles and zeros. Forming such a model for a three-dimensional structure, and using it for control simulations is almost a computational impossibility. Even if computational difficulties are alleviated, high modal density and system sensitivities introduce uncertainties that may result in a severely inaccurate model. Hence, implementing a model-based controller on a realistic structure to perform broadband control is not feasible. The study presented in this thesis implies that active structural acoustic control (ASAC) can be implemented without having to use an analytical or numerical model. Actuator to sensor transfer functions can be experimentally measured, and used to design an appropriate control system. Experimental results show that attenuation in both structural vibration and interior acoustics is possible over a broad frequency range.

A collocated sensor/actuator pair is desirable in achieving a control system that is robust to system uncertainties, such as environmental sensitivities and high frequency dynamics. The piezo-ceramic actuator PZT and the piezo-polymer PVDF form a good col-

located pair and provide sufficient controllability/observability of the structural modes of the system.

The controller used with the PZT-PVDF pair must remove energy from the system to result in improved performance. This can be achieved by designing a control law that adds damping to the structure over the frequency range of interest. Rate feedback is a desirable control technique because it adds damping through derivative action and is robust. In order for rate feedback to be effective, the actuator to sensor transfer function must be collocated, and must roll off to prevent high frequency instability. A transfer function taken from PZT to PVDF exhibits collocated behavior, but does not roll off. This roll off can be provided by including a second-order term in the denominator of the controller transfer function. The roll off must occur above the last modal frequency in the control bandwidth of interest. Hence, the resonant behavior that is observed/controlled by the collocated pair must vanish above the control bandwidth. This can be achieved by sizing the actuator and the sensor to spatially filter the structural modes that occur at frequencies above the control bandwidth of interest.

Experimental results showed better performance for structural vibration control than for interior acoustics control. This is mainly because the control was performed only on a few panels. Due to structural coupling, the disturbance induced by the PZT patch affects nearly all panels of the testbed, and causes them to radiate sound. Another reason is that the control action was only performed on the structure. Although interior acoustic pressure is the most direct performance metric, no feedback from interior acoustics was included in the control action. The control sensor (PVDF) and the performance sensor (microphone) were far from each other and they measured different properties. In other words, the system was *not output analogous* [Crawley, 1999]. In the case of structural vibration, the performance sensor (accelerometer) and the control sensor were relatively close. This implies

that the effectiveness of ASAC on interior acoustics may be improved by including some acoustic feedback in the control system. On the other hand, to achieve robustness, the sensors and actuators must be collocated; however, a microphone can not be collocated with a structural actuator. This introduces a trade-off between robustness and high performance that must be considered by the control designer.

5.3 Recommendations for Future Work

The experimental results showed promising closed-loop performance. This performance was obtained by instrumenting less than 10% of the testbed with sensors and actuators. As discussed in Chapter 3, frame members constitute a rough boundary for each panel. However, some level of structural coupling between the individual panel dynamics does exist: a disturbance that is induced at a specific location on the structure affects a large portion of the structure. Hence, interior noise results from the vibration of a large number of panels. For this reason, instrumenting a greater portion of the testbed with sensors and actuators is expected to produce greater reduction in the structural acceleration and the interior noise level.

Certain challenges in a large scale instrumentation do exist. Although the active plies contain sensors, actuators, and electrodes in an encapsulated package, control laws are implemented outside the active plies. There is a great deal of wiring between the active plies and the controllers. Instrumenting a large portion of the structure in the same manner would result in excessive number of wires which could introduce serious noise problems and debugging difficulties.

A more fundamental and somewhat long term approach to active structural control could be the *smart structure technology*. A smart graphite composite panel with embedded sensors, actuators and integrated control circuitry can be developed. The skin of the air-

craft fuselage can be manufactured with these smart panels. Several issues need detailed investigation. Composites require specific manufacturing procedures such as *curing* which is a high temperature heat treatment used to solidify the adhesive. Whether the embedded sensors, actuators and the control circuitry can endure this treatment is somewhat unclear and needs to be studied thoroughly. Once these manufacturing-related issues are understood and solved, smart panels can be used for active structural acoustic control. The work presented in this thesis can provide a significant background in performing active control using smart structure technology.

Appendix A

A.1 Equipment Specifications and Manufacturer Information

Equipment	Model	Company	Web site
PZT	5A 0.254mm thickness	Morgan-Matroc	www.morganmatroc.com
PVDF	P.N. 1-1004346-0 0.0508mm thickness	Measurement Specialties Inc.	www.msiusa.com
Accelerometer	352B22	PCB Electronics	www.pcb.com
Microphone	130B10	The Modal Shop	www.modalshop.com
Copper-Kapton	Etch-A-Flex 2500-HH-SS 0.0127mm thickness	Southwall Technologies Inc.	www.southwall.com
Epoxy	Epotek 301 Parts A and B	Epoxy Technology	www.epotek.com
Thermoplastic Adhesive	Thermobond 557EG 0.0635mm thickness	3M	www.3m.com
Data Acquisition Unit	Siglab 20-42	MTS (DPS Technology Division)	www.dspt.com
DSP Interface	Input: DS2003 Output: DS2103 Processor: C40	dSpace Inc.	www.dspace.de

Table A.1: Model, company, and web site information of experimental equipment.

References

- Bailey, T., and Hubbard, J., "Distributed Piezoelectric Polymer Active Vibration Control of a Cantilever Beam," *Journal of Sound and Vibration*, vol.8, no.5, Sept.-Oct. 1985, pp. 605-11.
- Blevins, R.D., "Formulas for Natural Frequency and Mode Shape," *Krieger Publishing*, Malibar, FL, 1979, pp. 293-321.
- Brennan, M.J., Day, M.J., Elliott, S.J., and Pinnington, R.J., "Distributed piezoelectric actuators and sensors for active vibration control," *Proceedings of Topical Symposium VI on Intelligent Materials and Systems of the 8th CIMTEC-World Ceramics Congress and Forum on New Materials TECHNIA*, Faenza, Italy, 1995, pp. 299-306.
- Concilio, A., De Vivo, L., and Sollo, A., "A Comparison of Different Strategies for Interior Active Noise Control by Piezoactuators," *Proceedings of the International Conference on Noise and Vibration Engineering*, Heverlee, Belgium, September 1996, Vol.1, pp. 247-258.
- Crawley, E.F., and de Luis J., "Use of piezoelectric actuators as elements of intelligent structures," *AIAA Journal*, vol.25, no.10, Oct. 1987, pp.1373-85.
- Crawley, E.F., and Hall, S.R., "Dynamics of Controlled Structures," *SERC Report # 10-91-I*, July 1991.
- Crawley, E.F., Campbell, M., and Hall, S.R., "High Performance Structures: Dynamics and Control-draft manuscript," *to be published by Cambridge University Press*, 1999.
- D'Cruz, J., "Active Suppression of Aircraft Panel Vibration with Piezoceramic Strain Actuators," *Journal of Aircraft*, Vol. 35, No. 1, Jan-Feb 1998, pp. 139-144.
- Elliot, S.J., Boucher, C.C., and Sutton, T.J., "Active Control of Rotorcraft Interior Noise," *Innovation in Rotorcraft Technology; Proceedings of the Conference of Royal Aeronautical Society*, London, U.K., June 1997, pp. 15.1-15.6.
- Elliot, S.J., "Down with Noise; Destructive Interference for Sound Control," *IEEE Spectrum*, Vol. 36, No. 6, June 1999, pp. 54-61.
- Fanson, J.L., and Caughey, T.K., "Positive Position Feedback Control for Large Space Structures", *AIAA Journal*, Vol. 28, No. 4, April 1990, pp. 717-24.
- Franklin, G.F., Powell, J.D., and Workman, M., "Digital Control of Dynamic Systems," 3rd edition, *Addison-Wesley*, 1998
- Freidland, B., "Control System Design; An Introduction to State-Space Methods," *McGraw-Hill Inc.*, 1986
- Fripp, M.L., O'Sullivan, D.Q., Hall, S.R., Hagood, N.W., and Lillienkamp, K., "Test-bed Design and Modeling for Aircraft Interior Acoustic Control," in *Smart Structures and Materials: Smart Structures and Integrated Systems, Proceedings of SPIE*, Vol. 3041, 1997, pp. 88-99.

- Fripp, M.L., Atalla, M.J., Hagood, N.W., Savran, C.A., and Tistaert, S., "Reconfigurable Arrays for Broadband Feedback Control of Aircraft Fuselage Vibrations," *Proceedings of International Conference on Adaptive Structures (ICAST)*, 1999, pp. 447-457.
- Fuller, C.R., Hansen, C.H., and Snyder, S.D., "Experiments on Active Control of Sound Radiation from a Panel Using a Piezoceramic Actuator," *Journal of Sound and Vibration*, Vol. 150, No. 2, October 1991, pp. 179-90.
- Fuller, C.R., and Gibbs, G.P., "Active Control of Interior Noise in a Business Jet Using Piezoceramic Actuators," *Proceedings of the 1994 National Conference on Noise Control Engineering*, 1994, pp. 389-394.
- Goh, C.J., and Caughey, T.K., "On the Stability Problem Caused by Finite Actuator Dynamics in the Control of Large Space Structures," *International Journal of Control*, Vol. 41, No. 3, 1985, pp. 787-802.
- Grewal, A., Zimcik, D.G., Hurtubise, L., and Leigh, B., "Active Noise and Vibration Control of Turboprop Aircraft Cabins using Multiple Piezoelectric Actuators," *3rd AIAA/CEAS Aeroacoustics Conference*, Atlanta, GA, May 1997, pp. 1-11.
- Hall, S.R., Crawley, E.F., How, J.P., and Ward, B., "Hierarchic control architecture for intelligent structures," *Journal of Guidance Control & Dynamics*, vol.14, no.3, May-June 1991, pp. 503-12.
- Hu, H., "Self-excited Vibration of Controlled Elastic Structures," *Journal of Vibration Engineering*, Vol. 12, No. 2, June 1999, pp. 188-192.
- Kalman, R.E, and Bucy, R.S., "New Results in Linear Filtering and Prediction Theory," *Trans., ASME (J.Basic Engineering)*, Vol. 83D, No.1, March 1961, pp. 95-108.
- Laugwitz, F., Goernandt, A., and Groebel, K., "Simulations and Experimental Investigations on Active Damping of Vibration of Plates with Piezoactuators," *Proceedings of EUROMECH 373 Colloquium on Modeling and Control of Adaptive Mechanical Structures*, Magdeburg, Germany, March 1998, pp. 367-374.
- Leatherwood, J., "Summary of Effects of Infrasound on Man," *Symposium on Internal Noise in Helicopters*, University of Southampton, U.K., July 1979, pp. A2 29-30.
- Leverton, J.W., and Pollard, J.S., "Helicopter Internal Noise - An Overview," *Symposium on Internal Noise in Helicopters*, University of Southampton, U.K., July 1979, pp. A2 7-9.
- MacMartin, D.G., and Hall, S.R., "Structural control experiments using an H_∞ power flow approach," *Journal of Sound & Vibration*, vol.148, no.2, 22 July 1991, pp. 223-41.
- MacMartin, D.G., and Hall, S.R., "Control of uncertain structures using an H_∞ power flow approach," *Journal of Guidance Control & Dynamics*, vol.14, no.3, May-June 1991, pp. 521-30.
- MacMartin, D.G., and Hall, S.R., "Broadband control of flexible structures using statistical energy analysis concepts," *Journal of Guidance Control & Dynamics*, vol.17, no.2, March-April 1994, pp. 361-9.

- Maitland, J.E., "Effects of Internal Noise on Helicopter Operation - An Aircrew View," *Symposium on Internal Noise in Helicopters*, University of Southampton, U.K., July 1979, pp. A1 1-2.
- Martin, G.D., and Bryson, A.E., "Attitude Control of a Flexible Aircraft," *Journal of Guidance and Control*, Vol. 3, No. 1, January-February 1980, pp. 37-41.
- Mathur, G.P., Tran, B.N., Simpson, M.A., and Peterson, D.K., "Broadband Active Structural Acoustic Control of Aircraft Cabin Noise-Laboratory Tests," *3rd AIAA/CEAS Aeronautics Conference*, Atlanta, GA, May 1997, pp. 422-431.
- Moreland, S., "U.S. Army Working Group on Aircraft Noise," *Symposium on Internal Noise in Helicopters*, University of Southampton, U.K., July 1979, pp. A2 1-24.
- Niesl, G., and Laudien, E., "Impact of Acoustic Loads on Aircraft Structures," *AGARD Meeting*, Lillehammer, Norway, May 1994, pp. 265.
- O'Sullivan, D., "Aircraft Interior Structural Acoustic Control Design," *S.M. Thesis, Dept. of Mechanical Engineering, Massachusetts Institute of Technology*, Cambridge, MA, 1998.
- Palumbo, D.L., Padula, S.L., Lyle, K.H., Cline, J.H., and Cabell, R.H., "Performance of Optimized Actuator and Sensor Arrays in an Active Noise Control System," *NASA Langley Research Center*, 1996, pp. 14.
- Rossetti, D.J., and Norris, M.A., "A Comparison of Actuation and Sensing Techniques for Aircraft Cabin Noise Control," *AIAA/ASME Adaptive Structures Forum*, Hilton Head, SC, April 1994, pp. 65-72.
- Savran, C.A., Atalla, M.J., and Hall, S.R., "Broadband Active Structural Acoustic Control of a Fuselage Testbed Using Collocated Piezoelectric Sensors and Actuators," *to appear in Smart Structures and Materials: Smart Structures and Integrated Systems, Proceedings of SPIE, 2000*.
- Schaeter, D., "Optimal Local Control of Flexible Structures," *Journal of Guidance and Control*, Vol. 4, No. 1, 1981, pp. 22-26.
- Siljak, D.D., "Decentralized Control of Complex Systems," *Academic Press Inc.*, Boston, 1991.
- Smith, T., and Furner, T., "Active Noise Control, the Proven Reality," *Aircraft Cabin Systems; Proceedings of the Conference of Royal Aeronautical Society, London, U.K.*, December 1996, pp 2.1-2.9.
- Thomas, D.R., Nelson, P.A., Pinnington, R.J., and Elliot, S.J., "An Analytical Investigation of the Active Control of the Transmission of Sound Through Plates," *Journal of Sound and Vibration*, Vol. 181, No. 3, 1995, pp. 515.
- Von Flotow, A., Mercedal, M., Maggi, L., and Adams, N., "Vibration and Sound Control," *Aerospace Engineering*, Vol. 17, No. 10, October 1997, pp. 12-14.
- Warnaka, G.E., Kleinle, M., Tsangaris, P., Oslac, M.J., and Moskow, H.J., "A Lightweight Loudspeaker for Aircraft Communications and Active Noise Control," *Proceedings of the Fourth Aircraft Interior Noise Workshop*, NASA Langley Research Center,

1992, pp. 316-327.

Xu, W., Afagh, F.F., Grewal, A., and Zimcik, D., "The Effects of Segmented Piezoelectric Actuator Configuration on Aircraft Noise Control Performance," *39th AIAA/ASME/ASCE/AHS/ASC Structures, Structural Dynamics, and Materials Conference and Exhibit and AIAA/ASME/AHS Adaptive Structures Forum*, Long Beach, CA, April 1998, pp. 2257-2264.

